AD-A064 136 MISSION RESEARCH CORP LA JOLLA CA F/G 9/1
HARDNESS ASSURANCE FOR LONG-TERM IONIZING RADIATION EFFECTS ON --ETC(U)
MAR 78 A R HART, J B SMYTH, J P RAYMOND DNA001-76-C-0201
UNCLASSIFIED MRC/SD-R-23 DNA-4574F NL

1 OF 2
AD
A064136

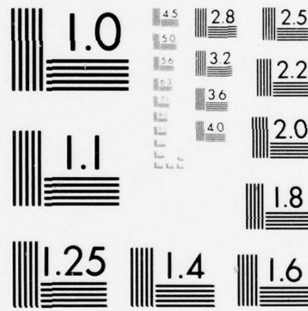

MICROCOPY RESOLUTION TEST CHART
NATIONAL BUREAU OF STANDARDS-1963-A

(12) LEVEL III AD-E300 417

DNA 4574F

HARDNESS ASSURANCE FOR LONG-TERM IONIZING RADIATION EFFECTS ON BIPOLAR STRUCTURES

AD A064136

Mission Research Corporation
P.O. Box 1209
La Jolla, California 92038

March 1978

Final Report for 1 April 1977—1 March 1978

CONTRACT No. DNA 001-76-C-0201

DDC FILE COPY

APPROVED FOR PUBLIC RELEASE;
DISTRIBUTION UNLIMITED.

THIS WORK SPONSORED BY THE DEFENSE NUCLEAR AGENCY
UNDER RDT&E RMSS CODE B323077464 Z99QAXTE50103 H2590D.

DDC
RECEIVED
FEB 5 1979
B

Prepared for
Director
DEFENSE NUCLEAR AGENCY
Washington, D. C. 20305

78 12 05 032

Destroy this report when it is no longer
needed. Do not return to sender.

PLEASE NOTIFY THE DEFENSE NUCLEAR AGENCY,
ATTN: TISI, WASHINGTON, D.C. 20305, IF
YOUR ADDRESS IS INCORRECT, IF YOU WISH TO
BE DELETED FROM THE DISTRIBUTION LIST, OR
IF THE ADDRESSEE IS NO LONGER EMPLOYED BY
YOUR ORGANIZATION.

UNCLASSIFIED

SECURITY CLASSIFICATION OF THIS PAGE (When Data Entered)

REPORT DOCUMENTATION PAGE		READ INSTRUCTIONS BEFORE COMPLETING FORM
1. REPORT NUMBER: DNA 4574F	2. GOVT ACCESSION NO.	3. RECIPIENT'S CATALOG NUMBER
4. TITLE (and Subtitle): HARDNESS ASSURANCE FOR LONG-TERM IONIZING RADIATION EFFECTS ON BIPOLAR STRUCTURES		5. TYPE OF REPORT & PERIOD COVERED: Final Report for Period 1 April 1977—1 March 1978
		6. PERFORMING ORG. REPORT NUMBER: MRC/SD-R-23
7. AUTHOR(s): Arthur R. Hart, John B. Smyth, Jr., James P. Raymond, Victor A. J. van Lint		8. CONTRACT OR GRANT NUMBER(s): DNA 001-76-C-0201
9. PERFORMING ORGANIZATION NAME AND ADDRESS: Mission Research Corporation, P.O. Box 1209, La Jolla, California 92038		10. PROGRAM ELEMENT, PROJECT, TASK AREA & WORK UNIT NUMBERS: NWED Subtask Z99QAXTE501-03
11. CONTROLLING OFFICE NAME AND ADDRESS: Director, Defense Nuclear Agency, Washington, D.C. 20305		12. REPORT DATE: March 1978
		13. NUMBER OF PAGES: 160
14. MONITORING AGENCY NAME & ADDRESS (if different from Controlling Office)		15. SECURITY CLASS (of this report): UNCLASSIFIED
		15a. DECLASSIFICATION/DOWNGRADING SCHEDULE

16. DISTRIBUTION STATEMENT (of this Report)

Approved for public release; distribution unlimited.

17. DISTRIBUTION STATEMENT (of the abstract entered in Block 20, if different from Report)

18. SUPPLEMENTARY NOTES

This work sponsored by the Defense Nuclear Agency under RDT&E RMSS Code B323077464 Z99QAXTE50103 H2590D.

19. KEY WORDS (Continue on reverse side if necessary and identify by block number)

Bipolar Transistors	Total Dose Effects
Gain Degradation	Surface Potential
Modelling	Surface States
Long-Term Ionizing Radiation Effects	Surface Recombination Velocity

20. ABSTRACT (Continue on reverse side if necessary and identify by block number)

This work assessed the theoretical understanding of long-term ionization effects in semiconductor bipolar devices in support of developing hardness assurance techniques. The principal effort was directed at investigating transistor gain degradation mechanisms by use of models relating semiconductor physical and electrical parameters to surface properties. Ionizing radiation effects on surface properties were used to identify critical physical parameters for use in hardness assurance procedures. Model

DD FORM 1 JAN 73 1473 EDITION OF 1 NOV 65 IS OBSOLETE

UNCLASSIFIED

SECURITY CLASSIFICATION OF THIS PAGE (When Data Entered)

20. ABSTRACT (Continued)

implications and predictions were then compared with existing data to evaluate accuracy and usefulness.

This investigation demonstrated that current theories regarding the surface of bipolar transistors appear to describe the major parameter dependencies if ionizing radiation effects are not considered. It is when radiation effects are incorporated into these theories (models) that fundamental questions arise as to their completeness or validity.

Specific questions were found when the surface models originally defined by Reddi and Grove were used to predict the experimental radiation data observed by Sivo.

ACCESSION for
NTIS White Section
DDC Buff Section
UNANNOUNCED
JUSTIFICATION
BY
DISTRIBUTION/AVAILABILITY CODES
Dist. AVAIL. and/or SPECIAL
A

TABLE OF CONTENTS

SECTION		PAGE
	LIST OF ILLUSTRATIONS	3
	LIST OF TABLES	6
	DEFINITION OF TERMS	7
1.0	INTRODUCTION	9
2.0	THEORETICAL MODEL AND IONIZING RADIATION EFFECTS	15
	2.1 Introduction to Theoretical Model	15
	2.1.1 Theoretical Model Description	16
	2.1.1.1 Field-Induced Depletion Layer Term (I_{FIDL})	26
	2.1.1.2 Surface Recombination Velocity Term I_{SO}	28
	2.1.2 Pre-Radiation Gated Transistor Data Comparison to Model Predictions	31
	2.1.2.1 "Bulk" Base Current Terms	33
	2.1.2.2 I_{SO} Term	37
	2.1.2.3 I_{FIDL} Term	41
	2.1.2.4 Other Current Terms Related To The FIDL Region	42
	2.1.2.5 Summary of Prediction Accuracy	43
	2.2 Radiation-Inclusive Bipolar Transistor Model	44
	2.2.1 Radiation Effects on Surface Physical Characteristics	45
	2.2.1.1 Trapped Hole and Surface State Generation Mechanisms	48

83 12 05 032

(Continued)

2.2.1.2 Surface Potential Distribution Due to Oxide Charge and Surface State Build-Up 51

2.2.1.3 Measurement Techniques for Analyzing Radiation Effects 58

2.2.2 Radiation Effects on Base Current Terms 62

2.2.2.1 Recombination-Generation Surface Terms 62

2.2.2.2 Surface Dependent Bulk Diffusion Currents 63

2.2.3 Radiation Data Comparison to Model 66

2.2.3.1 Shifting, Broadening and Increases In Gated Transistor Base Current Curves 73

2.2.3.2 Bias Effects During Irradiation 88

2.2.3.3 Process Variations 90

2.3 Other Bipolar Structures and Applications 91

2.3.1 P-N-P Transistor DC Gain Degradation 92

2.3.2 Saturation ($V_{CE(SAT)}$) 95

2.3.3 JFETs and Diodes 96

2.3.4 Integrated Circuits 99

3.0 CONCLUSIONS 100

REFERENCES 104

APPENDIX A - FIELD INDUCED DEPLETION LAYER

APPENDIX B - SURFACE RECOMBINATION

APPENDIX C - DESCRIPTION OF "BULK" BASE CURRENT TERMS IN DC GAIN COMPONENTS

APPENDIX D - MODEL DEVELOPMENT FOR SURFACE POTENTIAL (IRT Subcontract Report)

APPENDIX E - RECOMBINATION CENTER EFFECTIVE CONCENTRATION

ILLUSTRATIONS

FIGURE		PAGE
2.1	A schematic representation of the five base current components.	17
2.2	Base current components over collector current vs. emitter-base forward bias and collector current for the 2N2222 transistor model (Motorola).	20
2.3(a)	Carrier concentration, electric field strength, and recombination rate in an idealized junction.	23
2.3(b)	The effect of the n and p carrier concentrations on the recombination rate near and at the surface of the base region.	23
2.4	Surface base current components associated with a p-n junction.	24
2.5	Band representation of a p-type silicon intersection with the surface.	26
2.6	Cross-sectional views of experimental surface controlled transistors (circular symmetry).	31
2.7	Base current vs. gate voltage for the transistor shown in Figure 2.6.	34
2.8	Comparison of the theoretical to experimental I_{SO} term. The experimental points result from Figure 2.7.	39
2.9	Comparison of experimental and theoretical gate voltage shift vs. V_{BE} for peak I_B.	40
2.10	The Si-SiO_2 interface energy diagram during irradiation.	49
2.11	The Si-SiO_2 interface energy diagram after irradiation showing trapped charge effects.	49
2.12	The pre-irradiation Si-SiO_2 energy diagram showing surface state assumptions.	51

ILLUSTRATIONS (Continued)

2.13	Idealized electric field lines in oxide due to junction modeled as a parallel plate capacitor.	53
2.14	Pre-irradiation electric field for a non-gated transistor at the surface of the base due to the E-B junction voltage vs. distance from the edge of the E-B depletion layer.	53
2.15	The space-charge region and electric field associated with a p-n junction where the n-type is more heavily doped.	54
2.16	Dependence of surface potential ϕ_S on interface electric field in silicon dioxide, for various values of surface state density D_{ss} (in units of cm^2 $eV)^{-1}$).	56
2.17	Field-dependent influences on surface potential vs. distance from E-B junction for irradiated standard ungated transistor.	57
2.18	Illustration of gate structure placed over the E-B junction of an n-p-n transistor as a diagnostic tool for measuring surface properties of bipolar devices.	59
2.19	Pre-irradiation electric field for a gated transistor at the surface of the base due to the E-B junction voltage vs. distance from the edge of the E-B depletion layer.	60
2.20	Field-dependent influences on surface potential vs. distance from E-B junction for irradiated gated transistor.	61
2.21	Effect of bias and measurement current on current gain degradation.	64
2.22	2N1613 transistor, I_E = 1 mA, V_{CB} = 10 V, Cobalt 60 irradiation.	65
2.23	Total-dose induced degradation of n-p-n upgain transistor for two forms of advanced I^2L.	66
2.24	Standard interpretation of a non-irradiated gated bipolar transistor base current curve vs. gate voltage.	67
2.25(a)	Effect of ionizing radiation on the I_B vs. V_G curves at various injection levels.	70
2.25(b)	Effect of ionizing radiation on the I_B vs. V_G curves at various injection levels. This illustration is a continuation of Figure 2.25(a).	71

ILLUSTRATIONS (Continued)

2.25(c)	An example of high dose effects on the base current, I_B.	72
2.26	Gate voltage necessary to peak I_B vs. dose for several applied emitter-base voltages.	74
2.27	Gate voltage necessary to peak I_B vs. applied emitter-base voltage for several dose levels.	74
2.28	Example of the absence of substantial radiation induced broadening of the I_B peaks in a group of transistors which had a high initial oxide charge.	79
2.29	Predicted change in base current vs. dose for the ungated 2N2222 transistor model using only field-dependent build-up of Q_{ox} and N_{ss} for doses greater than 10^4 Rads.	83
2.30	Experimental data from Figure 2.25 at $V_G = 0$ describing the change in base current vs. dose for a gated 2N2222 transistor.	83
2.31	Predicted change in base current vs. dose for the ungated 2N2222 transistor model using the field-dependent build-up of Q_{ox} and N_{ss} plus a super-position of a field-independent $\Delta N_{ss} = 1.2 \times 10^6$ states/cm^2 per dose.	85
2.32	Combination of gated transistor experimental data with two cases considered by the model for an ungated transistor of the same type.	85
2.33	Ungated transistor experimental data for a Fairchild 2N1613 device type.	87
2.34	Normalized base current increase vs. total gamma dose for devices with varying junction electric field strengths during irradiation.	89
2.35	Effect of ionizing radiation on the I_B vs. V_G curves of a p-n-p transistor at various injection levels.	93
2.36	Illustration of the various current components of I_B in the I_B vs. V_G plot of an unirradiated p-n-p transistor.	94
2.37	Breakdown voltage vs. gate voltage characteristics of a p^+-n gate controlled diode before and after X-irradiation.	98
2.38	Breakdown voltage vs. gate voltage characteristics of an n^+-p gate-controlled diode before and after X-irradiation.	98

TABLES

TABLE		PAGE
2.1	Physical parameters used for Reddi's transistor in Figure 2.5.	32
2.2A	Experimental data and models concerning production of new interface states with increasing dose in biased, oxidized silicon.	46
2.2B	Experimental data and models concerning radiation-induced changes in biased oxidized silicon surfaces; fixed charge (Q_{ox}) and surface recombination velocity (S_o).	47
2.3	Physical parameters for the 2N2222 transistors (transistor is circular geometry) used in Sivo's ionizing radiation experiments.	69

DEFINITION OF TERMS

A_e = area of the projected emitter-base junction (cm^2)

A_g = A_G = area under the gate over the base surface (cm^2)

D_n = electron diffusion constant in p-type Si = $\frac{kT\ \mu_n}{q}$ (cm^2/sec)

D_p = hole diffusion constant in n-type Si = $\frac{kT\ \mu_p}{q}$ (cm^2/sec)

D_{ss} = energy density of surface states (states/cm^2-eV)

d_{ox} = thickness of oxide (Å)

N_B = base doping (atoms/cm^3)

N_{BS} = base doping at surface (atoms/cm^3)

N_E = emitter doping (atoms/cm^3)

N_{ES} = emitter doping at surface (atmos/cm^3)

N_{ss} = spatial density of surface states (states/cm^2)

n_i = intrinsic carrier concentration (carriers/cm^3)

P_e = emitter periphery (cm)

P_{eg} = emitter periphery under gate (cm)

P_G = gate periphery (cm)

R_i = intrinsic carrier recombination rate (sec^{-1})

R_{is} = intrinsic carrier recombination rate near the surface (sec^{-1})

v_{th} = limiting thermal velocity (cm/sec)

W_b = vertical width of base under the emitter (cm)

W_{sc} = vertical distance between collector and loweredge of surface field-induced depletion layer (cm)

ψ_o = built-in potential for emitter-base (E-B) junction (eV)

ψ_{os} = built-in potential for E-B junction at the surface (eV)

ϕ_F = Fermi potential (eV)

$\chi_{d_{max}}$ = maximum width of the Field-Induced Depletion Layer (FIDL) (cm)

χ_e = width of E-B depletion layer (cm)

χ_{es} = width of E-B depletion layer at surface (cm)

σ = capture cross section (cm^2)

τ_b = minority carrier lifetime in base (sec)

τ_e = minority carrier lifetime in emitter (sec)

β = q/kT (eV^{-1})

SECTION 1

1.0 INTRODUCTION

This effort assessed the theoretical understanding of long-term ionization effects in semiconductor bipolar devices in support of developing hardness assurance techniques. Technical effort was performed by Mission Research Corporation with the subcontract support of IRT Corporation. Results of this investigation complement the work of Dr. Alan Stanley at JPL and the current AFWL procurement to investigate hardness assurance screens and process controls.

The principal effort has been directed to the evaluation of transistor gain mechanisms in a model relating physical and electrical parameters. By evaluating the worst-case variations in these parameters based on processing variations and applications, hardness assurance techniques can be identified.

Most investigators of long-term ionizing radiation effects on bipolar devices (both theoretical and experimental) will agree that ionizing radiation effects are complex functions dependent on several parameters. This evaluation isolated the critical parameters through investigation of the pre-irradiation surface related contributions to the bipolar transistor DC gain, review of ionizing radiation mechanisms, and extension to the radiation-inclusive model.

Identifying the critical parameters does not however develop hardness assurance techniques, especially for long-term ionization effects.

Much of the difficulties in evaluating existing models was in estimating values for the parameters. This limitation was one of the most important problems to overcome. Once reasonable parameter values were obtained, the comparison of model implications with experimental data showed whether the models evaluated contained the necessary dependencies. The technical approach was organized by the following tasks:

a) Estimate the electric field distribution in the passivation insulator under normal bias conditions.

b) Estimate the generation and transport of holes to the interface due to ionizing radiation.

c) Estimate the distribution of trapped holes and interface states as a function of reasonable values of the hole trapping and interface state creation efficiencies.

d) Estimate the parameter changes resulting from trapped holes and interface states.

e) Estimate an upper limit on electrical parameter changes due to long-term ionizing radiation effects as a function of basic device parameters (e.g., silicon resistivity, oxide thickness, junction perimeter).

f) Formulate means to use these relations as hardness assurance controls for long-term ionization effects.

g) Check available data to compare predicted trends with experimental results.

The IRT effort was directed principally to tasks a) - c). The MRC effort consisted of incorporating the IRT results and those of a wide variety of previous studies in tasks d) - g).

The bipolar transistor structure was selected as the basis of the study. Parameter variations considered include those representative

of device and integrated circuit technologies (with the possible exception of some of the transistor elements in I^2L arrays using minimum-geometry logic cells).

Two basic effects have been identified as the long-term result of ionizing radiation exposure:

1) trapped charge build-up in the oxide near the silicon interface, and

2) creation of interface states at the silicon-silicon dioxide interface.

Process induced trapped charge and interface states can be identified in semiconductor devices and ionizing radiation induces a significant increase in each. In modeling radiation effects, several assumptions were made:

a) the basic radiation interaction is the same for both silicon MOS and bipolar devices,

b) MOS structures can be used to obtain radiation effects data on materials and interfaces used in bipolar devices, and

c) surface-related mechanisms are the only contribution to gain degradation due to long-term ionizing radiation (i.e., bulk displacement damage effects are not significant).

Each assumption simplifies the approach in applying mathematical expressions for the analysis of experimental data on gain degradation, and in obtaining estimates for upper limits on electrical parameter changes. These assumptions are incorporated in this report; their known limitations will be identified where appropriate.

The major contributions that this effort makes to the present understanding of the effects of ionizing radiation on bipolar transistors include:

a) the interpretation and implication of base current contributions due to added recombination sites at the Si-SiO_2 interface,

b) field related changes in the surface potential due to ionizing radiation and the influence this change has on the base current,

c) the identification of important relationships between ionizing radiation and physical changes and their application to hardness assurance controls for transistors.

Critical parameters which influence the gain degradation due to ionizing radiation effects were identified as:

a) surface potential,

b) surface state density,

c) acceptor dopant concentration (base doping for n-p-n transistors, emitter and collector doping for p-n-p devices),

d) emitter periphery,

e) emitter periphery - emitter area ratio,

f) base surface area between the edge of the E-B junction and base contact for n-p-n transistors, and

g) applied emitter-base voltage used during ionizing radiation exposure and post-irradiation measurement (V_{BE}).

The distribution of the surface potential and surface states over the base and emitter-base (E-B) metallurgical junction surface regions (for n-p-n transistors) and over the E-B metallurgical junction and emitter surface regions (for p-n-p transistors) is most critical.

In general, this program considered each reasonable base current term related to surface parameters and evaluated its usefulness in explaining all or part of the available experimental pre-irradiation data for DC gain effects. The result was the identification of two major base current terms (I_{SO} and I_{FIDL}) directly related to changes in surface properties. These two terms involve recombination-generation (R-G) mechanisms usually defined for a bulk space charge region or depletion layer by Shockley-Read-Hall statistics but the boundary conditions are different. They are maximized for the surface when the majority carrier concentration equals the minority carrier concentration (i.e., n = p, defined as crossover) and are dependent on the density of recombination centers (or surface states). When the surface properties are such that a full depletion layer is induced near the surface, crossover occurs in the bulk silicon. The additional base current I_{FIDL} due to these recombinations is dependent on bulk trap centers. When a complete depletion layer does not exist at the surface, crossover can occur at the surface. For this condition, the surface states act as recombination centers. The added base current due to this mechanism is defined as I_{SO} (this term contains the so-called surface recombination velocity). This contribution can be found even at zero surface potential due to the intersection of the crossover in the E-B metallurgical junction with the surface. Positive surface potential (such as induced by ionizing radiation) influences the position of the intersection of the crossover with the surface and results in a change in the base current due to increasing recombination centers and increasing effective surface area.

In n-p-n transistors, the base surface region is where I_{SO} is most important. In contrast, for p-n-p transistors the gain degradation appears to be dependent on the emitter surface region due to the effect of a positive surface potential on the dopant concentration. Both types of devices are thus critically dependent on the acceptor dopant concentration (N_A) at the surface. By knowing the distribution of surface potential, ϕ_s, the surface state density, N_{ss}, and surface geometry, I_{SO} can be evaluated and added

to the pre-irradiation base curent. Therefore,

$$\Delta \frac{1}{h_{FE_s}} = \text{Function of } (\phi_s,\ N_{ss},\ \text{geometry},\ N_A).$$

For hardness assurance applications, we do not necessarily require the exact values for each critical parameter. An upper bound for each parameter will allow for conservative designs and reasonable screening techniques useful to the system designer. To upper bound the critical parameters, several approximations can be made based on the understanding of the physics principles defined in the model.

To estimate an upper bound on the surface potential and surface state density (N_{ss}), field dependent properties of the build-up of trapped charge in the oxide (Q_{ox}) and surface-state density N_{ss} at the Si-SiO_2 interface can be approximated by maximum geminate recombination mechanisms defined by Metal-Oxide-Semiconductors (MOS) studies. This distribution can be added to the field-independent build-up of these parameters to form a reasonable estimate.

According to theory, a lower doped base region in a n-p-n transistor requires less positive surface potential to force the surface to crossover. Since the base doping concentration parameter can be approximated by the emitter-base breakdown voltage (BV_{ebo}), a screen on BV_{ebo} appears to be an excellent way to control this parameter for ionizing radiation effects (assuming all other parameters are also controlled). The other important parameters can easily be controlled in the processing stage of fabrication. The emitter periphery, ratio of emitter area to periphery, and base surface area are mask design features and therefore controllable in selected military process lines. Thus, based on the parameters defined by the model as being important in predicting the long-term ionization effects on bipolar devices, hardness assurance techniques appear to be possible.

SECTION 2

2.0 THEORETICAL MODEL AND IONIZING RADIATION EFFECTS

This section is divided into two main parts. In Section 2.1 the pre-irradiation theoretical model is introduced and evaluated against gated bipolar transistor data. In Section 2.2 the effects of ionizing radiation on the model are examined and compared to existing experimental data.

2.1 Introduction to Theoretical Model

A detailed and systematic investigation of the surface effects on the base current of n-p-n transistors is presented in this section. The theory of surface space-charge regions based on Metal-Oxide-Semiconductor (MOS) structure theories is extended to the bipolar structure. The following assumptions are applied in the analysis. 1) Carrier recombination is not limited by the flow of carriers to the surface, 2) low-level injection is the only case considered near the surface, 3) surface recombination proceeds through a discrete energy level in the band gap and obeys Shockley-Read-Hall statistics, and 4) for comparison to gated devices, the electron density underneath the field-plate is uniform (in its effect on the surface potential and the surface electron concentration).

A transistor reciprocal gain model is usually used to illustrate the contributions to base current from various regions of the structure.

Surface contributions will be assumed to be an additive change in the reciprocal gain. These additional contributions are primarily recombination-generation currents associated with depleted semiconductor regions. Each is examined and compared to experimental non-irradiation n-p-n gated transistor data in this section.

2.1.1 Theoretical Model Description

To relate long-term ionization damage to its effects on bipolar transistor DC gain, the relationship of gain to basic physical parameters must first be determined. A physical parameter model for gain of an n-p-n bipolar transistor can be defined which segregates the transistor into five basic current components. The term gain, (h_{FE}), refers to the forward common-emitter transistor gain with a reverse-biased collector junction.

The five major contributions to the base current (shown in Figure 2.1) are:

a) electron recombination in the base region, I_{RB},

b) hole recombination/transport in the emitter region, I_D',

c) recombination-generation in emitter-base depletion layer, I_{RG},

d) collector-base junction leakage, I_{CBO}, and

e) surface recombination, I_S.

These components form an expression for reciprocal gain defined as:

$$\frac{1}{h_{FE}} = \frac{I_B}{I_C} = \frac{I_{RB}}{I_C} + \frac{I_D'}{I_C} + \frac{I_{RG}}{I_C} - \frac{I_{CBO}}{I_C} + \frac{I_S}{I_C}$$

Figure 2.1 describes the location of each contribution. The form of each contribution in physical terms was obtained mainly from understanding provided by Phillips[1] and Larin.[2]

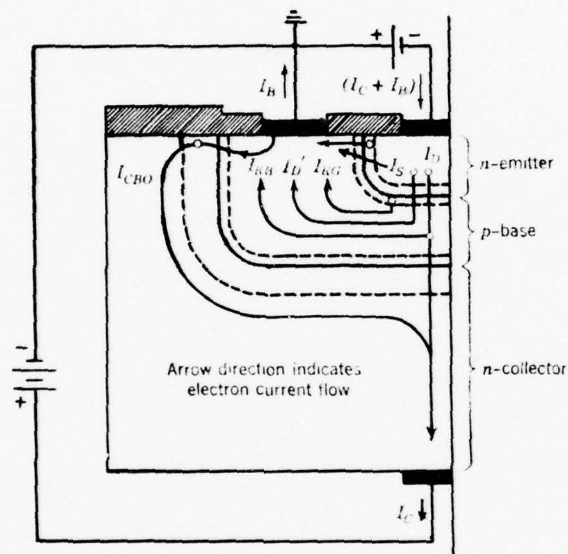

Figure 2.1. A schematic representation of the five base current components.[2]

The I_{RB}/I_C contribution defines the effect on the gain from the reduced number of minority carriers reaching the collector from the emitter through recombinations in the base region. Since a recombination requires an electron and hole, the base contact must supply additional majority carriers to preserve space-charge neutrality in the base. Therefore, the base current increases, reducing the gain. This term is directly dependent on the base width squared and inversely dependent on the minority carrier lifetime and diffusion constant in the base region. Narrow base width, long lifetimes and large diffusion constants minimize this term.

The contribution I_D'/I_C is related to hole recombination and transport in the emitter region. As the reverse diffusion current (I_D') increases, the base contact must supply additional majority carriers to the base to maintain space-charge neutrality. The result is an increase in base current and a decrease in gain. For maximum efficiency (i.e., minimum I_D'/I_C), the reverse diffusion current should be as small as possible. This implies that the base sheet resistivity should be as large as possible with respect to the emitter sheet resistivity (i.e., the emitter is much more highly doped than the base). Other design problems limit the extent that this principal can be fully implemented (i.e., base pushout).

The recombination-generation of electrons and holes in the emitter-base depletion layer is accounted for by the I_{RG}/I_C contribution. In a junction at thermal equilibrium the net recombination rate equals the net generation rate. When a forward bias is applied, the carrier concentration rises. The recombination rate must increase, requiring that the base contact supply more majority carriers (current). To minimize this term requires a high relative base and emitter doping. The largest relative contribution from this term occurs at low-injection (i.e., more than an order of magnitude below the collector current at which h_{FE} is at its peak value).

The contribution I_{CBO}/I_C results from the additional majority carriers introduced into the base from the collector. The mechanisms for this term are similar to that for the emitter-base junction. For the collector-base junction under normal DC gain operation, the junction is reverse-biased. Carriers generated in the depletion layer are swept out and the holes become majority carriers in the base region. This effect is only significant at very low collector currents. The problem at low currents is that I_{CBO} is an erratic contribution and can turn on the transistor forcing the minimum operating point to a higher base current to maintain control of the gain. The contribution to I_S from I_{CBO} near the surface will be discussed later in the report in a qualitative fashion.

These contributions (I_D', I_{RG}, etc.) actually are present for the projected emitter area and the sidewall area. In a diffused structure the base doping concentration, N_B, increases with distance up from the bottom of the emitter well. Thus the injected emitter electron current density decreases versus distance toward the surface of a standard diffused n-p-n transistor. Also, the sidewall area is usually more than an order of magnitude less than the emitter well projected area, hence the base currents associated with this region for the pre-irradiation case are generally on the order of a few percent and neglected. The hole current density into the emitter (I_D') does not necessarily have this same characteristic. Because of the way diffused bipolar structures are made, lateral doping gradients in the emitter can also be assumed (under the emitter oxide window edge). Thus the emitter doping at the E-B junction near the surface is usually less than the doping level under the emitter contact. This means that the hole current density near the surface can be larger than expected. For the post-irradiation case, we will see that the dependency on emitter doping near the surface for the reverse diffusion term along with its dependency on an effective surface emitter minority carrier lifetime may change these assumptions (especially for p-n-p transistors).

Simplified equations for the first four terms are presented in Appendix C.[1-3] It should be pointed out that these terms, I_{RB}/I_C, I_D'/I_C, I_{RG}/I_C and I_{CBO}/I_C are generally assumed to be independent of ionizing radiation. This is not generally true.†

Shown in Figure 2.2 are the "bulk" terms for the 2N2222 (Motorola) transistor versus collector current. The current components at medium collector currents are comparable with experimental data.[4] Aside from the

† The collector-base junction leakage current, I_{CBO}, can have substantial changes due to ionizing radiation, and under the proper conditions so can I_{RB}, I_D', and I_C for a given V_{BE}.

surface contribution (not shown) it can be seen that the major contributions to the base current at low collector currents are from I_{RG} and I_{CBO}.

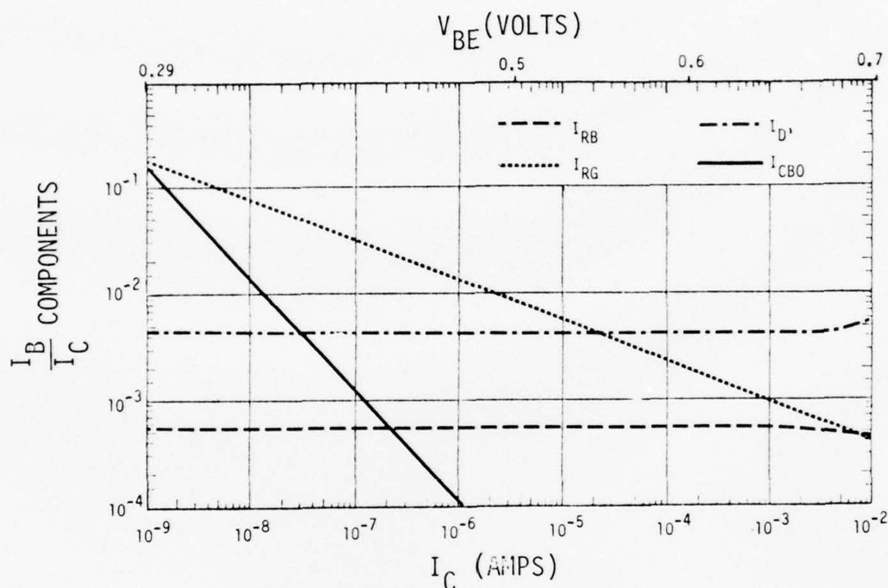

Figure 2.2 Base current components over collector current vs. emitter-base forward bias and collector current for the 2N2222 transistor model. (Motorola)

The surface related contribution, I_S/I_C, is an effect on the gain from depletion layer recombination and generation of holes and electrons at the surface. Since the dependence on V_{BE} is experimentally determined to be approximately proportional to $e^{(V_{BE}/2)}$, the major relative significance of this contribution occurs at low injection levels. As will be seen in Section 2.2, long-term ionization effects are reflected at the surface in the change in surface potential and surface state density.

The understanding of the recombination-generation process is inseparable from the understanding of surface effects. The theory of the recombination-generation process in bulk material was proposed by Shockley and Read[5] and independently by Hall.[6] It is based on a recombination rate, U, that is dependent on the product of the carrier concentrations (specifically $n \cdot p = n_i^2$) and on the distribution of the recombination centers.

According to the theory of silicon material, certain allowed energy states exist in the region of the forbidden-energy band. These states are called recombination-generation centers and are attributed to impurities or structural defects in the crystal lattice. The centers act to capture either a free electron from the conduction band or an electron from the valence band, leaving a hole behind (generation). Likewise, the filled center may be emptied by capturing a hole or releasing its electron back to the conduction band. Recombination occurs when the center captures a free electron and holds it until emptied by capturing a hole. Thus, the recombination center may be considered as a "stepping stone" in the gap between the bands.

The single-level recombination consists of four steps: namely, electron capture, electron emission, hole capture, and hole emission. The Shockley-Read-Hall (SRH) theory is based on probability considerations employing Fermi-Dirac statistics. The probability of a carrier recombining at a recombination center is dependent on several factors, viz., (1) the concentration of recombination centers in the silicon, (2) the concentration of the free carriers, (3) the capture probability of the centers, and (4) the concentration of centers that are normally filled under equilibrium conditions. The last factor is dependent on the position of the centers in the band gap with respect to the Fermi level, since this would determine the degree of occupancy of the centers.

At thermal equilibrium where $n \cdot p = n_i^2$ there is no net recombination current. When voltage is applied to the junction, the minority carrier

densities on both sides of the junction are changed, and $n \cdot p$ is no longer equal to n_i^2. Under reverse-bias, $n \cdot p < n_i^2$, the dominant R-G processes are those of emission. Thus under the reverse-biased condition, a generation current exists.

Under a forward bias, $n \cdot p > n_i^2$. The major R-G processes are those of capture. Thus a recombination current exists.

Figure 2.3 (a) illustrates the carrier concentration, electric field, and the recombination rate, U, for a forward-biased symmetric junction in bulk silicon when two different doped silicon materials form a junction. Since the recombination process requires both a hole and an electron for completion, the maximum rate occurs when n = p. Mathematically, this is seen from the simplified recombination rate (U) equation from the SRH theory which has the form:

$$U = \sigma v_{th} N_t \frac{p \cdot n - n_i^2}{n + p + 2n_i \cosh\left(\frac{E_t - E_i}{kT}\right)}$$

where σ = capture cross section,

v_{th} = carrier thermal velocity,

N_t = trap density,

E_t = trap energy level,

E_i = intrinsic Fermi level,

and n_i = intrinsic carrier concentration.

For non-equilibrium ($p \cdot n > n_i^2$), a net recombination rate produces a base current. The "driving force" for this net recombination is defined by the nunerator which is the deviation from the equilibrium condition. The increase in U depends upon increases in "n" and "p". Thus U is maximum when the sum (n + p) is at its minimum value. This occurs when n = p.

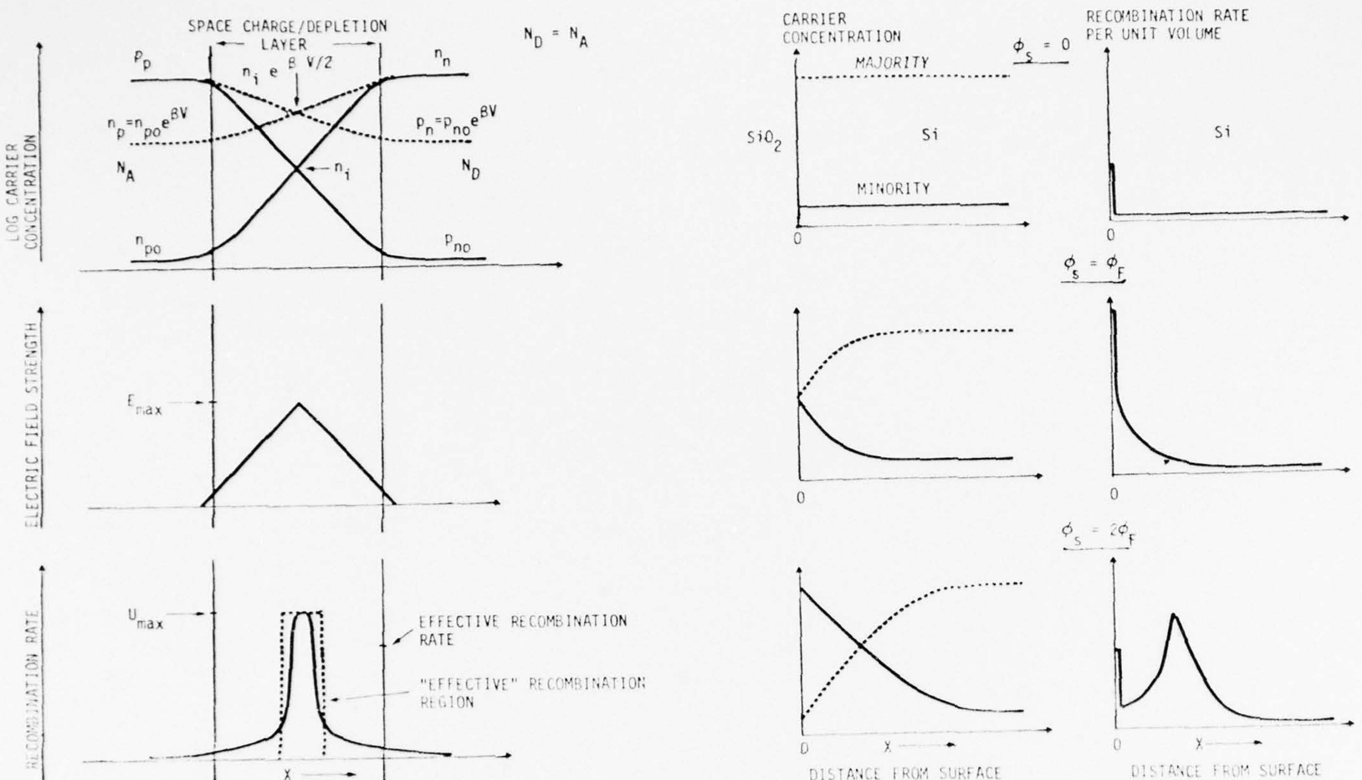

Figure 2.3 (a). Carrier concentration, electric field strength, and recombination rate in an idealized junction. Crossover is where n = p.

Figure 2.3 (b). The effect of the n and p carrier concentrations on the recombination rate near and at the surface of the base region.

In a space-charge region or depletion layer, both n and p carrier concentrations vary exponentially across the junction and consequently the recombination rate falls off quickly on either side of where n = p. The point where n = p is referred to as "crossover". The concept of crossover is crucial in the understanding of surface effects.

Figure 2.3 (b) illustrates the carrier concentration, and its effect on the recombination rate at the base surface for several surface potentials (ϕ_S). The surface states act as additional recombination centers when crossover occurs at the surface as indicated in Figure 2.3 (b) when the surface potential equals the Fermi potential of the underlying doped silicon material (ϕ_F); $\phi_S = \phi_F$. When crossover occurs below the surface (i.e., $\phi_S = 2\ _F$), the bulk centers determine the recombination rate.

The surface contribution to the base current is generally accepted to be comprised of two major current components;[7,8] one a current associated with a surface space-charge region (SSCR) or field-induced depletion layer, I_{FIDL}, and another consisting of the current associated with crossover (n = p) intersecting the surface, I_{SO}. These regions are illustrated in Figure 2.4.

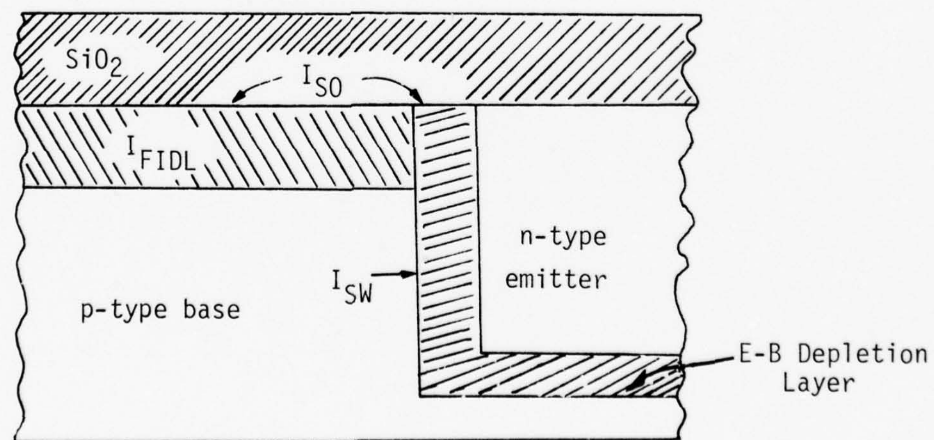

Figure 2.4. Surface components associated with a p-n junction. I_{SW} = Sidewall current.

A surface-space-charge region (SSCR) modifies the E-B space-charge region and leads to changes in the total junction currents.† The SSCR is formed by a buildup of charge in the oxide, usually within several hundred Angstroms of the surface,[9] that creates an electric field at the silicon-silicon dioxide ($Si-SiO_2$) interface. In essence, the charges in the oxide "push" charges in the silicon away from the surface. In band theory this is referred to as band bending. Illustrated in Figure 2.5(a) is a band diagram indicating the case of no charge in the oxide (this is referred to as "flat band"). In Figure 2.5(b) the effect of induced charge in the oxide is shown by the bending of the energy bands. E_C and E_V are the lower edge of the conduction band and the upper edge of the valence band in energy space, respectively. The energy difference between these two bands is the gap energy, which for silicon is approximately 1.1 volts. E_i is the intrinsic energy level which generally lies very close to the middle of the band gap.[10] The Fermi level (or energy), E_F, is dopant dependent. For p-type silicon, it lies below the intrinsic energy level and approaches the valence band energy for greater doping concentrations. For n-type, E_F is above E_i and lies close to E_C for heavily doped n-regions. The surface potential, ϕ_s, is the "amount" that the bands are bent. In this case a positive charge in the oxide will cause the bands to bend toward the Fermi level. This means that the p-region is less p-type. The effect of the surface potential diminishes as distance increases from the interface to the semiconductor. Thus, far from the surface, the p-type material is unchanged. A depletion or space-charge region can therefore be defined near the surface, and additional bulk recombination-generation processes result from surface effects. This added current is defined as I_{FIDL}. If the bands are bent such that the intrinsic energy level coincides with the Fermi energy, then the cross-over condition exists ($n_s = p_s$) at the surface. At this point, both n and p carriers are acting to make surface traps (recombination centers or surface states) most effective. The recombination current thus is maximized. The

---

† From another point of view, the superposition of the FIDL effect on the E-B metallurgical junction space-charge region could be interpreted as an increase of the emitter sidewall area extending into the base.

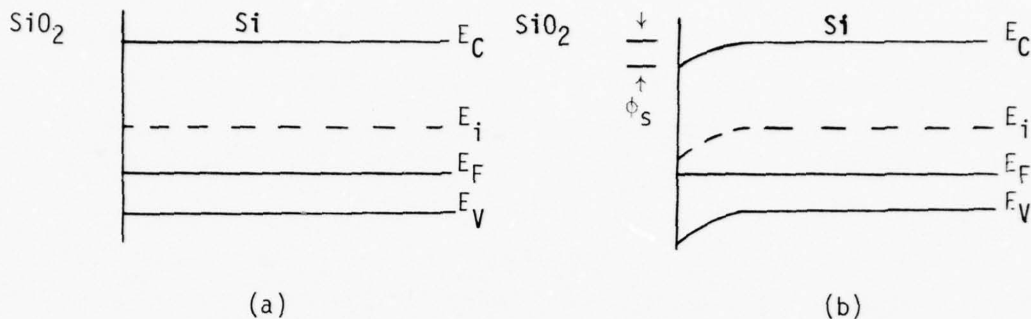

Figure 2.5. Band representation of a p-type silicon intersection with the surface.

effects of recombinations at the surface are incorporated in the current term defined as I_{SO}.

Further increase in the surface potential, pushes the crossover point into the bulk base material. The surface region is now more n-type than p-type and the recombination rate diminishes. Strong inversion occurs when the surface potential completes the SSCL. It occurs at a surface potential of approximately:[11,12]

$$\phi_s(\text{inv}) = (V_a + 2\phi_F) \text{ Volts}$$

where V_a is the applied junction bias, V_{BE}. The surface potential required for strong inversion is dependent on the junction bias and is larger for a reverse-biased junction.†

2.1.1.1 Field-Induced Depletion Layer Term (I_{FIDL}). At the surface potential ϕ_s(inv), the field-induced depletion layer has reached a maximum thickness. This thickness is given by[12,13]

$$x_{d_{max}} = \sqrt{\frac{2 K_S \varepsilon_o \phi_s(\text{inv})}{q N_A}} \quad \text{cm},$$

† This means that the I_{SO} and I_{FIDL} components of the surface current will peak or contribute significantly at lower surface potentials for increasing V_{BE}. This is experimentally found to be true in the data presented by Reddi.

In an extreme case (higher surface potentials), a conducting channel may form between the emitter and the base contact. Once the field-induced depletion layer has been formed, it should behave like a new p-n junction over the base region, only its origin is different from that of the metallurgical E-B junction; the E-B junction was brought about by a metallurgical process.

The above assumes that a full depletion layer exists in the bulk material just below the entire surface. This full depletion layer exists because the surface has been inverted. Crossover exists, somewhere in this depletion layer allowing us to define an effective volume for an additional bulk recombination-generation mechanism.

"Emitter" diffusion currents related to the field-induced depletion layer at a given V_{BE} are determined in the same manner as under the projected emitter-well (i.e., by the net doping and width of the base and the minority carrier lifetime.† These parameters influence the currents in the same way as they do under the emitter well. The density of these field-induced diffusion currents are generally significantly smaller than those generated under the emitter well; especially in high gain double diffused transistors with very narrow base widths. We will call these terms I_{RBDL} and I'_{DDL} where DL denotes the depletion layer and the remaining subscripts designate the current components as they did in Figure 2.1.

The total increase in emitter and base currents (I_E and I_B) due to surface inversion depend also on the area of inversion. As we shall see later, if a substantial part of the emitter current is borne by the field-induced space-charge layer then the emitter current density under the emitter well is reduced, thus, easing emitter crowding.

---

† The base here means the distance from the bottom of the field-induced junction to the collector-base junction, assuming that the width is still small compared to the diffusion lengths.

2.1.1.2 Surface Recombination Velocity Term I_{SO}. When the depletion layer is only partially formed such that the crossover region intersects the surface, there is an additional current associated with the recombination between the carriers aided by the interface states. This base current is defined as the I_{SO} contribution to the base current. It is this term that contains the often referred to "surface recombination velocity".[14,15] Surface states can be considered as imperfections within the Si-SiO_2 interface crystal lattice having energy levels that lie within the forbidden band gap (i.e., surface states are additional recombination centers resulting from surface properties). The surface recombination current associated with the surface states may be expressed for each trap energy site as[15†]

$$I_{SO} = \frac{\frac{1}{2} A_s \, q \, n_i \, N_{ss} \, (C_n C_p)^{\frac{1}{2}} \left[e^{\beta V_{BE}} - 1 \right]}{\cosh \beta(\phi_s - \phi_t - \phi_o) + e^{\beta V_{BE}/2} \cosh \beta(\phi_s - \phi_F - \phi_o + V_{BE}/2)} \text{ Amps}$$

where n_i = intrinsic carrier concentration ($\#/cm^3$),

N_{ss} = effective surface state (recombination center or trap) density ($\#/cm^2$),

$C_n = v_{th} \sigma_n$ (cm^3/sec),

$C_p = v_{th} \sigma_p$ (cm^3/sec),

σ_n = electron cross-section (cm^2),

σ_p = hole cross-section (cm^2),

v_{th} = thermal limiting velocity (1×10^7 cm/sec),

$\beta = q/kT = (0.026 \text{ Volts})^{-1}$,

ϕ_s = surface potential (Volts),

ϕ_t = trap (recombination) potential (Volts),

† A brief development can be found in Appendix B.

and ϕ_o = energy equivalent to the ratio of capture possibilities, (Volts).[†]

For a given V_{BE}, I_{SO} has a maximum value with respect to variations in ϕ_s of

$$I_{SO(MAX)} = \frac{\frac{1}{2} A_s \, q \, n_i \, N_{ss} \, (C_n \, C_p)^{\frac{1}{2}} \left[e^{\beta V_{BE}} - 1 \right]}{\cosh \beta(\phi_s - \phi_t) + e^{\beta V_{BE}/2}} \quad \text{Amps}$$

This occurs at a specific surface potential, ϕ_s, given by[††]

$$\phi_s = \left(\phi_F - \frac{V_{BE}}{2} \right) \text{ Volts.}$$

Thus, the maximum I_{SO} current occurs at a surface potential equal to one-half the surface potential for strong inversion ($\phi_s(\text{inv}) = 2\phi_F - V_{BE}$), and is indicative of the crossover ($p_s = n_s$) point. This term must be integrated over all trap energies (ϕ_t) to obtain the total I_{SO} current. The surface recombination term (I_{SO}) decreases rapidly as the surface potential increases beyond crossover in the same way as recombination currents are described for the E-B junction.

Two contributions to the I_{SO} term can actually be defined. One is related to a region that forms a crossover at higher ϕ_s, and the other is related to crossover existing from zero ϕ_s.[†††] The contribution to I_{SO} when ϕ_s=0 is where the E-B junction intersects the surface. Crossover in the E-B junction also terminates at the surface. Thus, for a small surface region, I_{SO} will be at a maximum even for zero surface potential. An increase in surface states will therefore produce a significant effect even at low build-up

---

† $\left(\phi_o \equiv \frac{\ln C_p/C_n}{2\beta} \right)$ In Appendix B before the cross-section ratio is taken into the hyperbolic cosine argument it is easily seen that as C_p/C_n deviates from 1 (equal capture probability) the surface current diminishes.

†† Note: we assumed that the capture cross-sections for holes and electrons were the same; i.e., $\phi_o \approx 0$.

††† These two parts of I_{SO} are actually extensions of each other since higher ϕ_s lowers the dopant on the base side of the E-B junction. This makes the E-B junction crossover "walk out" into the base region.

of trapped oxide charge. In a gated structure where a portion of the surface is inverted, this "zero ϕ_s" component reappears where the crossover point intersects the surface beyond the extension of the field plate and is influenced by fringing fields of the gate. This term is often overlooked and is responsible for an increase in I_B, that is not related to I_{FIDL}, when the base is strongly inverted.

2.1.2 Pre-Radiation Gated Transistor Data Comparison to Model Predictions

A gated n-p-n transistor serves as a useful tool to test the theoretical surface model. For this structure, we can assume that depletion (and subsequently, inversion) in the base surface region occurs uniformly over a well defined surface area.† We can also assume that this depletion layer is sufficiently far removed from the metal contacts so that their influences on the profile of the depletion layer do not have to be considered. Generally, it is assumed that the presence of the gate does not interact with the surface states, N_{ss}, or the charge, Q_{ox}, built into the oxide.††

A gated n-p-n transistor reported on by Reddi[15] is shown below in Figure 2.6. The physical parameters defined, or inferred from his discussion, are shown in Table 2.1.

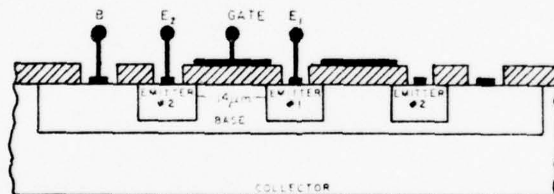

Figure 2.6. Cross-sectional views of experimental surface controlled transistors (circular symmetry).[15] Emitter structure: diffused emitter (both combined) area = 1.2×10^{-3} cm^2; gate area over the base = 1.0×10^{-4} cm^2; emitter periphery underneath the gate = 0.135 cm.

† Charge build-up in the oxide due to processing or exposure to ionizing radiation can occur over the Si-SiO_2 interface in some fashion other than uniform, but we will not consider these in this section.

†† These assumptions are to some degree invalid for radiation, but can be assumed valid for the pre-irradiation case.

Table 2.1. Physical parameters used for Reddi's transistor in Figure 2.5.

PHYSICAL PARAMETER	VALUE	PHYSICAL PARAMETER	VALUE
A_e	1.2×10^{-3} cm^2	$\sigma_n = \sigma_p$	1×10^{-15} cm^2
A_g (base region)	1.0×10^{-4} cm^2	v_{th}	1×10^7 cm/sec
N_{BS}	1.0×10^{18} atoms/cm^3	N_{ss}	1×10^{10} states/cm^2
N_{ES}	1.0×10^{20} atoms/cm^3 **	χ_{es} @ $V_{BE} = 0.1$ V	3.5×10^{-6} cm *
N_B	9×10^{16} atoms/cm^3 **	χ_e @ $V_{BE} = 0.1$ V	1×10^{-5} cm *
N_E	3×10^{18} atoms/cm^3 **	$\chi_{d_{max}}$ @ $V_{BE} = 0.1$ V	3.6×10^{-6} cm*
P_{eg} (under gate)	1.35×10^{-1} cm	D_n (base)	13.8 cm^2/sec*
P_e (not under gate)	2.1×10^{-1} cm	D_p (emitter)	1.95 cm^2/sec *
W_b	1×10^{-4} cm	ψ_{os}	1.06 eV *
W_{sc}	6×10^{-4} cm	ψ_o	0.9 eV *
τ_b	1×10^{-7} sec **	R_i	1.5×10^5 sec^{-1} **
τ_e	1×10^{-8} sec **	ϕ_{F_s}	0.468 eV*
d_{ox} (base)	2000 Å		

* Inferred/Calculated

** Assumed from similar information

Presented in Figure 2.7 are the resulting base currents obtained by varying the gate voltage for the transistor of Figure 2.6.

Several conclusions can be drawn from this data.

a) I_B is relatively independent of gate voltage for gate voltages ranging from $\approx$ -20 to +10 volts. The transistor characteristics in this regime are primarily related to "bulk" effects (i.e., I_{RG}, I_{RB} and I_D').

b) To the right of this flat region, the base current increases when considerable depletion has taken place and peaks when crossover occurs over the entire base surface region. As the surface is further "depleted" I_B diminishes.

c) At higher V_{BE} (higher collector currents) the importance of these surface contributions is reduced, relative to the "bulk" contributions.

d) the increase in I_B above the "bulk" contributions for high gate voltages to the right of the peak, is due to recombination currents associated with the field-induced depletion layer at strong inversion.

e) The usual interpretation for the increase in I_B with negative gate voltage for n-p-n transistors is due to accumulation effects near the base surface and depletion effects near the emitter surface.

2.1.2.1 "Bulk" Base Current Terms. We saw in Figure 2.7 that the region to the left of the peak I_B value (for n-p-n transistors) was fairly insensitive to gate voltage until large negative voltages are applied. The logical conclusion would be that this current includes all non-surface related contributions and thus includes all "bulk" related base current terms. These include I_{RG}, I_{RB}, I_D', and I_{CBO}. (I_{CBO} can be assumed zero for this data since the base was tied to the collector). The I_{RG} contribution at low collector currents (below 1.0 mAmp as seen in Figure 2.2) is the predominant term due to the dependence on V_{BE}.

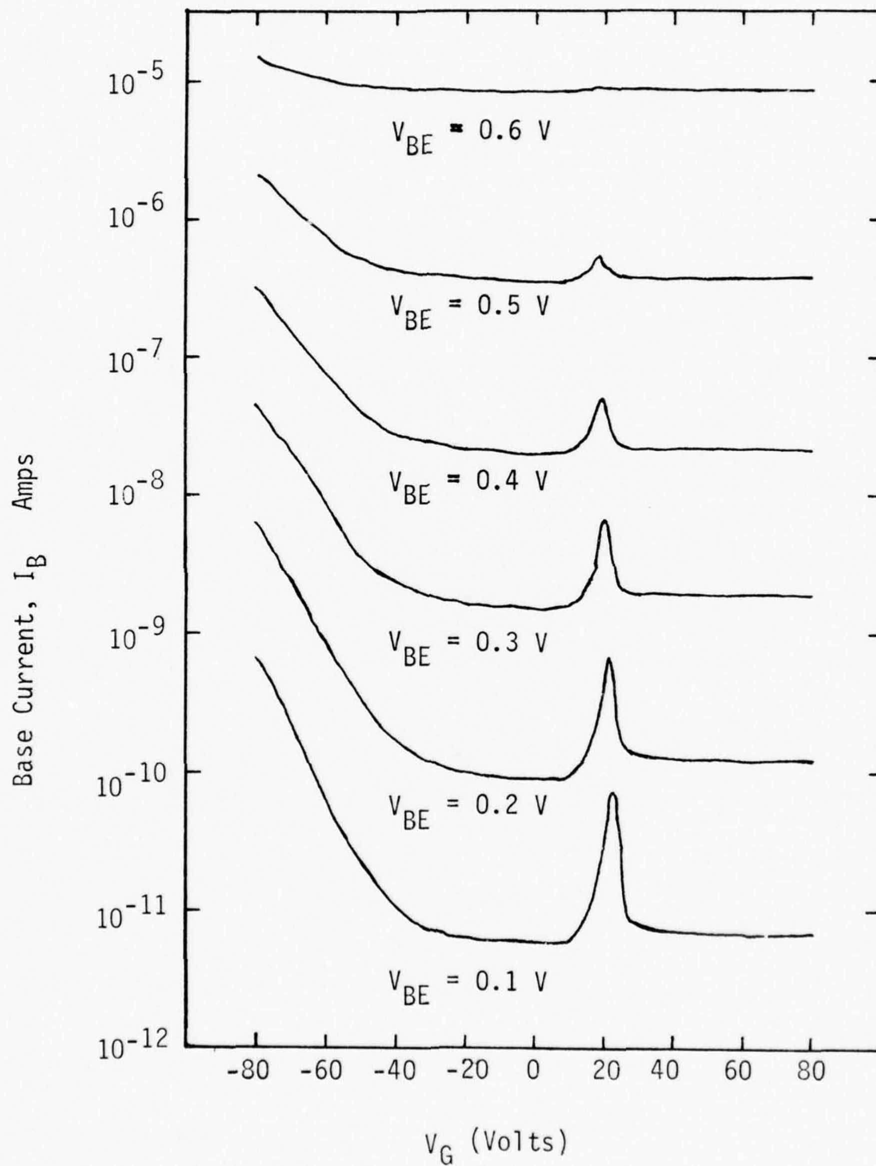

Figure 2.7. Base current vs. gate voltage[15] for the transistor shown in Figure 2.6.

Using Table 2.1 and Appendix C at low I_C conditions, we can evaluate the effect of each "bulk" term. This value will establish a lower limit to which all surface related terms must be added.

For $V_{BE} = 100$ mV:

(a)

$$I_{RG} = I_{RG_e} + I_{RG_{sw}} =$$

$$= \left(5.1 \times 10^{-12} + 4 \times 10^{-13}\right)\text{Amps}$$

$$= 5.5 \times 10^{-12} \text{ Amps},$$

where I_{RG_e} = recombinations in the E-B junction for the projected emitter area,

$I_{RG_{sw}}$ = recombinations in the E-B junction for the emitter sidewall area up to the surface (using averages for parameters)†

and

$$I_{RG} = \frac{q\pi A X_e R_i n_i}{\ln\left(\frac{N_E N_B}{n_i^2}\right)} e^{qV_{BE}\, 1.5/kT} \text{ Amps;}$$

(b)

$$I_{RB} = I_{RB_e} + I_{RB_{sw}}$$

$$I_{RB} = \left(1.1 \times 10^{-14} + 4.8 \times 10^{-16}\right)\text{Amps},$$

where

$$I_{RB} = \frac{qA\, W_b\, n_i^2}{2\tau_n\, N_B} e^{qV_{BE}/kT} \text{ Amps; and}$$

(c)

$$I_D = I_{D_e}' + I_{D_{sw}}'$$

† The parameters used to obtain the sidewall values for I_{RB} and I_D' were estimated from averages between the projected emitter values and those at the surface on Reddi's device. ($\overline{N}_{E_{sw}} \approx 3\text{x}10^{19}$ atoms/cm^3, $\overline{X}_{e_{sw}} = 6\text{x}10^{-6}$cm, $\overline{A}_{e_{sw}} = 1.7\text{x}10^{-4}$cm^2, $\overline{N}_{B_{sw}} = 3 \text{ x } 10^{17}$ atoms/cm^3, $\overline{R}_{i_{sw}} = 1.5\text{x}10^5$ sec^{-1}, $\overline{D}_{p_{sw}} \approx 1.6$cm^2/sec).

$$I_D' = (9.4 \times 10^{-15} + 1.2 \times 10^{-16}) \text{ Amps},$$

$$\text{where } I_D' = \frac{qA D_p n_i^2}{(D_p \tau_p)^{\frac{1}{2}} N_E} e^{qV_{BE}/kT} \text{ Amps.}$$

The theoretical "bulk" base current contribution for Reddi's transistor is therefore 5.5×10^{-12} Amps. The measured lower limit base current from Figure 2.7 was 5.9×10^{-12} Amps. The measured value contains mostly "bulk" contributions but some surface contributions may be present from the E-B metallurgical junction intersecting the surface.

From the above analysis, we see that the sidewall region (for Reddi's device) does not make a significant pre-irradiation contribution except for the R-G term (which contributes approximately 10%). Applying a negative gate voltage over the emitter-base surface region increases the effective base doping while decreasing the effective emitter doping. Thus the $I_{D_{sw}}'$ term becomes more significant especially in view of the lifetime decrease near the surface caused by changes in the lattice and impurity concentration from processing steps. Also the effects on the lifetime at the surface by process induced surface states will influence the importance of this term. These factors have not been used in the calculation of $I_{D_{sw}}'$. This increase in $I_{D_{sw}}'$ for large negative gate voltages is a candidate for influencing the shape of the left part of Figure 2.7. This part of the curve is usually referred to as accumulation. Other influences commonly associated with this region are increases in the RG sidewall term, increases in surface area for the E-B junction intersection with the surface, and tunneling currents. All but the I_D' and tunneling current contributions are related to R-G mechanisms which could not explain the sudden increase in I_B for high negative gate voltages (at lower V_{BE}). The $I_{D_{sw}}'$ contribution appears to have the necessary dependencies to explain the increases for both pre- and post-irradiations and for both n-p-n and p-n-p transistors.

This will be seen later when the post-irradiation condition is applied to the gated transistor and when p-n-p transistors are considered. It should be observed that at low V_{BE} in Figure 2.7 that R-G terms dominate over the diffusion terms under normal operating conditions ($V_G = 0$). At higher V_{BE}'s, the diffusion terms dominate the R-G terms. More work needs to be done to verify the contributions from accumulation. We will not pursue accumulation further in this section but a general discussion is included in Section 2.3 for p-n-p transistors where these mechanisms are important in describing the radiation response.

2.1.2.2 I_{SO} Term. The term describing the crossover intersecting the surface is I_{SO}. Two "separate" regions can be considered which satisfy this criteria (even though the second region can be thought of as an extension of the first). Region one (1) is where the metallurgical E-B junction intersects the surface. Crossover intersects the surface for zero gate voltage. Region two (2) is when ϕ_s (from gate voltage or oxide charge) has forced the base surface region to crossover. The general I_{SO} term† is described as

$$I_{SO} = \frac{\frac{1}{2}\, q\, n_i\, A\, N_{ss}\, \sigma\, v_{th} \left[e^{\beta V_{BE}} - 1\right]}{\cosh \beta(\phi_s - \phi_t) + e^{\beta V_{BE}/2} \cosh \beta\left(\phi_s - \phi_F + \frac{V_{BE}}{2}\right)} \text{ Amps}$$

$$\approx \frac{\frac{1}{2}\, q\, n_i\, A\, \frac{\pi kT}{q}\, D_{ss}\, \sigma\, v_{th} \left[e^{\beta V_{BE}} - 1\right]}{e^{\beta V_{BE}/2} \cosh \beta\left(\phi_s - \phi_F + \frac{V_{BE}}{2}\right)} \text{ Amps}$$

where $A \equiv$ the surface area at potential ϕ_s (cm^2)

ϕ_t = energy of the surface state in the silicon band gap (eV)

D_{ss} = density of surface states ($\#/cm^2$- eV)

σ = the capture cross-section (cm^2).

† Appendix A discusses the derivation of this term.

The hole and electron capture cross-sections were assumed equal and constant for all surface potentials since little information exists on this subject. Thus, $\phi_o = 0$ and $\sigma = (\sigma_p \cdot \sigma_n)^{\frac{1}{2}} = \sigma_n$. Also, as a first approximation, the energy density of surface states over the silicon band gap was assumed uniform.

For region (1) the surface area, where crossover interacts with the surface states, can be assumed to be the width of the depletion layer (χ_{es}) times the emitter periphery (P_e). Region (1) has a maximum I_{SO} contribution even at zero gate bias. Thus $I_{SO_{max}}$ for Region (1) must be added to the "bulk" contributions that formed the lower limit.† At $V_{BE} = 100$ mV;

$$I_{SO_{max}} \text{ (Region 1)} = 9.9 \times 10^{-13} \text{ Amps.}$$

In region (2), the surface area under the gate in the base region ($A = A_G$) is used. To obtain the peak base current theoretical value from this region, the gate voltage was increased to force a crossover at the *base surface region under the gate.*

$$I_{SO_{max}} \text{ (Region 2)} \approx 9.3 \times 10^{-11} \text{ Amps}$$

At the peak I_B, region (2) can be thought of as the region (1) crossover bent over and lying over the entire base surface under the gate. Therefore, in the region (2) I_{SO} calculation, region (1) I_{SO} does not exist.

The measured value of $I_{SO_{max}}$ (region (2)) was 7×10^{-11} Amps. This correlates very well with the predicted $I_{SO_{max}}$ in region (2).

---

† Assume D_{SS} is uniform over all regions of the transistor due to process induced factors.

Further calculations (for other V_{BE}'s) yield the results shown in Figure 2.8. In general the results are in excellent agreement with experimental data.

Both theory and experimental data show a decrease in gate voltage necessary to identify the maximum I_{SO} contribution from region (2) for higher V_{BE}. This is sometimes referred to as a shift in the peak to the left on the gate voltage (or surface potential) scale. The reason the theoretical curve shifts to the left vs. V_{BE} is because of the injection of minority carriers (n_s) into the base surface region. For higher V_{BE}, n_s approaches p_s without any additional gate voltage. Thus, less surface potential is required to generate the $n_s = p_s$ crossover condition.

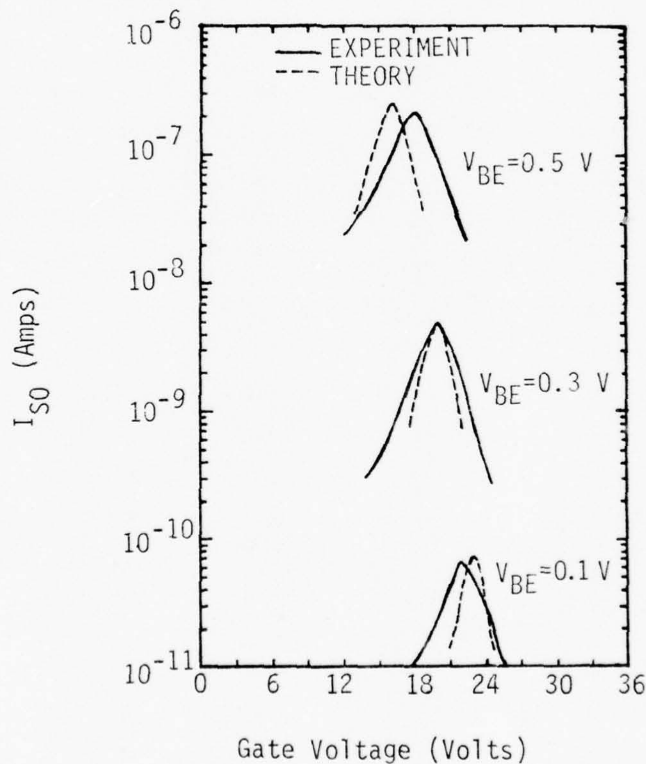

Figure 2.8. Comparison of the theoretical to experimental I_{SO} term.[15] The experimental points result from Figure 2.7. Theory was normalized to agree with experiment at V_{BE} = 0.3 V.

The theoretical I_{SO} curve shifts to the left with increasing V_{BE} faster than the experimental curve as shown in Figure 2.9. The I_{SO} term defined by Reddi calculates the base current associated with a region where ϕ_s, n and p are nearly constant. The assumption that n_s does not vary significantly as a function of distance from the edge of the E-B depletion layer is invalid for higher V_{BE}'s. The minority carrier concentration away from the E-B junction in the base is actually less than at the E-B edge due to the surface diffusion length. Thus, a larger gate potential is required than theory would predict to reach the peak base current.

This distribution of minority carriers would also account for the broadening of the peak for higher V_{BE}.

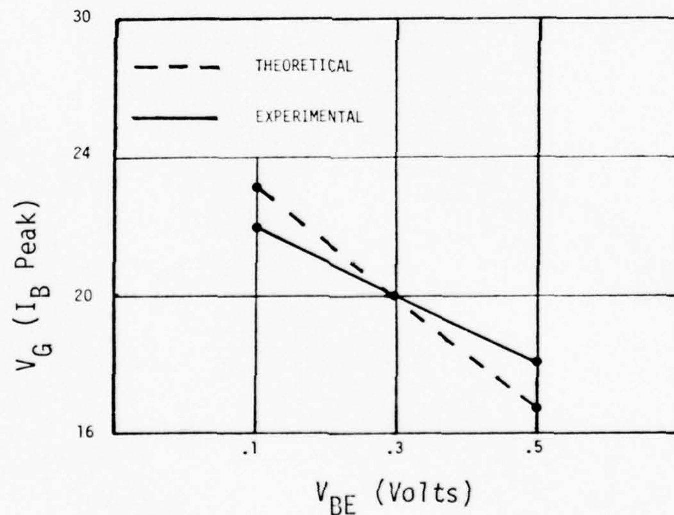

Figure 2.9. Comparison of experimental and theoretical gate voltage shift vs. V_{BE} for peak I_B. The theoretical curve is normalized to the 0.3 volt V_{BE} as in Figure 2.8.

2.1.2.3 I_{FIDL} Term. When high gate voltages are applied to a gated transistor, the entire region of the surface under the gate is assumed to be forced into strong inversion. For this condition a complete depletion region has been formed. The base current resulting from this region was modeled earlier as I_{FIDL}.

The maximum field induced depletion layer recombination-generation current, I_{FIDL}, may be approximated as†

$$I_{FIDL} = \frac{q}{2}\left(\frac{\pi\ kT}{q\ 2\phi_F}\right) \chi_{d(max)}\ A_i\ n_i\ R_i\ e^{\beta V_{BE}/1.5} \quad \text{Amps}$$

where R_i = intrinsic recombination rate.

A_i = the surface area having a surface potential of $\phi_s \geq 2\phi_F$.

Substituting the physical parameters into this relationship produces a value for I_{FIDL} @ V_{BE} = 100 mV of:

$$I_{FIDL} = 7.35 \times 10^{-14} \text{ Amps.}$$

The measured value for the I_{FIDL} term at V_G = 60 V is the difference between I_B at this gate voltage and the lower limit due to "bulk" terms discussed in the last section. (Note: This lower limit is present for all gate voltages.) The measured I_{FIDL} term was 1.4×10^{-12} Amps. The discrepancy can only be related to the definition of the intrinsic recombination rate (R_i) or carrier concentration (n_i)[16] near the surface of the base region. It is reasonable to expect that R_i is somewhat larger near the surface than below the emitter because the base diffusion concentration is higher near

† $\left(\frac{\pi\ kT}{q\ 2\phi_F}\right) \chi_d\ A_i$ is the effective volume in the field induced depletion layer where the $\pi\ kT/q$ portion is a constant of integration assuming a uniform trap energy distribution from E_v to E_c.

the surface.† If we define the value of R_i near the surface to be R_{is}, then from the measured value of I_{FIDL}, $R_{is} \approx 3 \times 10^6$/sec. We will use this value of R_{is} when discussing surface effects on I_B and I_C for Reddi's data.

2.1.2.4 Other Current Terms Related To The FIDL Region. With the surface inverted there exists a field-induced depletion layer that has similar properties as the E-B junction. The emitter current from this extension of the E-B junction can be modeled as;

$$I_{EFIDL} \cong \frac{q A_G D_b \Delta n}{W_{sc}} \text{ Amps}$$

where $\Delta n = \frac{n_i^2}{N_{BS}} e^{\beta V_{BE}}$ carriers/cm^3, and

W_{sc} = the "base width" from the field-induced depletion layer to the collector-base junction.

Since the base doping is greater near the surface of the base region, the emitter current density will be less, and the area is smaller. This additional emitter current for Reddi's transistor can be approximated as:

$$I_{EFIDL} \approx 2 \times 10^{-15} \text{ Amps (for } V_{BE} = 100 \text{ mV).}$$

This calculation shows that some new emitter current may be seen at strong inversion. The increase is small for this device.

The bulk base recombination current related to the FIDL region can be estimated from;

$$I_{RBDL} = \frac{q A_G W_{sc} n_i^2}{\tau_n (N_{BS} + N_B)} e^{\beta V_{BE}} \text{ Amps} = 9.3 \times 10^{-16} \text{ Amps.}$$

† The intrinsic recombination rate at the surface layer may be larger than in the bulk due to processing where: oxides are grown, oxides are stripped off, diffusion runs and drive-ins have perturbed the crystal lattice. There can be many more "intrinsic" imperfections and thus a higher rate than assumed in the bulk (1.5×10^5/sec).

where $\frac{N_{BS} + N_B}{2}$ = average base doping in the bulk base region extending from the edge of the field-induced depletion layer to the C-B junction ($carriers/cm^3$).

The reverse diffusion current I'_{DDL} is about an order of magnitude less than I_{RBDL} for this device and defined for the gated structure as;

$$I'_{DDL} = \frac{q \, A_G \, D_p^{1/2} \, n_i^2}{N_{BS} \, \tau_s^{1/2}} \, e^{\beta V_{BE}} \quad \text{Amps},$$

where τ_s = lifetime at the surface (sec).

2.1.2.5 Summary of Prediction Accuracy. The surface model is successful in predicting the maximum surface current, $I_{SO_{max}}$, associated with the crossover intersecting the surface. The number of surface states and the capture cross-section(s) are necessary input data. The ability to predict the added base current associated with the inversion of the base surface region, $I_{FIDL(max)}$, appears to be limited by the accuracy of the values for the intrinsic recombination rate at the surface. The lower limit to the measurement of each term is the total "bulk" base current (i.e., the base current due to the projected area under the emitter) which for higher V_{BE} washes out the surface terms. For the pre-irradiation case, the major surface terms of consequence were I_{SO} and I_{FIDL}. All other terms were at least an order of magnitude smaller than these.

The dependence of the various base current components on V_{BE} can be put into a general expression where

$$I \propto e^{\beta V_{BE}/n} .$$

For the FIDL term, n was measured experimentally as 1.5. This value of n is usually associated with a depletion layer recombination-generation current but caution should be exercised about conclusions drawn based on the slope

of a current.[17] If we examine the I_{SO} peaks presented in Figure 2.8 and select one gate potential (+20 V), we find that the slope of the total base current changes versus V_{BE}, yet the majority of the base current results from I_{SO}. This surface current term can have slopes of anywhere between $n \approx 1.3$ to $n \approx 2.7$ before being overtaken and washed out by the "bulk" and FIDL terms. The ungated transistor could not separately identify that the I_{SO} term was shifting and thus a conclusion might be reached that the changing slope is due to the interplay of several surface components.

2.2 Radiation-Inclusive Bipolar Transistor Model

The effects of long-term ionizing radiation on the DC gain of bipolar transistors can be described by examining the changes induced in each base current term discussed in Section 2.1 as a function of radiation. The base current for an n-p-n transistor will remain the vehicle for discussing ionizing radiation effects in bipolar structures.

To understand the surface mechanisms related to ionizing radiation effects, we first need to describe the distribution and build-up of oxide charge and interface states. Most of this understanding was obtained from metal-oxide-semiconductor (MOS) studies. The results of these studies will be extended to the n-p-n transistor. A uniform distribution of trapped oxide charge and surface states (MOS approach to bipolar structures) will be assumed initially (i.e., before irradiation) However, the non-uniform electric field in the oxide of bipolar transistors produced by the emitter-base junction will perturb the distribution of trapped charge in the oxide and surface states at the $Si-SiO_2$ interface due to ionizing radiation effects.

The total radiation-inclusive model for bipolar transistors will be compared to available experimental data (e.g., gated bipolar transistor data).

2.2.1 Radiation Effects on Surface Physical Characteristics

The direct physical result of ionizing radiation on silicon devices with an SiO_2 (silicon dioxide) passivation surface layer is to induce additional positive trapped charge throughout the oxide and produce electronic states (usually called interface or surface states) at the $Si\text{-}SiO_2$ boundary.†

Varying levels of trapped charge and surface states exist in both MOS and bipolar structures as a result of manufacturing processes. The effect, for example, is dependent on oxide growth time and temperature. For our purposes we will assume that the trapped charge is positive and uniformly distributed over the entire surface for the pre-irradiation case.

Ionizing radiation significantly increases both trapped charge in the oxide and surface states. A summary of worst-case estimates for both species at pre- and post-irradiation levels are shown in Tables 2.2A and 2.2B. These were obtained by reviewing the literature and from past experience.†† The effect of trapped positive charge above the $Si\text{-}SiO_2$ interface is to create an electric field in the oxide and for a short distance into the bulk silicon. If the trapped charge is uniform it will produce a surface potential similar to that created by a gate placed over the surface above the $Si\text{-}SiO_2$ interface.

---

† There exists evidence that negative trapped charge is also induced, however it is dominated by the trapped positive charge. The surface states are usually located within 200 Å of the ideal $Si\text{-}SiO_2$ boundary plane.[9]

†† Note: The review was performed by Andrew Holmes-Siedle under a consulting contract during the summer of 1977. The values established may eventually be useful for establishing hardness assurance limits.

Table 2.2A Experimental data and models concerning production of new interface states with increasing dose in biased, oxidized silicon.

	Radiation Dose, D, Rad(Si)				
	0	$1x10^4$	$3x10^5$	$1x10^6$	$3x10^6$
D_{SS}*(o) ($cm^{-2}eV^{-1}$)					
Sivo[18] Fig. 4 Bipolar	$8x10^{11}$	$1.2x10^{12}$	$2.2x10^{12}$	-	-
Sivo[18] Fig. 9 MOS	$3x10^{10}$	$4x10^{10}$	$1.5x10^{11}$	-	-
Sivo[18] Fig. 10 Al^+ Implanted MOS	$4x10^{10}$	$4x10^{10}$	$5x10^{11}$	-	-
Bruncke et al.,[19] Bipolar	$2x10^{11}$	-	$4x10^{11}$	$1x10^{12}$	$2x10^{11}$
Fitzgerald,[20] Bipolar	$5x10^{10}$	-	$5x10^{11}$	$8x10^{11}$	$1x10^{12}$
Brown,[21] Exp. 14 Bipolar (Worst case)	$1x10^{11}$	-	-	$\sim 1x10^{13}$	-
Brown,[21] Expt. 14, MOS	$1x10^{11}$	-	-	$2x10^{12}$	-
Tentative worst-case Model:	$1x10^{11}$	$1x10^{13}$	$2x10^{13}$	$5x10^{13}$	$1x10^{14}$

* Surface midgap surface state density - $D_{SS}(o)$ ($cm^{-2}eV^{-1}$). The effective number of surface states (N_{SS}) is assumed to be π kT/q D_{SS}. See Appendix E for development of the justification in using this assumption.

Table 2.2B Experimental data and models concerning radiation-induced changes in biased oxidized silicon surfaces; fixed charge (Q_{ox}) and surface recombination velocity (S_o).

	Radiation Doses, D, Rad (Si)				
	0	$1x10^4$	$3x10^5$	$1x10^6$	$3x10^6$
Q_{ox} (cm^{-2})					
Brown,[21] Expt. 14, Worst-case Bipolar	$3x10^{11}$	-	-	$1x10^{13}$	-
Brown,[21] Expt. 14, MOS	$3x10^{11}$	-	-	$3x10^{12}$	-
Snow,[22] Fig. 3, MOS	$2x10^{11}$	-	$5x10^{11}$	$1x10^{12}$	$1.5x10^{12}$
AH-S, Fig. 3, Worst-case MOS Model	$2x10^{11}$*	$1x10^{12}$	$8x10^{12}$	$1x10^{13}$	$1.5x10^{13}$
S_o (cm sec^{-1})					
Sivo,[18] Fig. 8, Bipolar	-	200	300	800	1500
Fitzgerald,[20] Fig. 2, Bipolar**	1	10	80	130	150

* Nominal 1-V offset due to fixed charge in 2000 Å oxide

** Dose estimated by AH-S

2.2.1.1 Trapped Hole and Surface State Generation Mechanisms. Ionizing radiation causes electron-hole pairs to be produced in the oxide. Without an electric field in the oxide many of these pairs will undergo geminate recombination. The probability of a hole and an electron escaping geminate recombination increases when an electric field is present. The electric field may be due to the emitter-base junction alone or combined with an applied voltage. Holes can be trapped in oxide centers, which are usually considered to be comprised of both deep and shallow traps. Since the electrons have a mobility in the oxide that is several orders of magnitude larger than that of the holes, the probability of capture is less for electrons.† "Hole hopping" mechanisms in the presence of an electric field move the trapped holes toward the interface into deeper trap sites where the "hopping" mechanism stops.[23] As these charges are swept toward and across the Si-SiO_2 interface into the bulk they appear at the terminal leads. The presence of an applied electric field by a gate over the oxide will alter this process. Ionizing radiation coupled with the existing electric field causes a build-up of positive trapped charge near the Si-SiO_2 interface. By using an energy band diagram, these mechanisms can be illustrated (see Figure 2.10). The result of this build-up of trapped charge is a change in the surface potential as viewed from the silicon substrate illustrated in Figure 2.11.

The surface states are not as well defined in terms of their physical interpretation but the present understanding is that they can be caused by broken bonds and impurities at the interface.[24,25] Both causes can result from processing techniques. Only the broken bonds are increased from ionizing radiation. The increase in broken bonds is thought to result

---

† Electrons having the opposite charge of the hole will travel in the opposite direction along the same field line.

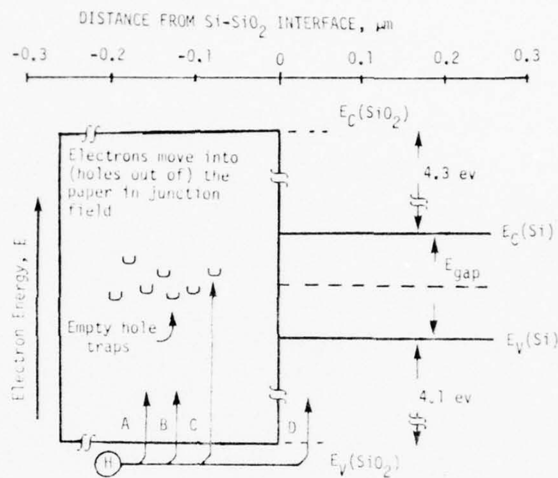

Figure 2.10. The Si-SiO_2 interface energy diagram during irradiation. The holes: A) recombine (geminate), B) recombine (non-geminate), C) are trapped, or D) discharged to recombine in the silicon.

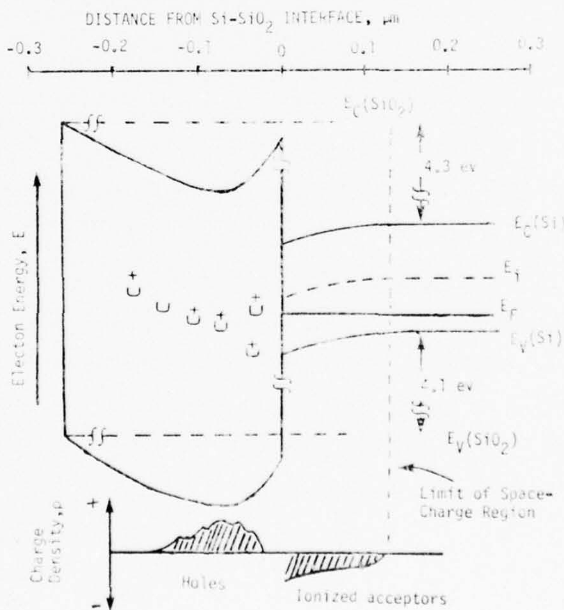

Figure 2.11. The Si-SiO_2 Interface energy diagram after irradiation.

from free holes produced in the oxide by the ionizing radiation which diffuse through or to the interface. It is unclear whether all of these holes stop at the interface or some of them pass into the silicon.[24] Regardless, the creation of surface states is postulated to result. The most complete analysis has been presented by Sah.[26] Surface states can act as donors or acceptors and are considered recombination-generation centers. They are usually assumed to be distributed uniformly in energy over most of the energy band gap of silicon.[†] Thus, the surface states act as extra recombination centers at the surface regions of the silicon substrate.

We will assume that surface states have a donor-like character (charge states neutral and positive) when they lie below the intrinsic level, and an acceptor-like character (charge states neutral and negative) when they lie above the intrinsic level. The surface states then are either neutral or positive in character for a "p-type" substrate. Positive surface states are those with energies between the intrinsic energy level and the Fermi level. If the intrinsic level shifts closer to the Fermi level but remains "p-type" in character, less surface states will appear positive (i.e., active). If the level shifts below the Fermi level then the material is inverted to "n-type" by definition. The surface states are negative for those with energies between the Fermi level and the intrinsic level. Figure 2.12 demonstrates this concept. Only the states near the intrinsic level are considered effective (whether positive or negative) for recombination, since it takes both holes and electrons to complete the recombination process and the crossover point has a near equal concentration of both. If the surface state is close to either edge of the bandgap (valence or conduction band), there is a lack of one of the two essential

---

† The above understanding of the mechanisms of charge build-up in oxides and the creation of surface states was provided by Andrew Holmes-Siedle. Near the conduction and valence bands, there has been much disagreement on what the distribution is really like. Since later we will only use those surface states near the intrinsic level, we can assume a uniform distribution. For more information on the distribution of surface states, see Reference 27.

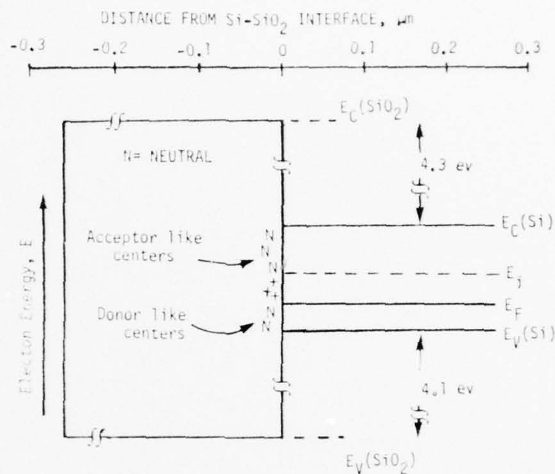

Figure 2.12. The pre-irradiation Si-SiO_2 interface energy diagram.

species and the probability of a recombination is small. Thus only the surface states within a few energy units (kT/q) of the intrinsic energy level are effective. The charge of these surface states also affects the surface potential as viewed by the charge carrier in the silicon.

<u>2.2.1.2 Surface Potential Distribution Due to Oxide Charge and Surface State Build-Up</u>. For the pre-irradiation case we assume that fabrication processes produce a uniform level of both trapped charges and surface states. These levels can widely vary as evidenced by the "0 Rads" column in Tables 2.1A and 2.1B.

Consider the post-irradiation condition. The trapped oxide charge and the density of surface states increase. The result is an increase in

surface potential and an increase in the density of recombination centers at the surface. The increases are not restricted to the uniform distribution discussed for the pre-irradiation case.

As seen earlier, the creation of free holes and the movement of those holes (through trapping/hole hopping mechanisms) is assumed dependent on the electric field in the oxide. For MOS structures where a gate is placed over the surface, the final trapped charge and surface distribution would remain fairly uniform due to the uniform electric field induced in the oxide by the gate. For bipolar structures, the E-B junction built-in potential is always present with or without a surface gate. The electric fields in the oxide produced by the presence of this junction produce a non-uniform distribution of trapped charge and surface state density versus distance from the junction.

For the standard off-the-shelf n-p-n bipolar transistor, the surface of the base region extends from the E-B junction to the base contact. Above this region (in the oxide), the electric fields are those from the E-B junction near the surface due to the built-in potential combined with the applied bias.† We thus obtain field lines in the oxide as illustrated by Figure 2.13. The E-B junction field lines can be modeled as originating from two metal blocks separated by the E-B depletion layer width, both ending at the surface interface. Modeling a bipolar transistor in this way generates an idealized field distribution shown in Figure 2.14. The fields decrease as $1/r$ (r = distance) from the edge of the depletion region. (For more details of this modeling effort, see Appendix D.)

For the surface area near the interface directly over the E-B junction (where it meets the surface) the electric field in the oxide can

---

† Fields extending from the base metal contact through the oxide to the emitter metal contact can be considered small in proportion to these E-B junction fields.

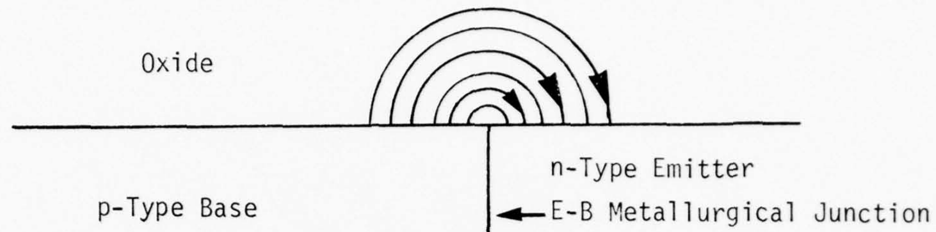

Figure 2.13. Idealized electric field lines in oxide due to junction modeled as a parallel plate capacitor. The arrows are in the direction of electron movement.

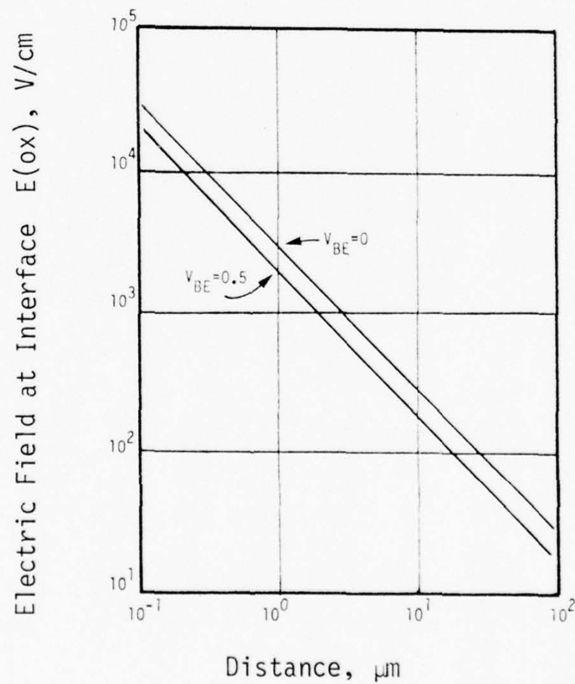

Figure 2.14. Pre-irradiation electric field for a non-gated transistor at the surface of the base due to the E-B junction voltage vs. distance from the edge of the E-B depletion layer.

can be approximated to be similar to the electric field within the junction. One dimensionally, this field across the E-B junction can be illustrated as in Figure 2.15.

During ionizing irradiation, the number of holes that escape geminate recombination in the oxide, and the movement toward the surface due to hole hopping mechanisms, were shown earlier to be dependent on the strength of the electric field. We also assume that the untrapped holes diffuse to the interface and form surface states. Under these assumptions and for bipolar transistors, we would expect that the distribution of trapped charge in the oxide and the number of surface states produced as a result of ionizing radiation could be modeled as diminishing from the edge of the E-B junction toward the base contact.

Since both the oxide charge and surface states increase with ionizing radiation, we must consider the total effect on the surface

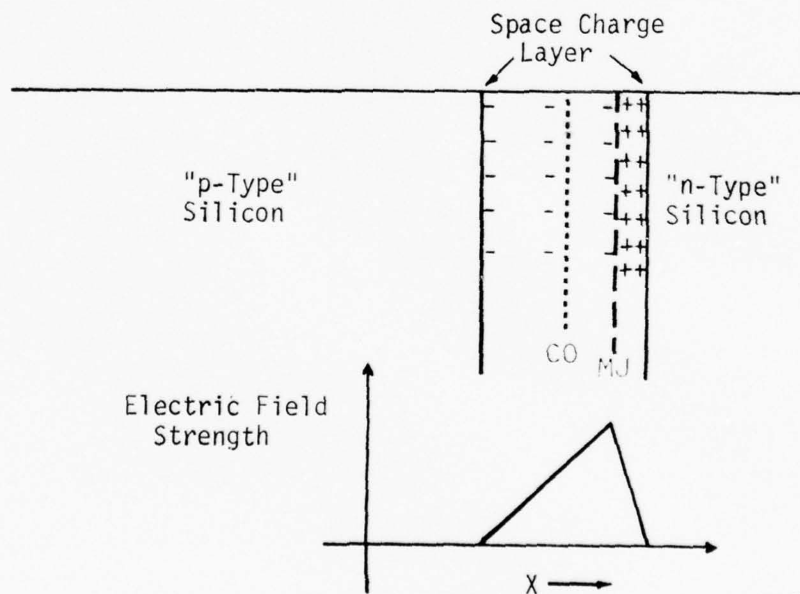

Figure 2.15. The space-charge region and electric field associated with a p-n junction where the n-type is more heavily doped. CO = cross-over (where n = p) and MJ = metallurgical junction.

potential as viewed from the substrate. As a result of the oxide charge build-up, the surface potential increases positively and pushes positive charges (holes) in the semiconductor away from the surface. The increase in surface states also has a net effect on the surface potential. This is based on the theory that as the energy bands are bent by the electric fields from the oxide charge, the intrinsic energy level moves closer to the Fermi energy level making many of the originally positive surface states, neutral.[28] Thus, there is an effective loss in total positive potential associated with the surface and a smaller positive potential will be seen by the carriers in the silicon substrate. The effect on surface potential by increasing the number of surface states for specific electric potentials at the surface is shown in Figure 2.16. The number of surface states influences the surface potential for a given electric field ($E_{(ox)}$).† The effect of increasing the number of surface states on the surface potential is to decrease or "saturate" the effect of an electric field at the Si-SiO_2 interface.

If we now apply all these ionizing radiation mechanisms simultaneously in an n-p-n bipolar transistor, we obtain a surface potential profile that looks like Figure 2.17(a) for $V_{BE} = 0$ and Figure 2.17(b) for $V_{BE} = 0.5$ volts. (This profile represents the surface potential as seen by the charge carriers in the semiconductor near the surface.) The surface potential is modeled from the edge of the E-B depletion layer versus distance from the metallurgical junction. Note that the applied V_{BE} diminishes the magnitude of the surface potential generated for each dose level.

It appears that for this field induced build-up of oxide charge and surface states, beyond 10 μm for this doping, the surface potential approaches its uniform pre-irradiation characteristics. Bäuerlein measured

---

† The energy density of surface states is assumed to be uniform throughout the energy band of silicon for the post-irradiation case. This is a reasonable approximation based on work done by Sivo. He showed that for higher radiation levels, the center of the energy band becomes more uniform. Since the effective surface states are those near and at the intrinsic energy level, any non-uniformity outside this region would not be effective.[29]

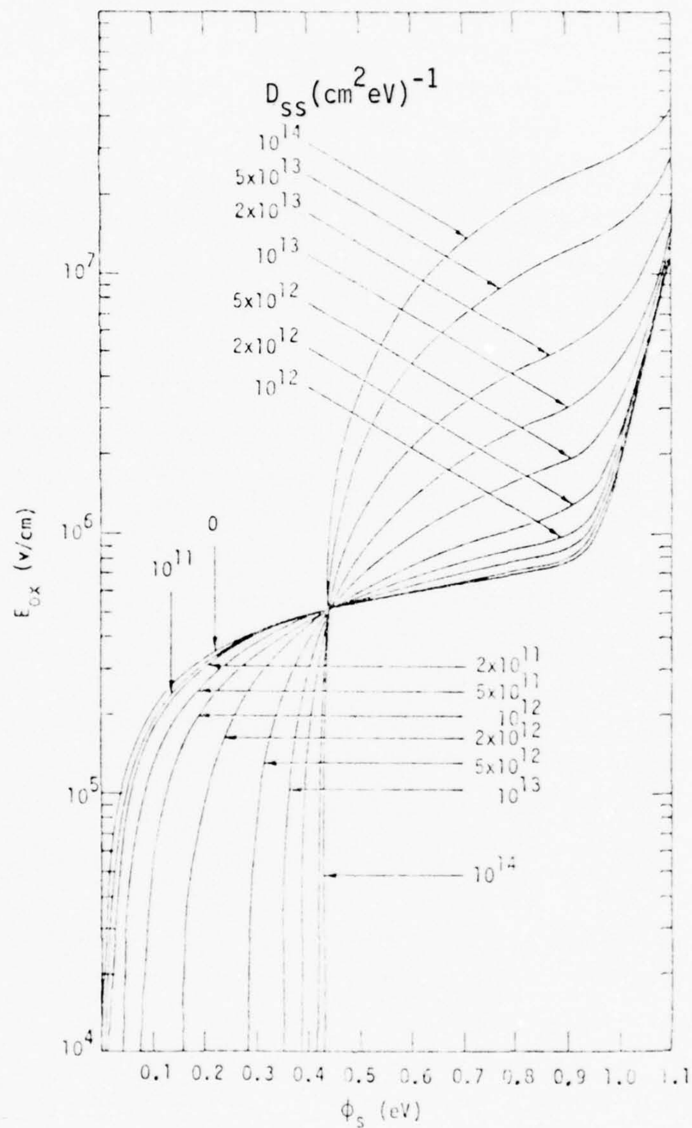

Figure 2.16. Dependence of surface potential ϕ_S on interface electric field in silicon dioxide, for various values of surface state density D_{SS} (in units of $(cm^2\ eV)^{-1}$). Zero surface potential is taken at flat band condition. Acceptor concentration in the silicon is $2 \times 10^{17}\ cm^{-3}$ for the model.

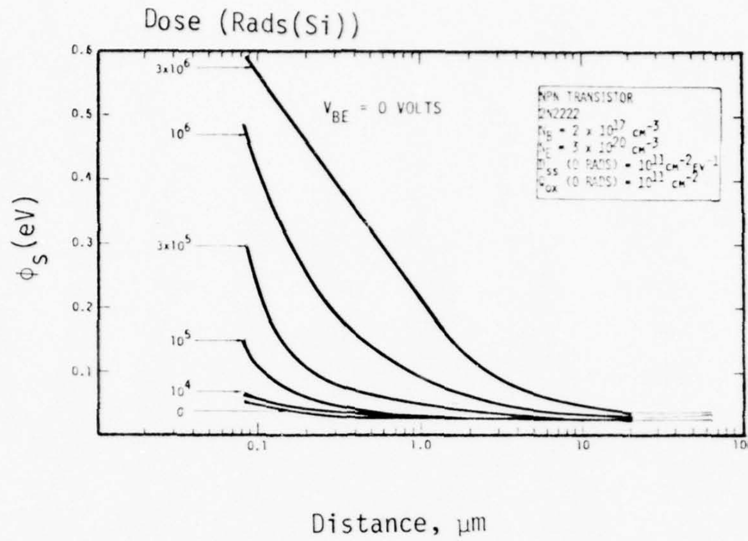

Note: $$D_{ss} = \left[\frac{4.6 \times 10^5}{\ell(\mu m)} \cdot \text{Dose (rads(Si))} + 1 \times 10^{11} \right] \frac{\text{states}}{\text{cm}^2\text{-eV}}$$

(a)

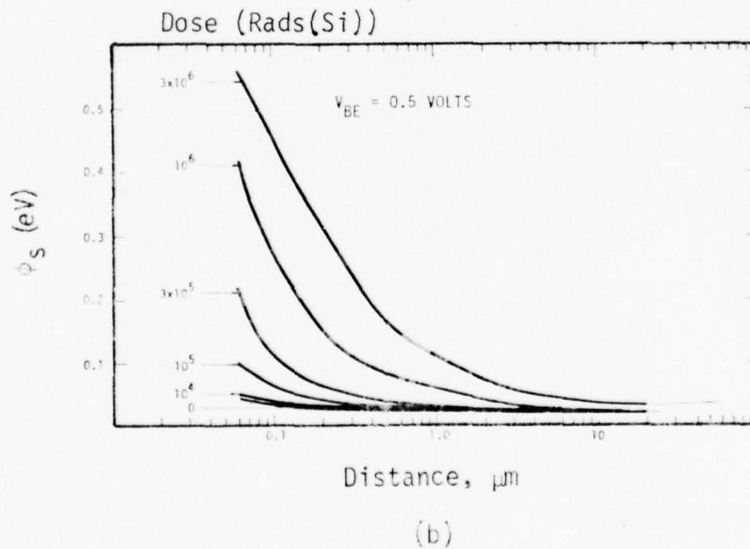

(b)

Figure 2.17. Field-dependent influences on surface potential versus distance from E-B junction for irradiated standard ungated transistor. V_{BE} represents the applied bias during irradiation. Passive and active biases during irradiation were used as examples since these two conditions represent real states for bipolar transistors in a deployed system.

an effective 10 μm zone next to the E-B junction by irradiating small regions of the base surface with an electron beam.[30] This experimental data supports the above predicted distributions. It appears that (at least for the low to moderate ionizing radiation case) the position of the base contact is not a critical parameter. Higher density technologies may change the importance of this parameter.

2.2.1.3 Measurement Techniques for Analyzing Radiation Effects. Initially, this report used MOS data to describe the basic transport properties of ionizing radiation created trapped holes in the silicon dioxide. The uniform effects could thus be modeled. The problem was complicated when the varying electric fields due to the E-B junction caused a non-uniform buildup of trapped charge.

Consider now the use of gated transistors as diagnostic tools. Several authors have used gated structures to evaluate ionizing radiation effects on the base current terms.[7,8,15]

For the gated transistor, a gate is placed over the E-B junction extending into both the emitter and base regions. Figure 2.18 is an illustration of this technique for a n-p-n structure.

Prior to irradiation, various components of the base current can be analyzed by varying the gate potential. We assumed that the oxide charge and surface states were uniform and the gate produced a uniform surface potential over the base region. The non-uniform effects from the E-B junction electric fields on the surface potential can be assumed small and are usually neglected. We saw in Section 2.1 how this tool can accent various components of the base current related to the surface. The gated transistor was thus considered to be a reasonable tool to dissect the effects of radiation on bipolar transistors.

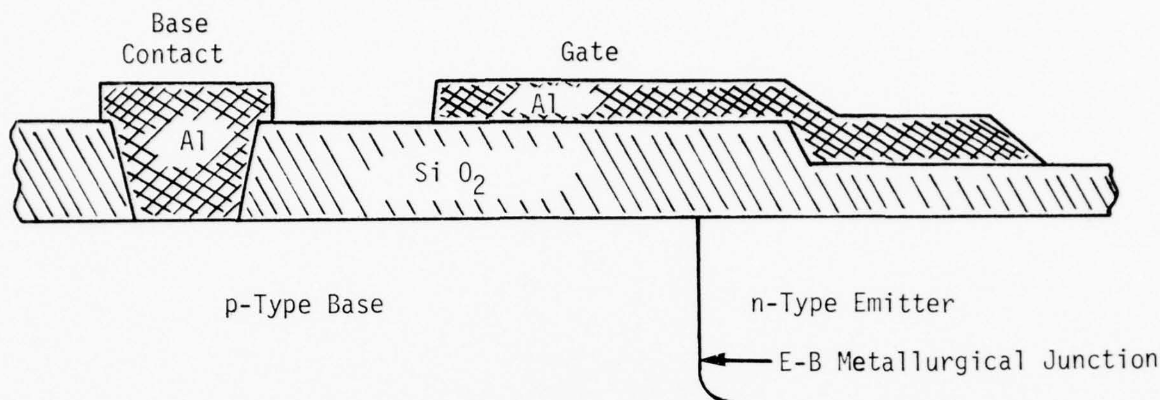

Figure 2.18. Illustration of gate structure placed over the E-B junction of an n-p-n transistor as a diagnostic tool for measuring surface properties of bipolar devices.

In actuality, the gate (when grounded during irradiation) produces another set of boundary conditions for the E-B junction fields in the oxide. The result is a difference in the electric field from the non-gated transistor which influences the distribution of trapped charge in the oxide and surface states. Figure 2.19 shows the predicted distribution of the pre-irradiation surface electric field produced by the E-B junction for the gated transistor. The electric field is spread out further (than for the non-gated transistor) into the base and the magnitude of the electric field is higher for more of the base surface region. The total effect from this gate for the post-irradiation case is the distribution of surface potentials as shown in Figure 2.20. We see that the presence of a gate has significantly perturbed the expected distribution of surface potential making the potentials larger and slightly more uniform at higher doses.† The effects from applied voltages are smaller (compared to the non-gated transistor).

† Note: no assumption of trapped charge saturation was used in the model for Figure 2.20. If a charge saturation was used,[22] with the maximum $Q_{ox} \cong 1 \times 10^{13}/cm^2$, the surface potential would reach a peak of 0.65 (eV) and remain constant thereafter. The dip seen near the edge of the E-B junction for very high dose level is the result of surface state effects illustrated in Figure 2.16.

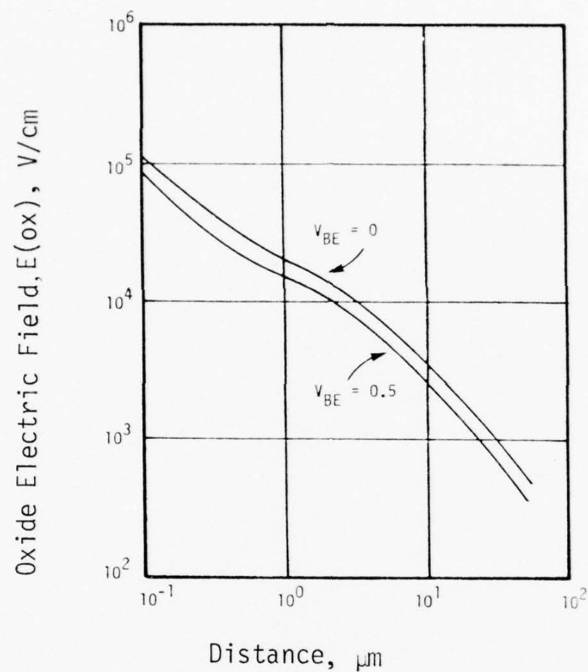

Figure 2.19. Pre-irradiation electric field for a gated transistor at the surface of the base due to the E-B junction voltage vs. distance from the edge of the E-B depletion layer.

The result of this analysis is that the gate perturbs the distribution of surface potential due to ionizing radiation and thus the response of the transistor. One should therefore be careful in applying gated transistor data to describe non-gated transistor response in hardness assurance screens.

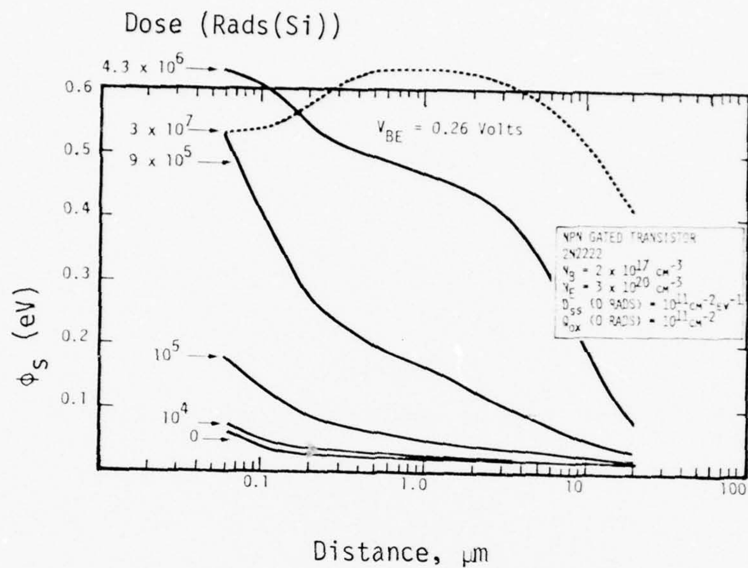

(a)

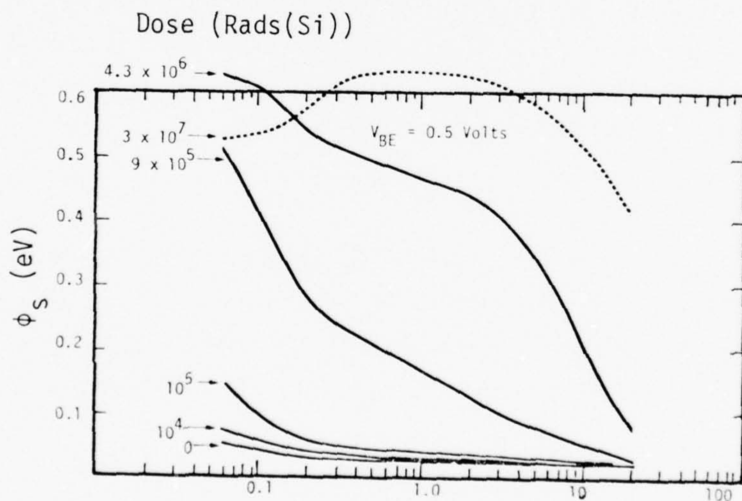

Distance, μm

(b)

Figure 2.20. Field-dependent influences on surface potential versus distance from E-B junction for irradiated gated transistor. V_{BE} represents bias during irradiation.

2.2.2 Radiation Effects on Base Current Terms

The surface related base current terms introduced in Section 2.1.1 were composed of recombination-generation type terms and diffusion related terms. The recombination-generation terms at the surface were defined for depletion layers (DL) near the surface of the semiconductor. These terms described the contributions to the base current from a field-induced depletion region formed in the base near the surface (I_{FIDL}), and the recombination-generation at the surface, I_{SO}, (sometimes referred to as the surface velocity term).†

Two other possible surface terms were defined when the new surface depletion layer was complete and exist only after I_{SO} has peaked. These terms were I_{RBDL} and $I_{D'DL}$.

The "bulk terms" are usually assumed to remain unchanged due to ionizing radiation. We will use this assumption initially. As will be seen later, after the surface terms are evaluated, this assumption will have to be modified. The total effect on gain from ionizing radiation is the sum of all contributions, surface and bulk.

2.2.2.1 Recombination-Generation Surface Terms. The same recombination-generation surface terms defined in Section 2.1.2 (I_{FIDL} and I_{SO}) will be used in the evaluation of ionizing radiation effects. For $V_{BE} \geq 100$ mV, the crossover expression, I_{SO}, can be simplified to

$$I_{SO} \approx \frac{.5q\, A\, n_i\, v_{th}\, \sigma_n\, N_{ss}\, e^{\beta V_{BE}/2}}{\text{Cosh}\ \beta(\phi_s - \phi_F + V_{BE}/2)} \quad \text{Amps.}$$

Evaluation of this term's maximum for Reddi's transistor at V_{BE} = 0.1, 0.3 and 0.5 volts gave values that closely matched corresponding experimental

† The I_{SO} term includes all surface areas where $n_s \approx p_s$ (defined as crossover).

data assuming uniform surface potential. If we apply this term to the case of a non-uniform surface potential, such as for the post-irradiation case, only a small portion of the base surface area will be peaked; namely the portion of the surface where $n_s \approx p_s$. The other base surface regions will have values of I_{SO} that are less than the peak depending on the local values of the surface potential, carrier concentrations, and the density of interface states. For regions where the surface potentials are greater than that needed to reach peak I_{SO}, the I_{FIDL} term will contribute by increases in the depth of the depletion layer from the surface. Ionizing radiation may also effect the recombination rate near the surface which also will increase the FIDL current for very high dose levels.[31]

At higher doses, another effect is predicted. From Figure 2.16 we observed that electric field effects on the surface potential (ϕ_s) were less significant over a large range of electric field strengths for high interface state densities. Therefore at high dose levels when the surface state density becomes dominant, the surface potential is forced toward the crossover point thus peaking I_{SO} (for a given n_s and p_s) over most of the base surface region regardless of the oxide charge distribution. This means that under these conditions the quantity of oxide charge is relatively unimportant. Thus, measurement techniques which supposedly measure the charge in the oxide (Q_{ox}) may not provide accurate values of the surface potential for all dose levels.

2.2.2.2 Surface Dependent Bulk Diffusion Currents. Large surface potentials can induce a full depletion layer at the surface. Another viewpoint of this depletion layer is an extension of the E-B junction depletion layer. Additional I_{RB} and I_D' contributions related to this new surface field-induced depletion layer are theoretically produced under certain conditions.† We called these terms, in Section 2.1, I_{RBDL} and $I_{D'DL}$.

---

† If the base surface doping is not too different from that under the emitter well and if the well depth is comparable to the base width (a factor of 2 or so) then the emitter current density flowing into the base from the field-induced depletion layer will be comparable to the emitter current density under the well.

The only radiation variable contained within these two terms is the surface lifetime in the $I_{D}{}'_{DL}$ current.

Within the relationship that $\tau_S = (N_{ss}\ \sigma\ v_{th})^{-1}$ seconds, the conclusion is reached that $I_{D}{}'_{DL}$ is proportional to the interface state density to the one-half power. This term is usually small (pre-irradiation at low V_{BE}) relative to I_{SO}. I_{SO} is also more sensitive to N_{ss} directly and dominates the total surface current; especially at low V_{BE}.

Now let us introduce the indirect mechanism of decreasing emitter crowding. This mechanism is only found at high currents by definition of emitter crowding. The increase in emitter area (from the viewpoint of an extension of the E-B depletion layer) is the cause. The FIDL region acts like an extension of the original sidewall region which causes added collector current given the right conditions. As more emitter current is injected through the sidewall, the effective emitter current density decreases and crowding decreases (for the same measured collector current). Appendix C discusses the effect of crowding on the "bulk" base current terms used to determine DC gain. Figure 2.21 shows the effects of bias and measurement current on gain degradation. The author states that the slope of the change in reciprocal gain due to ionizing radiation is similar in behavior to the normal base spreading resistance term caused by emitter crowding.[23] In

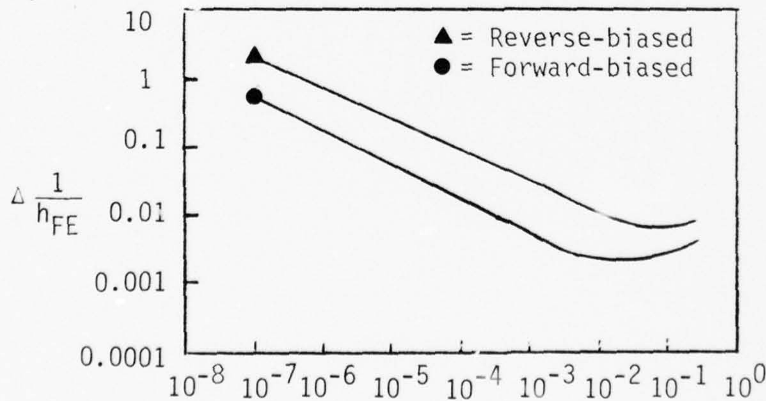

Figure 2.21. Effect of bias during exposure and measurement current on current gain degradation.[23]

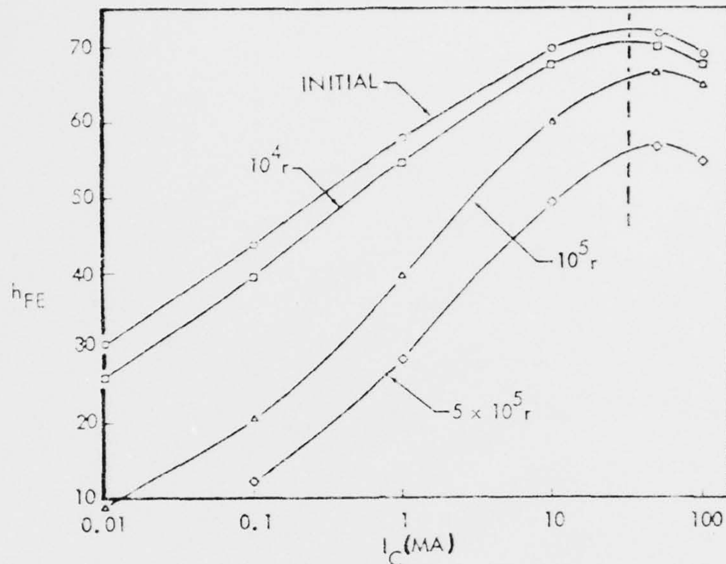

Figure 2.22. 2N1613 transistor, I_E = 1 mA, V_{CB} = 10 V, Cobalt 60 irradiation.[32]

Figure 2.22, the gain is measured versus collector current for various dose levels.[32] The peak gain is usually associated with the point where current crowding and high injection effects become significant. A shift of this point and/or a change in the slope of the curve beyond this point would indicate changes in the current density through the base region. Figure 2.22 shows such a shift and slope change. Since the shift is to the right (higher current required to obtain peak h_{FE}), current crowding could be interpreted as being reduced for higher radiation levels. Also, the slope of the curve beyond the peak is not as severe. This indicates that the crowding (or high injection effects) has been reduced. A final example is a comparison of gain versus collector current for several transistor structures included in I^2L integrated circuits (IC's).[33] Figure 2.23 shows the same effect on these structures from ionizing radiation. The position of peak gain and slope (after peak gain) have been significantly changed. Thus "bulk" terms not directly related to surface changes can be affected indirectly by the change in the surface due to ionizing radiation.

transistors can provide insight as to the individual mechanisms contributing to the total base current and how they change versus radiation. Figure 2.24 is an example of the pre-irradiation curves generated by varying the gate voltage over the base region. The standard interpretation of each contribution to the total base current is also shown.

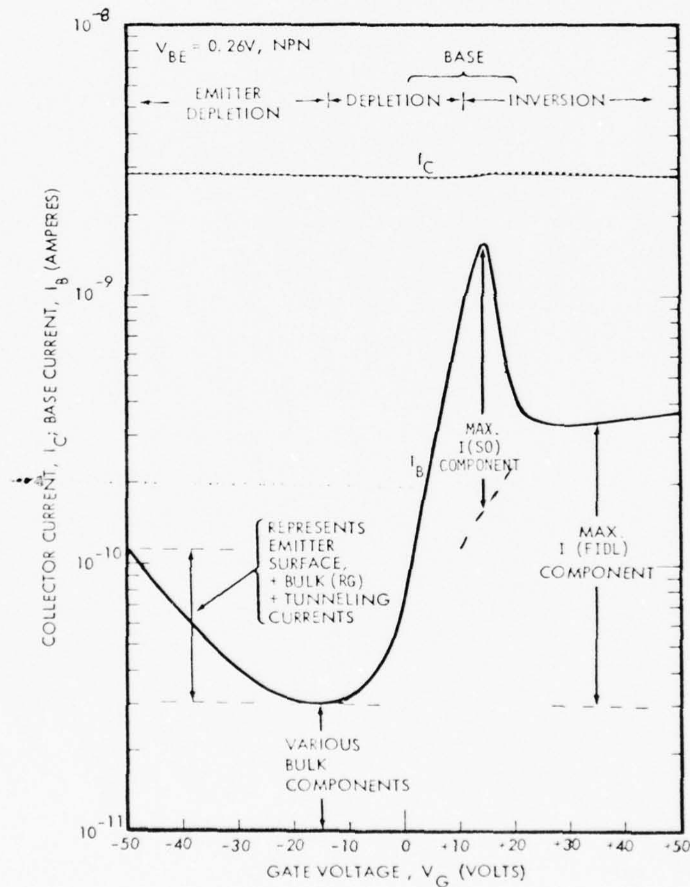

Figure 2.24. Standard interpretation of a non-irradiated gated bipolar transistor base current curve versus gate voltage.[7]

The trouble with using standard off-the-shelf transistors is that several mechanisms interact at the same time. Separating the mechanisms for understanding and modeling efforts for hardness assurance are very difficult. This is the reason the data used by investigators to evaluate models are from gated transistor experiments.

Using someone else's past data for comparison with the radiation-inclusive model poses two problems. One, important physical parameters are often unknown and some of the critical physical parameters have to be assumed from similar devices or the same manufacturer. Two, other tests useful in evaluating new model predictions, cannot be tested on the same samples (i.e., breakdown voltage vs. dose).

For the non-irradiation case, we used Reddi's[15] gated transistor due to the availability of detailed physical characteristics. This data was introduced in Section 2.1. Unfortunately, Reddi did not perform radiation tests on these devices. Therefore, we must introduce a second set of data to be used as a vehicle for discussing radiation effects. The data is from Sivo's work.[7] Unfortunately, Sivo did not include all the needed physical parameters. The physical parameters for the 2N2222 transistor are presented in Table 2.3 and assumed similar for devices used by Sivo. Figure 2.25 introduces Sivo's experimental data for a circular geometry device with a one dot emitter inside the base diffusion well. The transistor curves are for a gated transistor structure operating at several V_{BE} levels.

As will be seen in the following discussions, each of the surface related terms can be identified from experimental data. Broadening and shifting of the various portions of the gated transistor curves are discussed

Table 2.3. Physical parameters for the 2N2222 transistors (transistor is circular geometry) used in Sivo's[7] ionizing radiation experiments.

PHYSICAL PARAMETER	VALUE	PHYSICAL PARAMETER	VALUE
A_e	1.2×10^{-4} cm^2 *	v_{th}	10^7 cm/sec
A_g (base region)	1.3×10^{-4} cm^2	N_{ss} (pre-radiation)	1.2×10^{10} states/cm^2 *
N_{BS}	3×10^{18} atoms/cm^3	X_{es} @ V_{BE}=0.26 Volts	2.2×10^{-6} cm *
N_{ES}	2×10^{20} atoms/cm^3 **	X_e @ V_{BE}=0.26 Volts	1.2×10^{-5} cm *
N_B	9×10^{16} atoms/cm^3 **	$X_{d_{max}}$ @V_{BE}=0.26 Volts	1.8×10^{-6} cm *
N_E	3×10^{18} atoms/cm^3 **	D_n (base)	13.8 cm^2/sec *
P_e	3.9×10^{-2} cm*	D_p (emitter)	1.95 cm^2/sec *
P_G (edge of gate)	5.5×10^{-2} cm*	ψ_{os}	1.1 eV *
W_b	1×10^{-4} cm **	ψ_o	0.9 eV *
W_{sc}	3×10^{-4} cm **	n_i	1.45×10^{10} cm^{-3}
τ_b	7×10^{-7} sec **	R_i	1.5×10^5 ** sec^{-1}
τ_e	1.35×10^{-8} sec **	R_{i_s}	1.6×10^7 ** sec^{-1}
d_{ox} (base)	(6000 ± 1000) Å	ϕ_{F_s}	0.498 eV *
σ	5.8×10^{-16} cm^2		

* Inferred/Calculated
** Assumed from similar information

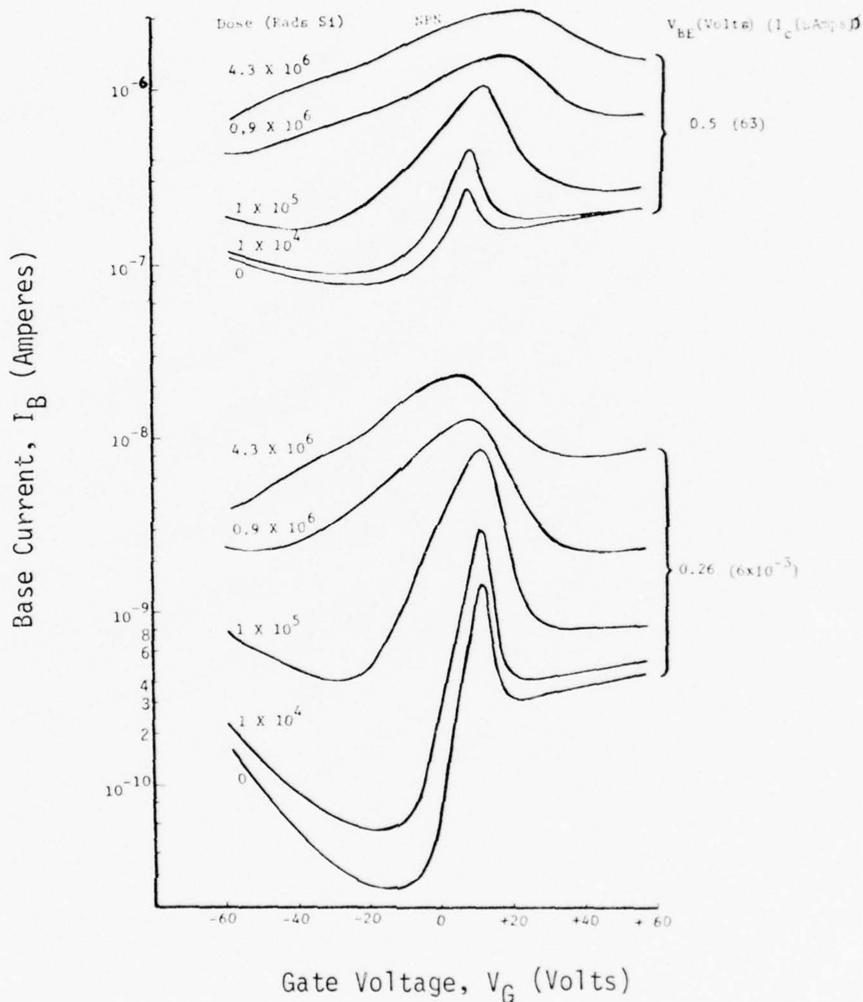

Figure 2.25 (a). Effect of ionizing radiation on the I_B vs. V_G curves at various injection levels. Note the increases in the surface and bulk (FIDL) components of I_B as well as the changes in the shapes of the current peaks ("broadening"). The illustration is continued in the next figure.[7]

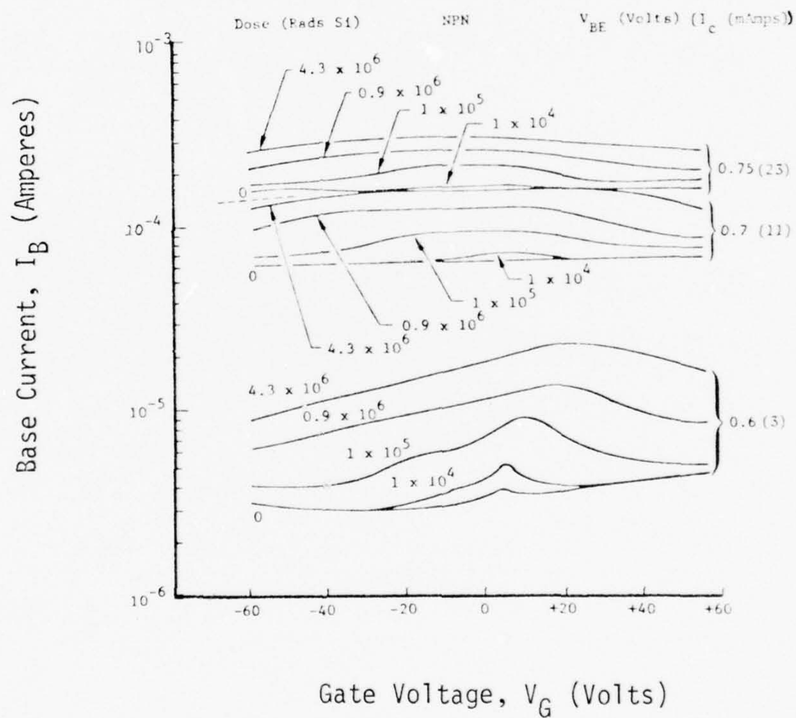

Figure 2.25 (b). Effect of ionizing radiation on the I_B vs. V_G curves at various injection levels. This illustration is a continuation of Figure 2.25(a).[7]

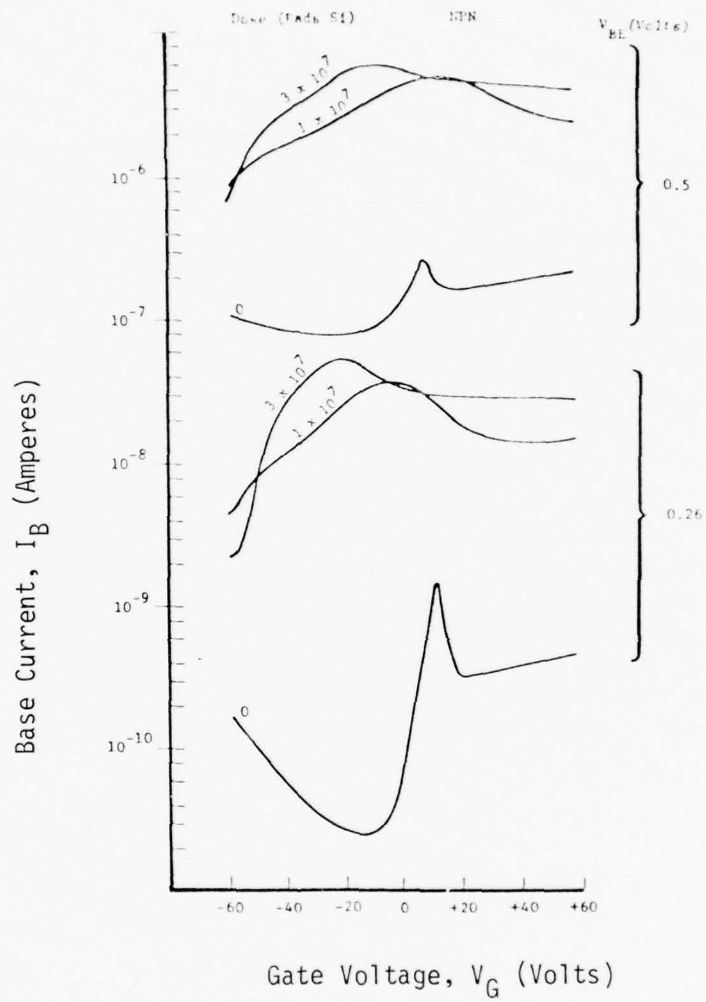

Figure 2.25 (c). An example of high dose effects on the base current, I_B.[34]

as related to model predictions. Changes in the magnitude of base currents are also evaluated in relation to model predictions.

The bias conditions during irradiation are also very important for development of hardness assurance screens. These will be discussed as natural extensions of the modeling effort. We will see that the worst-case bias conditions for n-p-n bipolar transistors is when the C-B and E-B junctions are reverse-biased. This condition produces the maximum fields in the oxide allowing more electron-hole pairs to escape geminate recombination and more "hole-hopping".

As a last subject in this section (process variations), we will discuss mechanisms that may explain or identify the cause of "mavericks" (or "outliers").

2.2.3.1 Shifting, Broadening And Increases In Gated Transistor Base Current Curves. Comparing pre-irradiation curves with post-irradiation curves for gated transistors shows a shifting of the peak (associated with the I_{SO} component) to lower gate voltage (at V_{BE}=0.26 Volts) for high radiation dose levels. At higher V_{BE}, the peaks shifted to larger gate voltage versus dose level. These relationships are defined in more detail in Figures 2.26 and 2.27. Figure 2.26 describes the shifting versus dose level for several applied V_{BE}'s while Figure 2.27 describes the shifting versus V_{BE} for several dose levels.

The model description of I_{SO} contains a dependency on surface potential. For increased surface potential, the maximum I_{SO} contribution would occur at lower gate voltages. Trapped oxide charge and interface states created by ionizing radiation would increase the surface potential and reduce the necessary external gate voltage required to force the surface to crossover. The theoretical result is a shift of the peak to lower gate voltages for higher doses.

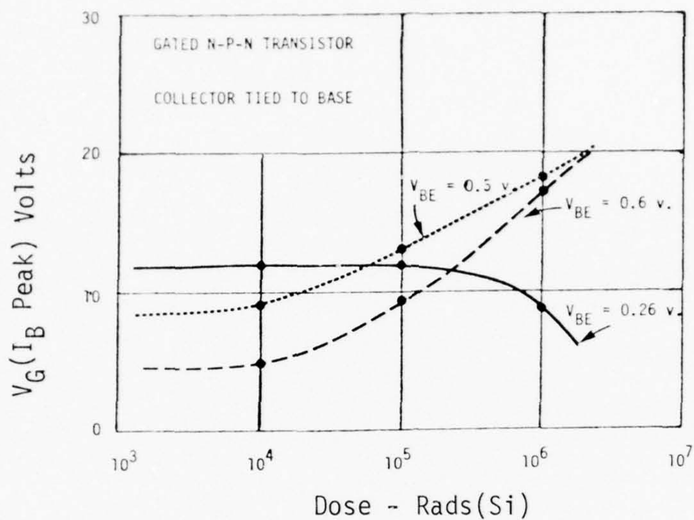

Figure 2.26. Gate voltage necessary to peak I_B vs. dose for several applied emitter-base voltages. Data is from Figure 2.25.

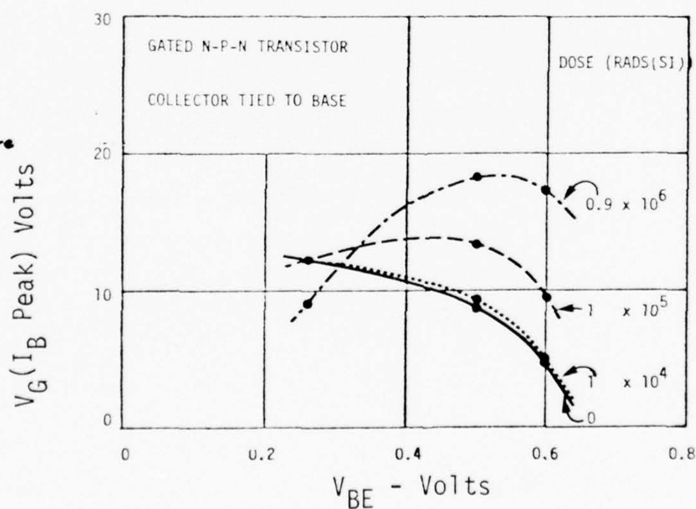

Figure 2.27. Gate voltage necessary to peak I_B vs. applied emitter-base voltage for several dose levels. Device is the gated n-p-n transistor used by Sivo in Figure 2.25.

The theoretical model described in Section 2.1 fits the experimental data at low V_{BE}. At higher V_{BE}'s and low dose levels, the model prediction is a reasonable approximation. For higher V_{BE} at moderate to high dose levels, the model does not appear to contain the correct dependencies until very high dose levels (as illustrated in Figure 2.25(c), very high dose levels show a dramatic shift to lower gate voltages).

Possible explanations for this discrepancy in the model predictions are found in the simplification techniques employed in the I_{SO} term. These were used to make it easier to apply to actual devices with limited knowledge of the physical parameters. For example, the minority carrier concentration is assumed uniform for all regions under the gate and V_{BE} determines the assumed concentration. At low V_{BE} the injected minority carrier concentration from the emitter is representative of a relatively small increase and thus large minority carrier gradients do not result. Consequently, low V_{BE} applications satisfy the assumptions used in the I_{SO} term.

At higher V_{BE}, the injected minority carrier concentration (n_p) from the emitter becomes more substantial and a larger carrier gradient results. The V_{BE} applied at the E-B junction determines n_p at the base edge of the E-B depletion layer. In the base region, the minority carrier concentration decreases versus distance from the junction. This decrease is due to the diffusion length of electrons in a "p-type" base which is dependent on lifetime. Therefore, at one diffusion length into the base from the E-B junction, the "uniform" minority carrier concentration used to evaluate local I_{SO} is not associated with the V_{BE} found by using the Boltzmann relationship at the junction edge.

The applied V_{BE} is therefore only representative of the immediate base surface region next to the edge of the E-B depletion layer. The structure geometry (i.e., interdigitated, circular, etc.) also determines how significant this mechanism will be in causing deviations between the model predictions and experimental data.

For the post-irradiation case it is conjectured that increases in the density of interface states will reduce the lifetime at the surface. This may make the minority carrier concentration fall off even more severely versus distance from the E-B junction. The gate extends over the base region well beyond the E-B junction. Thus, the peak I_{SO} may be representative of any base surface region out to the edge of the gate. The gate voltage necessary to peak I_{SO} would be determined by an n_p that could be associated with a lower "effective V_{BE}" increasing the predicted peak gate voltage. The effect of increased surface states from ionizing radiation can therefore be thought of as a lifting of the pre-irradiation curve in Figure 2.27 back toward a horizontal line whose value is determined by the low V_{BE} value. This effect is observed. This mechanism cannot however explain the increase of the curves above the horizontal position.

A second possibility that may add to the above effect relates to the assumption that the ratio of the capture cross-sections for holes (σ_p) and electrons (σ_n) at the surface was not very different from "1" and was radiation independent. Using these assumptions allowed us to simplify the I_{SO} term by eliminating ϕ_o ($\phi_o = 1/\beta \ln \sigma_p/\sigma_n$) from the argument in the cosh portions of I_{SO}.

There is very little data about the ratio of the cross-sections because it is hard to measure and for most applications, the important parameter is σ (where $\sigma = (\sigma_p \cdot \sigma_n)^{\frac{1}{2}}$). The only data found was from Sivo's report[18] which shows a change in σ versus dose for a gated transistor. This may indicate that the ratios may be changing as well which may change ϕ_o and shift the peak.

With the assumption that for increasing V_{BE}, the minority carrier concentration increases and for higher gate voltage, the effective majority carrier concentration near the surface is reduced, then the gate voltage required to force the surface to crossover (and thus peak I_B) is predicted

to decrease for higher V_{BE}. Radiation effects (increase in positive surface potential) should accent this decrease versus V_{BE}.

The above two possibilities assume the model is in a correct and complete form. Another possibility is that some as yet undefined radiation dependent mechanism is influencing the experimental data. (Observing Figure 2.27, we conclude that obviously some physics is missing in the present state-of-the-art description and understanding of ionizing radiation effects in semiconductors).

We have a model that, when simplified, can be used generally at low V_{BE} or at high V_{BE} (low dose levels) without introducing a significant deviation from the worst-case experimental data. For the other cases, the discrepancies must be resolved before applying the model generally. Since the discrepancies will require future work, we will limit our discussions to the low V_{BE} case for this section and show how the terms explain other features of the experimental data.

Along with the shifting, a broadening of the peak associated with the I_{SO} contribution was observed. The broadening mechanism is contained in the I_{SO} model via N_{ss} and ϕ_s. The interplay between N_{ss} and ϕ_s as well as their individual distributions change as a function of dose. For a non-uniform distribution of surface potential, we would not expect a sharp peak for I_{SO}. Some surface areas will reach crossover with a specific applied gate voltage while other regions would have surface potentials that will correspond to one side or the other of the peak. The result is a "broadening" due to the structure influences on I_{SO}.

Broadening can also be caused by the increase in surface states due to ionizing radiation. According to Figure 2.16, high dose levels will

eventually pull the surface potential for each base surface region to crossover regardless of the oxide charge distribution. The result will be a maximum I_{SO} contribution independent of the gate potential. This translates into a broadening so severe that the characteristics of the pre-irradiation curve are washed out. Figure 2.25 shows this effect.

To confirm these predictions, Sivo used a transistor in his gated transistor experiment that was processed with a high initial oxide charge. The gate was placed over part of the base surface area next to the E-B junction (the same as for the previous experiments). For the pre-irradiation case, we can assume that this oxide charge is distributed uniformly over the entire base surface region. We would expect that this built-in surface potential (ϕ_s) would act like a "built-in" gate voltage in the experimental data. Figure 2.28 shows the results of Sivo's experiment using this structure.

For increasing dose levels (up to 10^6 Rads), the peak is not broadened due to the relatively small radiation induced non-uniform oxide charge distribution added to a large process induced uniform distribution. The only effects of ionizing radiation on this device should be due to increasing surface state density (N_{ss}). The I_{SO} term should increase with radiation for each region of the base surface area.

After inversion (at high gate voltages), the increase due to radiation results partly from the I_{SO} contribution for the region at the end of the gate where the crossover is forced back to the surface and where a uniform increase in N_{ss} occurs. The width of this surface area is affected by the fringing fields at the end of the gate. Other contributions may come from $I_{D_{SW}}'$ when the field-independent build-up of N_{ss} changes the surface lifetime in the emitter.

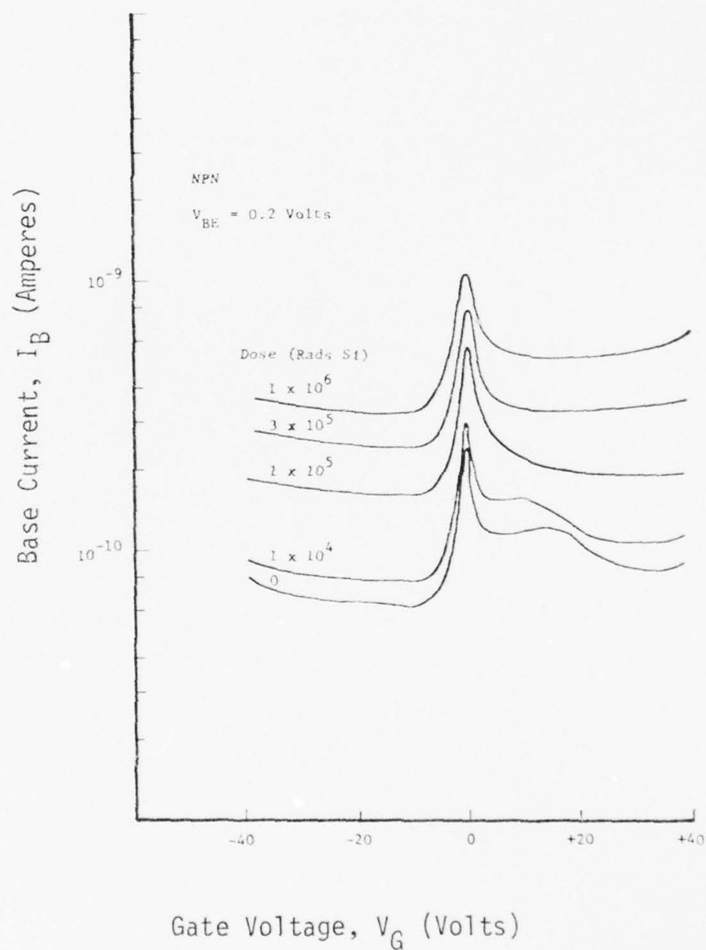

Figure 2.28. Example of the absence of substantial radiation induced broadening of the I_B peaks in a group of transistors which had a high initial oxide charge.[35]

Let us now use the model to predict the magnitude of the response of the gated transistors. We must first establish the lower limit on the base current for these transistors due to the "bulk" base terms (I_{RG}, I_{RB}, and I_D'). Table 2.3 defines the physical parameters. For V_{BE} = 0.26 volts;

$$I_{RG} = \frac{q \pi A_e \chi_e R_i n_i}{\ln\left(\frac{N_E N_B}{n_i^2}\right)} e^{\beta V_{BE}/1.5} = 3.6 \times 10^{-11} \text{ Amps}$$

$$I_{RB} = \frac{q A_e W_b n_i^2}{2 \tau_b N_B} e^{\beta V_{BE}} = 7.4 \times 10^{-14} \text{ Amps}$$

$$I_D' = \frac{q A_e D_p n_i^2}{(D_p \tau_e)^{1/2} N_E} e^{\beta V_{BE}} = 3.7 \times 10^{-13} \text{ Amps}$$

The predicted pre-irradiation lower limit of base current (I_{BLL}) is the sum of these terms. $I_{BLL} \approx 3.6 \times 10^{-11}$ Amps. The measured lower limit (assumed to be the minimum value on Figure 2.25(a) for zero radiation) was found to be $\approx 2.4 \times 10^{-11}$ Amps. The measured and predicted values compare very well considering the uncertainty in some of the physical parameters assumed for these transistors, especially R_i. We must subtract this lower limit base current from the total base current to estimate the contributions from surface terms in Figures 2.25 and 2.28.

Another term that can be assumed to be contributing to this pre-irradiation lower limit is I_{SO} for the surface region where the E-B depletion layer intersects the surface. This will be called $I_{SO(1)}$.

$$I_{SO(1)} = 1/2 \; q \, n_i \, A_{(1)} \, \sigma \, \upsilon_{th} \, N_{ss} \, e^{\beta V_{BE}/2} \text{ Amps}$$

$$= 1.1 \times 10^{-12} \text{ Amps,}$$

where $A_{(1)} = P_e \cdot X_{es}(cm^2)$ = surface area over E-B junction intersection with surface.

$I_{SO(1)}$ does not make a significant contribution to I_{BLL} for the pre-irradiation case.

The peak I_{SO} contribution for the transistors in Figure 2.25 (pre-irradiation) is;

$$I_{SO(PEAK)} = 1/2\ q\ n_i\ A_G\ \sigma\ v_{th}\ N_{ss}\ e^{\beta V_{BE}/2} \quad \text{Amps}$$

$$= 1.6 \times 10^{-9} \text{ Amps.}$$

The measured value for the peak was approximately 1.4×10^{-9} Amps, which is in excellent agreement.

Finally, for the region of base current at high gate voltages where the FIDL term is maximum,

$$I_{FIDL} = q \frac{\pi kT}{4q\ \phi_{FS}} X_{d_{max}}\ A_G\ n_i\ R_{is}\ e^{\beta V_{BE}/1.5} \quad \text{Amps}$$

$$= 2.8 \times 10^{-10} \text{ Amps.}$$

The measured value was approximately the same. Thus with the physical parameters assumed for Sivo's devices and the present collection of surface terms, we can describe each pre-irradiation portion of Figure 2.25.

Post-irradiation, the curves become more complex because of the broadening due to a non-uniform distribution of oxide charge and surface state build-up over the base surface region. Also the minority carrier concentration gradient becomes more severe undermining the uniform carrier concentration assumption.

If we use the low dose levels of 10^4 to 10^5 Rads, the broadening effects are minimized. For a dose level of 1×10^4 Rads, Sivo measures the ΔN_{SS} to be approximately 1.2×10^{10} states/cm^2 by using MOS structures.[36] With the value of ΔN_{SS} of 3.6×10^{10} states/cm^2 for 3×10^4 Rads, I_{SO} peak at a dose of 3×10^4 Rads would be predicted by the model to be four times that for pre-irradiation. Measured values show a factor of ≈ 3.5 increase in the peak I_B. Thus the radiation estimates using the peak I_{SO} term are very good at low dose.

The two important parameters that determine the base current are the surface potential ϕ_S, and the interface (surface) state density. At this time these parameters must be estimated in order to apply the model as a hardness assurance technique. As one approximation, we assumed that the interface state density builds up with the same field dependence as the trapped charge. The resulting field-dependent surface potential distribution (presented earlier in Figure 2.17(a)) was used in determining the added base current resulting from ionizing radiation for an ungated 2N2222 transistor. By assuming a simple approach for adding the contributions of I_{SO} and I_{FIDL} from 25 circular ring segments of this distribution vs. distance (ℓ) from the E-B junction, an estimate of ΔI_B for this 2N2222 model was obtained versus dose.† The predicted field-dependent surface contribution to I_B is shown in Figure 2.29.

The only experimental data for comparison was from the gated device (of the same type) shown in Figure 2.25. Experimental data from this figure produces Figure 2.30. The values were taken at $V_G = 0$. In comparing these two figures, we see that the rate of build-up of field dependent interface states is too slow to explain the sublinear line experimentally found.††

---

† An assumed uniform Q_{OX} of 1×10^{11} charges/cm^2 and N_{SS} of 8×10^9 states/cm^2 was used for the pre-irradiation condition.

†† One must remember that when comparing gated transistor data to model predictions based on an ungated transistor model, the gate will accent the predicted values.

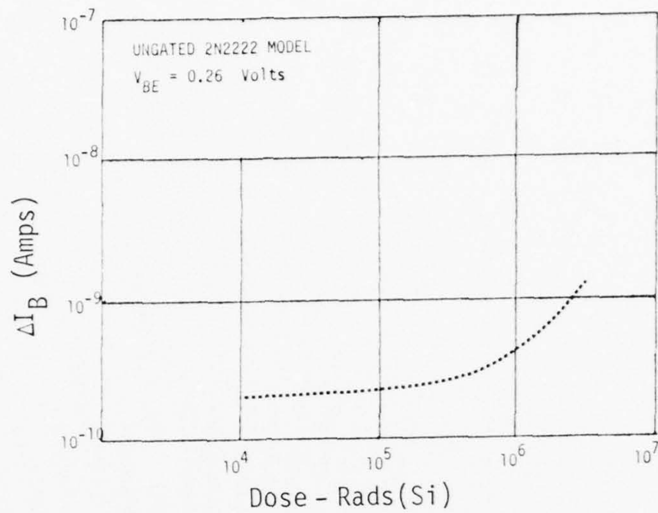

Figure 2.29. Predicted change in base current vs. dose for the ungated 2N2222 transistor model using only field-dependent build-up of Q_{ox} and N_{ss}† for doses greater than 10^4 Rads.

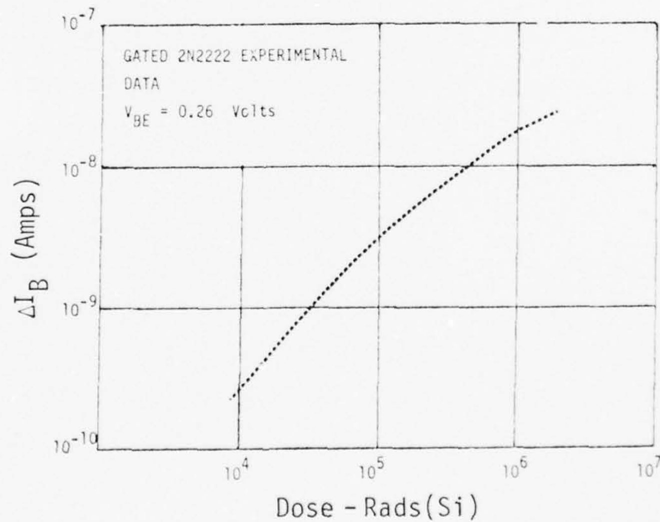

Figure 2.30. Experimental data from Figure 2.25 at V_G = 0 describing the change in base current vs. dose for a gated 2N2222 transistor.

---

† By taking the total number of surface states under the gate, we can determine ΔN_{SS}/dose used in the field-dependent curve (Fig. 2.29) as equal to 7.2 x 10^3 states/cm^2 - dose.

By comparing the total change in surface states measured by Sivo (ΔN_{ss} = 1.2 x 10^{10} states/cm^2 at 1 x 10^4 Rads(Si)) to the field-dependent ΔN_{ss} modeled for the ungated transistor, a conservative field-independent ΔN_{ss} estimate was obtained. The same technique was used at 10^5 Rads on the same data resulting in a consistant value of ΔN_{ss} (field-independent) per dose. This worst-case field invarient distribution was added to the field-dependent distribution and a new predicted value for ΔI_B was obtained. If we assume that the field-independent production of surface states is linear with dose, Figure 2.31 is obtained. The effect of the field-independent build-up on the surface area beyond the gate was also included in the calculation.

The added field-independent surface states cause ΔI_B to increase earlier with dose and actually cross through the data curve (see Figure 2.32). Since the increase in surface states (at higher doses) has the effect to "hold" the surface potential at crossover, the predicted curve flattens out at very high dose levels.

The rate of build-up is apparently too fast as exhibited by the "saturation" at 10^6 rads. A smaller field-independent interface state production rate and the addition of any field-independent trapped oxide charge build-up should result in a better comparison with the data. Both of these estimates will have to be defined by further MOS studies.

To determine if ungated transistors would compare more favorably with the model predictions (which evaluated the base current for an ungated transistor), another piece of data is presented. This data represents a group of Fairchild 2N1613 transistors.[37] These devices were used by Sivo to show the effect of the bias from the collector-base (C-B) junction on the base current increase due to ionizing radiation. The hypothesis that the C-B junction fields can extend into the ambient above the chip and increase the density of holes injected into the oxide over the base surface

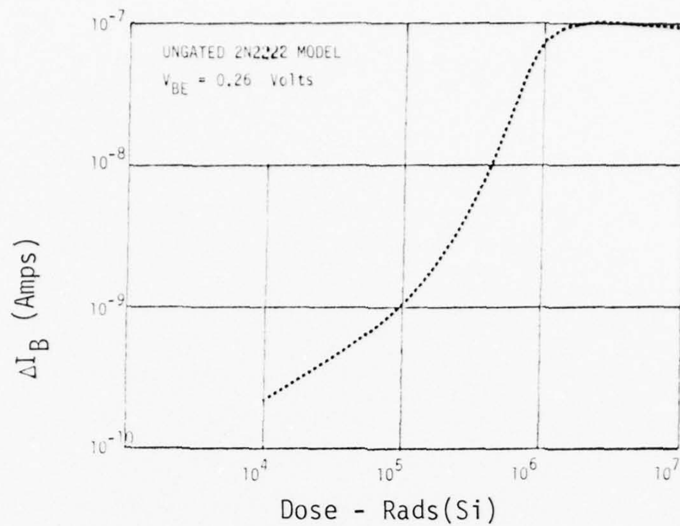

Figure 2.31. Predicted change in base current vs. dose for the ungated 2N2222 transistor model using the field-dependent build-up of Q_{ox} and N_{ss} plus a super-position of a field-independent $\Delta N_{ss} = 1.2 \times 10^6$ states/cm^2 per dose.

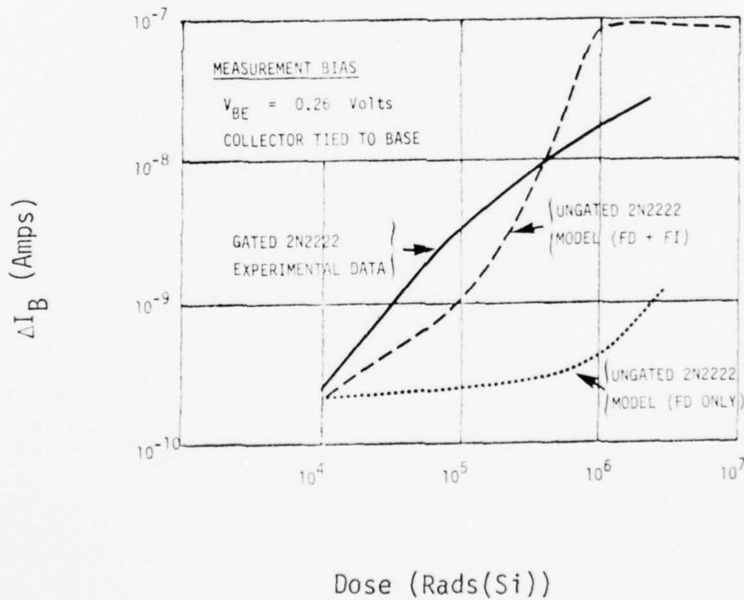

Figure 2.32. Combination of gated transistor experimental data with two cases considered by the model for an ungated transistor of the same type. Field dependent (FD) build-up of Q_{ox} and N_{ss} are considered with and without the addition of field-independent (FI) build-up of N_{ss}.

region was confirmed by previous Boeing experiments. If we assume that, for the active device, a large reverse bias is applied to the C-B junction and that the additional holes injected into the base region oxide by the C-B junction field effects were distributed uniformly, then the effect of the C-B junction is to add a large uniform (E-B field-independent) build-up of N_{ss} to the base surface region. Figure 2.33 shows the resultant change in base current for the active (biased) and passive (unbiased) irradiation bias conditions. Our assumptions used to obtain the ungated 2N2222 model prediction (FD + FI) curve in Figure 2.32 appear to be reasonable considering that we used a conservative field independent build-up of N_{ss}. The unbiased experimental data for the Fairchild 2N1613 shows that the actual dependence of ΔI_B on the build-up of Q_{ox} and N_{ss} is somewhere between the assumptions of field-dependent mechanisms only and the addition of large field-independent mechanisms. The data also shows that to predict the worst-case degradation to the DC gain for moderate dose levels, large field-independent mechanisms must be assumed by the user in order to account for possible C-B junction effects. Therefore, Table 2.2 can be used with the model to upper bound the long-term ionization effects. If supplemental information is known about the device construction (i.e., the ambient in the device package above the chip is not conducive to ionization effects or a metallization layer is placed over the C-B junction oxide to restrict the extension of the C-B junction field lines above the oxide) then this additional conservative approach can be relaxed.

By using the device data represented in Figure 2.28, estimates can also be made of the effects from increasing values of N_{ss}. The devices represented in this figure had a high oxide charge fabricated into the device (assumed uniform); the process induced surface state density was unknown. At zero gate voltage, the pre-irradiation oxide charge has forced the entire base surface region to crossover. Therefore, $I_{SO(PEAK)}$ pre-irradiation is independent of the gate area and the uniform built-in N_{ss} over the entire base region can be approximated. The model predicts;

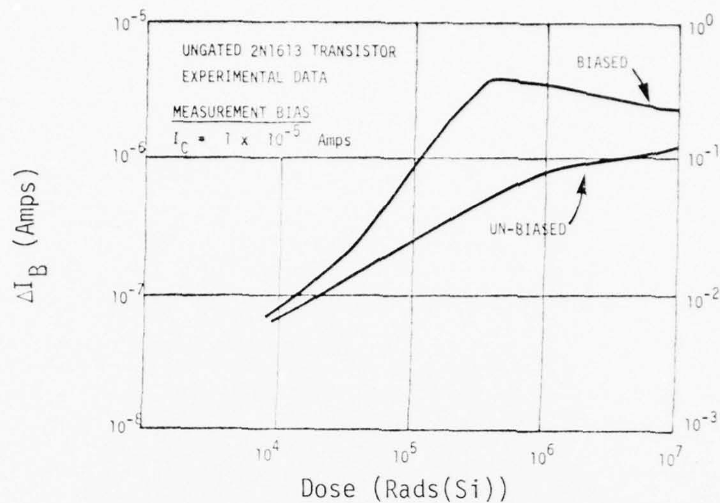

Figure 2.33. Ungated transistor experimental data for a Fairchild 2N1613 device type.[37] Biased conditions refers to the device being active during irradiation. Unbiased refers to the passive condition. Note that the measurement bias represents a higher V_{BE} (i.e., $V_{BE} \approx 0.5$ Volts) than for the 2N2222 data presented in Figure 2.32. Also, this device type showed a large C-B junction effect.

$$I_{SO(PEAK)} = 1/2\ q\ n_i\ A_b\ \sigma\ v_{th}\ N_{ss}\ e^{\beta V_{BE}/2} \quad \text{Amps}$$

$$= 4.4 \times 10^{-20}\ N_{ss}\ \text{Amps},$$

where $A_b \approx A_G \pm 20\%$ †

The measured peak I_{SO} (Figure 2.28) was approximately 1.6×10^{-10} Amps. This indicates that $N_{ss}(0) \approx 3.8 \times 10^9$ states/cm^2 and implies that in the

† The area of the base surface region for this high oxide charge case can be approximated by assuming that the base current curves to the left of the peak are the result of the gate voltage countering the built-in oxide charge under the gate. Thus for the pre-irradiation case, the ratio of the peak base current to the lowest base current value (to the left of the peak) is approximately the ratio of the entire base surface area to the base surface area beyond the gate (over to the base contact). This ratio was calculated to be ≈ 5.4. Thus the entire base surface area can be approximated to be equal to the gate area over the base (A_G) with only a maximum of a 20% error. We have assumed that $I_{SO(1)}$ is still small for the pre-irradiation case.

processing of higher oxide charge, the effective interface states density was reduced.

In the post-irradiation case (10^4 Rads) for the normally processed device, the peak I_{SO} increased by 1.4×10^{-9} Amps while the initial high oxide device showed an increase in the peak I_{SO} of 6.6×10^{-11} Amps. (NOTE: the high oxide device was tested at a lower V_{BE}.) If the assumption is made that N_{ss} is the only parameter to vary with dose when I_{SO} is peaked, i.e., that the relative minority carrier surface profile does not change and that the recombination cross-sections are radiation invarient, then the change in N_{ss} is approximately 1×10^{10} states/cm^2 for the normal device. This compares favorably to that given by Sivo measured on a MOS structure. The same calculation for the high oxide device yields a ΔN_{ss} of 1.5×10^9 states/cm^2. From this, the conclusion could be drawn that the rate of radiation induced interface density creation is dependent on the initial values of oxide charge. The accuracy of the two assumptions used to get this conclusion still needs to be determined as discussed earlier. The results of MOS studies may help to evaluate the validity of these conclusions.

The above analysis is an example of how the model may be used to analyze available data, and possibly generate relationships between physical parameters and radiation effects to develop hardness assurance techniques. The analysis also points out that a dependency on oxide processing exists, which has been known for some time.

2.2.3.2 Bias Effects During Irradiation. Experimental data has shown that the bias applied during irradiation has an effect on the degradation of DC gain.[25] Figure 2.34 is a good example. We observed that for a bipolar transistor the built-in E-B junction produced electric fields in the oxide. These fields provided the conditions necessary to increase the probability for separation of holes and electrons from ionizing radiation interaction in SiO_2. Applying V_{BE} modifies the field in the oxide by adding to (reverse

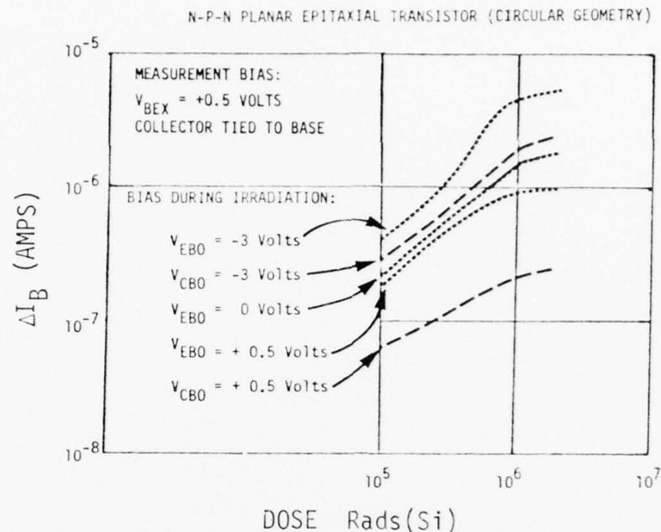

Figure 2.34. Normalized base current increase vs. total gamma dose for devices with varying junction electric field strengths during irradiation.[25]

bias) or subtracting from (forward bias) the built-in junction potential. Therefore, since higher fields in the oxide produce higher generation of free holes to influence the surface potential, we would predict that reverse-biasing the E-B junction is the worst case condition for hardness assurance screens.

Figure 2.34 also shows that for higher reverse-biased E-B junctions, the field-independent build-up of Q_{ox} and N_{ss} cannot be ignored. This fact was seen earlier in the model predictions when a large radiation-induced field-independent build-up of both Q_{ox} and N_{ss} had a significant effect with the same shaped curve.

Another important junction effect has been experimentally identified. It is the increase in base current by reverse biasing the collector-base (C-B) junction. This condition produces large field lines that extend into the higher oxide layers and into the ambient space above the chip. Sivo has reviewed the available data that supports this model and reviews the techniques currently used to eliminate this C-B bias dependence.[37] The two

most popular techniques are to (1) reduce the atmosphere over the chip to a low ionizing medium, and (2) extend the base metal over the C-B junction so that the field lines are confined to the localized base region near the C-B junction.†

The worst degradation of DC gain (experimentally) in a n-p-n transistor occurs when both junctions are reverse-biased during irradiation. The gain degradation was experimentally shown to be smallest for a saturated device where both junctions are forward-biased (hence a smaller field) during irradiation.[23] Therefore the predicted dependency of surface potential on the applied voltage during irradiation appears to be valid.

2.2.3.3 Process Variations. Both intentional and unintentional process variations in the oxide properties can have a large effect on proposed hardness assurance screens. We saw in the last two sections that the trapped oxide charge can result from direct radiation hole-electron generation or from indirect charge transfer at the surface of the oxide. By applying various layers of oxide materials, these rates of charge buildup can be changed significantly. Stanley discussed the changes produced by glassivation layers and various doping techniques in the oxide.[39] All have their advantages and disadvantages.

Process variations that are unintentional can be referred to as differences in processing techniques (i.e., equipment, quality control, etc.). By reducing the contaminants at the interface between the $Si\text{-}SiO_2$ layers, the number of surface states is reduced. Non-uniformity of this contamination may result in high surface state generation in a random distribution by the radiation. Also the number of surface states activated by the ionizing radiation may be reduced. The result of these concepts may explain the existence of "Mavericks" (or "outliers").[40] These devices deviate (sometimes wildly) from the radiation response of near neighbor devices. Since the surface potential and surface state distribution are so important to the model, changes in the expected distributions by these random discontinuities would cause differences in the radiation response. The above

† It was found that the gated devices were harder than non-gated devices of the same type and on the same wafer.[38]

variations may also show why, in the past, attempts to relate oxide charge build-up to fixed surface state densities have failed.[41] Process variations are therefore a very important consideration in developing any hardness assurance procedures.

2.3 Other Bipolar Structures and Applications

In this section we discuss the extension of the model to other bipolar structures (p-n-p transistors, JFETs and diodes, and integrated circuits) and a quick look at the implications for the saturation case (i.e., $V_{CE(SAT)}$). As we will see, p-n-p transistors can be modeled similarly to n-p-n except that a different region is predominant in describing the ionizing radiation effects. For $V_{CE(SAT)}$ little can be said due to the lack of accurate models describing the saturation mechanisms. In previous reports on neutron displacement damage,[4,17,42] the general models proposed for saturation by several sources were shown to be ineffective in predicting changes in $V_{CE(SAT)}$. The point where a transistor is no longer in saturation (i.e., forced gain equals the natural gain) appears to be the sole existing accurate model in the $V_{CE(SAT)}$ case. We would expect the natural-gain base-current terms to be useful for this case.

Diodes and JFETs show changes in the reverse current and breakdown voltage, but the JFET is much more susceptible to ionizing radiation than the diode. This is because the JFET also shows significant changes in the gate leakage current, drain-to-source current and the pinch-off voltage at 10^5 Rads(Si) and above.

Finally a section on bipolar ICs is presented which describes briefly the impact of these modeling efforts in more complex structures.

2.3.1 P-N-P Transistor DC Gain Degradation

Now that we have described a model that incorporates the surface effects on n-p-n transistors, it is reasonable to expect the same physics to be applicable to p-n-p transistors. An assumption is made that there is no dopant interaction with the oxide growth that is different for n- or p-type material. Then the main difference between n-p-n and p-n-p transistors that must be recognized is that the field lines in the oxide generated by the E-B junction near the surface force the ionizing radiation-induced trapped holes to the emitter side of the junction (now the p-type material). This means that positive oxide charges can induce a space-charge region over the emitter rather than the base. Therefore, the E-B junction can widen into the emitter and the intersection of the E-B metallurgical junction with the surface term will increase in importance. The widening process is not as severe as was the case of the n-p-n transistor due to the higher doping in the emitter (compared to the base). Even so, the widening is more severe than a 10^{20} cm^{-3} average surface dopant density of the emitter would indicate. The construction of the emitter usually is done by a diffusion process through a window cut into the oxide. Since the diffusion of dopant is not limited to the vertical direction, a diffusion gradient can develop laterally along the surface under the protective oxide (in the same fashion as for n-p-n transistors). This makes the emitter less heavily doped at the surface next to the E-B junction and allows the widening to be greater for moderate positive charges trapped in the oxide.

It also makes I_D' near the surface much more significant than for n-p-n transistors. With a positive gate bias placed over the emitter surface (or positive surface potential increasing for higher dose levels), the effective emitter doping decreases. This effect occurs just near the E-B junction where the doping is least due to the lateral diffusion in the emitter. Thus, considering positive oxide charge effects, the $I_{D_{SW}}'$ term should become more significant at a lower gate voltage for the post-irradiation case. If we now add the effect of increasing surface states, the minority carrier lifetime at the surface, τ_s, will also be a factor that makes $I_{D_{SW}}'$ more significant.

Field-independent generation of oxide charge and surface state density build-up over the entire surface (base regions as well as emitter regions) will therefore be a critical parameter for evaluating ionizing radiation effects in p-n-p transistors. Modeling for p-n-p transistors still needs to be completed. Ionizing radiation effects in p-n-p gated transistors are shown in Figure 2.35. This figure shows similar curves to those presented earlier for the gated n-p-n transistor structure but the shape is reversed. The accumulation portion of the curve will be most important for predicting post-irradiation effects in p-n-p transistors.

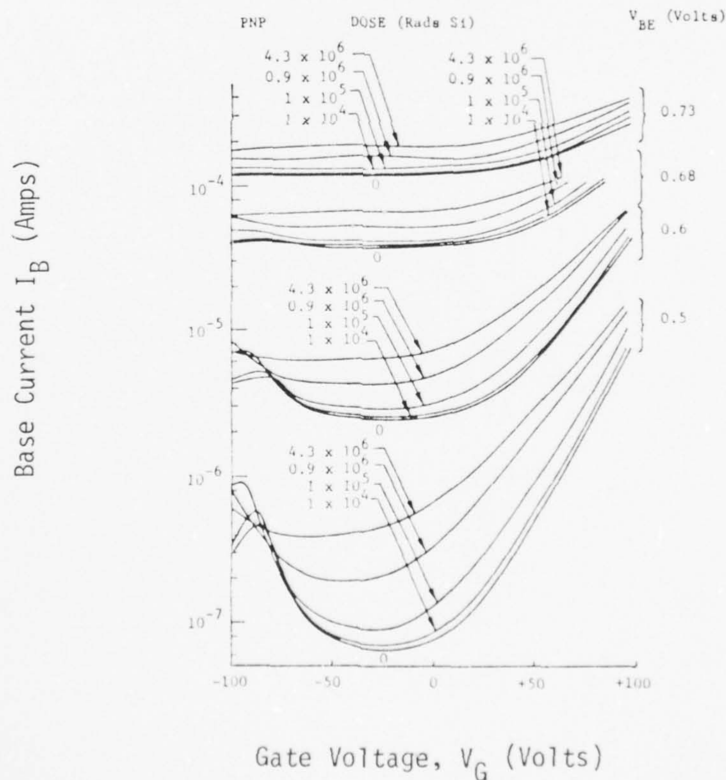

Figure 2.35. Effect of ionizing radiation on the I_B vs. V_G curves of a p-n-p transistor at various injection levels.[43]

AD-A064 136 MISSION RESEARCH CORP LA JOLLA CA F/G 9/1
HARDNESS ASSURANCE FOR LONG-TERM IONIZING RADIATION EFFECTS ON --ETC(U)
MAR 78 A R HART, J B SMYTH, J P RAYMOND DNA001-76-C-0201
UNCLASSIFIED MRC/SD-R-23 DNA-4574F NL

2 OF 2

AD
A064136

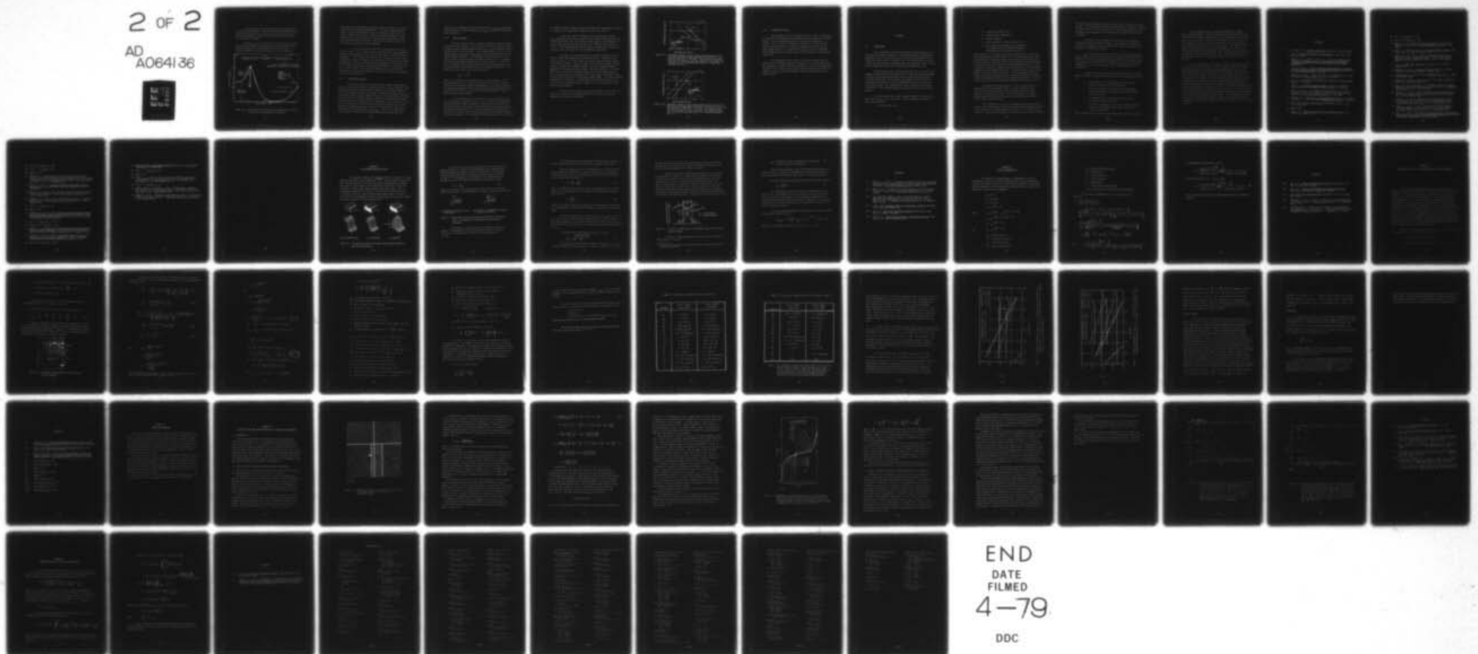

END
DATE
FILMED
4-79
DDC

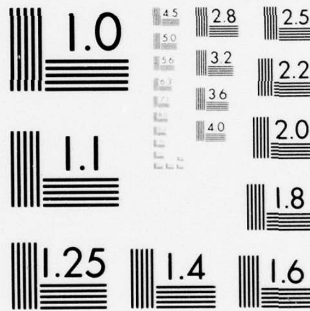

MICROCOPY RESOLUTION TEST CHART
NATIONAL BUREAU OF STANDARDS-1963-A

Positive charge in the oxide produced by ionizing radiation acts like a positive gate voltage. Figure 2.36 shows the usual interpretation of a gated p-n-p transistor curve. Since the p-n-p transistor has a n-type base, field-independent N_{ss} build-up over the base may force the base to less n-type near the surface.

Both the $I_{D_{sw}}'$ and the RG contribution related to the E-B junction intersecting the surface are predicted to be significant factors in determining the surface base current contribution in p-n-p trnasistors. A logical implication to this prediction would be that p-n-p transistors

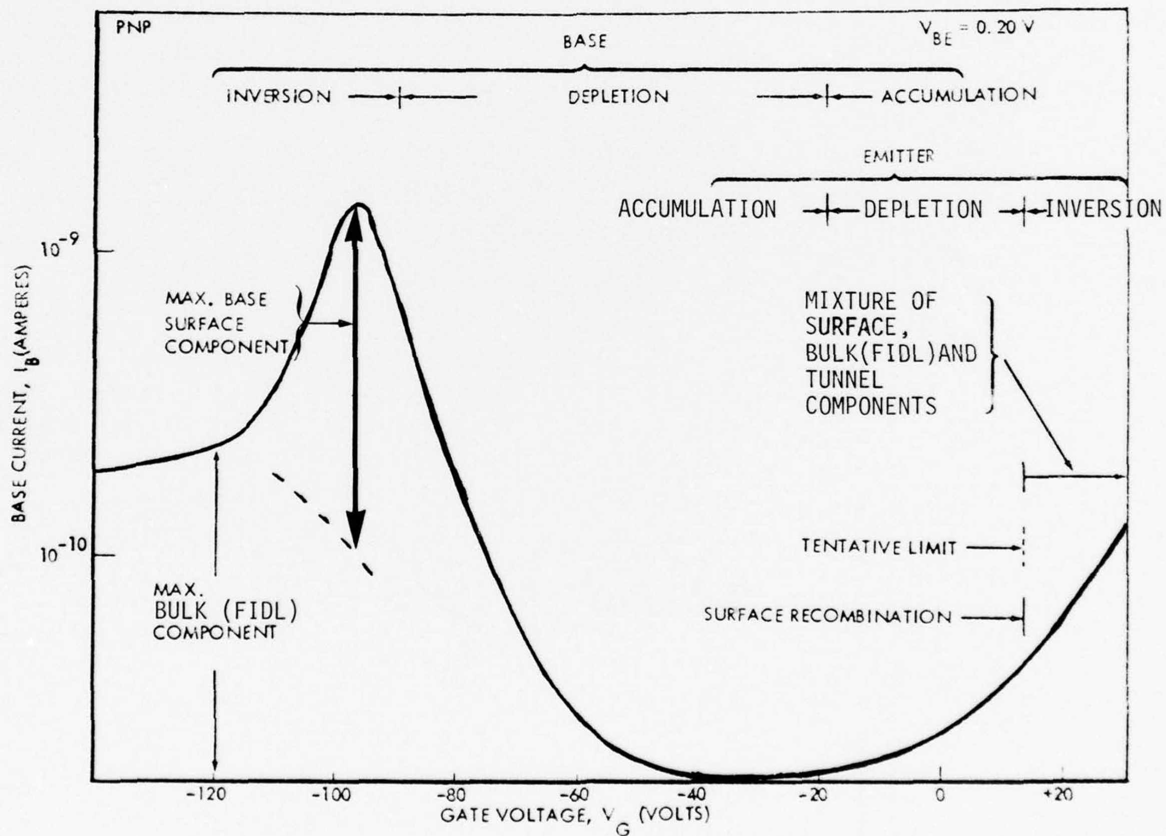

Figure 2.36. Illustration of the various current components of I_B in the I_B vs. V_G plot of an unirradiated p-n-p transistor.[44]

with large emitter peripheries would have the largest effect. This model prediction was verified experimentally.[45] For p-n-p transistors (all grown at the same time under very similar conditions), devices with the largest periphery were the most sensitive to ionizing radiation. Also everything else equal, the devices with the largest periphery-to-emitter area ratio were the most sensitive. More work is required in this area to confirm the existence of these mechanisms.

Up to this point, we have only considered the region near the E-B junction. If we consider the C-B junction region, I_{CBO} degradation could be a real problem in p-n-p's even at low doses; in fact, even before irradiation. This is due to the fact that the collector is lightly doped. Consequently, surface inversion can be introduced by relatively small charge accumulation. However, in order to avoid I_{CBO} problems associated with the initial fixed oxide charge, the manufacturers diffuse a P^+ guard ring into the collector surface close to the C-B junction to stop the inversion. Fortunately, this step also eliminates in most cases, serious I_{CBO} problems, at both low and high doses.[46]

2.3.2 Saturation ($V_{CE(SAT)}$)

We saw for the n-p-n transistor that the current crowding mechanisms were delayed and softened in importance due to ionizing radiation. Some theories have been discussed previously related to the possible importance of current crowding for explaining changes in saturation voltages ($V_{CE(SAT)}$).[3] If the oxide charge creates a depletion layer at the surface which acts as an extension of the E-B junction sidewall, then the ionizing radiation effects on the saturation case could possibly be explained. With an increase in sidewall area added to the emitter area and with crowding forcing the current through the periphery region of the emitter, an increase in sidewall area could reduce the crowding effects on $V_{CE(SAT)}$. The result is that higher oxide charge and shallow emitter depths will possibly provide the most

effective way of reducing the sensitivity of devices to $V_{CE(SAT)}$ degradation. More work needs to be done on modeling the $V_{CE(SAT)}$ mechanisms to confirm the above speculation.

2.3.3 JFETs and Diodes

Two basic types of JFETs are usually considered: junction isolated and dielectrically isolated. For an n-channel junction isolated JFET, large increases in gate-to-source leakage currents (I_{GSS}) can be caused by relatively low dose levels ($\approx 10^5$ Rads(Si)).[47] This leakage current is a result of the lightly doped n-region and a strong function of the bias applied to the gate junction during irradiation. The mechanisms for this effect appear to be similar to those discussed earlier for bipolar transistors (i.e., a build-up of positive oxide charge and an increase in surface states). At this dose level, some devices show a minimum increase of an order of magnitude in I_{GSS} due to an increase in the surface potential and surface state density. At higher total dose levels, I_{GSS} can vary with dose as

$$I_{GSS} = (K \cdot D)^n$$

where K is a constant, D is the dose and n is a factor between 2 and 5.[47] The extreme case is when an inversion layer forms at the surface. Changes in the saturation current, channel transconductance and pinch-off voltage do not appear to be affected by the long-term ionizing radiation effects for dose levels below 10^8 Rads(Si). This is due to their relationship to location within the bulk silicon material.

For the dielectrically isolated JFET, the long term effects from ionizing radiation are much more severe. This is because of the added interface formed directly under the channel in the dielectrically isolated (DI) region which allows trapped charge and interface states to form and influence the channel parameters directly. The same mechanisms as discussed for the surface oxide also apply for the isolation region but an additional mechanism can eventually dominate. This mechanism is described by Neamen as the build-up

of trapped electrons (negative charge) for higher dose and apparently reduces the effect of the trapped holes produced at lower dose levels.[48]

At dose levels above 10^5 Rads(Si) the drain-to-source current (I_{DSS}) and pinch-off voltage ($V_{GS}(off)$) increase dramatically with dose level for n-channel JFETs (DI). This increase peaks around 4×10^6 Rads(Si) for several tested devices and then decreases to or below the pre-irradiation levels.[48] The transconductance did not change as dramatically with dose in the same tested devices but it still followed the same trend.

For diodes, the same mechanisms as discussed for transistors are used to explain the changes due to ionizing radiation. Depending on the structure (n^+-p or p^+-n), oxide charge and surface states can produce changes in the reverse currents. Also, the effects on the effective dopant near the surface can change the breakdown voltage. Since the breakdown voltage is dependent on the doping on the lower doped side of the junction, a p^+-n diode would show a decrease in breakdown voltage due to oxide charge build-up. This is because the positive charges in the oxide reduces the dopant in the p^+ region (which makes the n region appear higher doped). The reverse analysis would hold for a n^+-p diode. The same effect can be created by the use of a gate over the lower doped region. Figures 2.37 and 2.38 show this effect from ionizing radiation.

The result of this analysis of JFETs and diodes is that JFETs are relatively insensitive to ionizing radiation while diodes have the same mechanisms as defined for transistors.

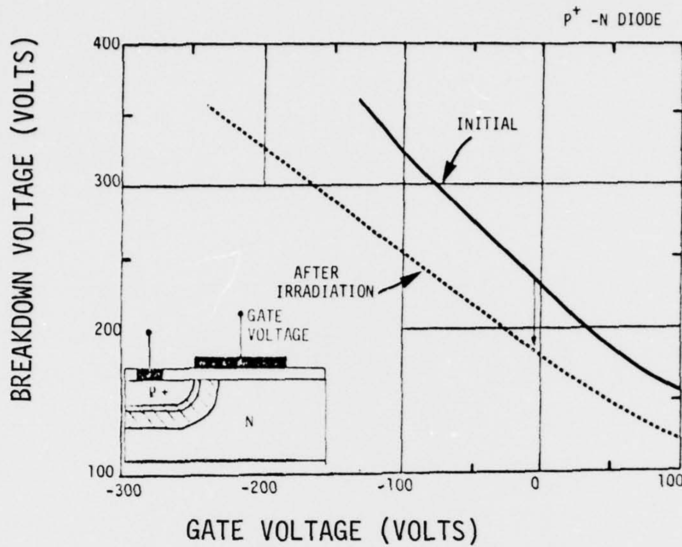

Figure 2.37. Breakdown voltage vs. gate voltage characteristics of a p^+-n gate controlled diode before and after X-irradiation.[49] The radiation dose was 3 x 10^5 Rads. The device was irradiated with +45 volts applied to the gate and V_J=0. The doping concentration of the n-substrate was $5x10^{14}$ cm^{-3}; the oxide thickness was 0.8 μ.

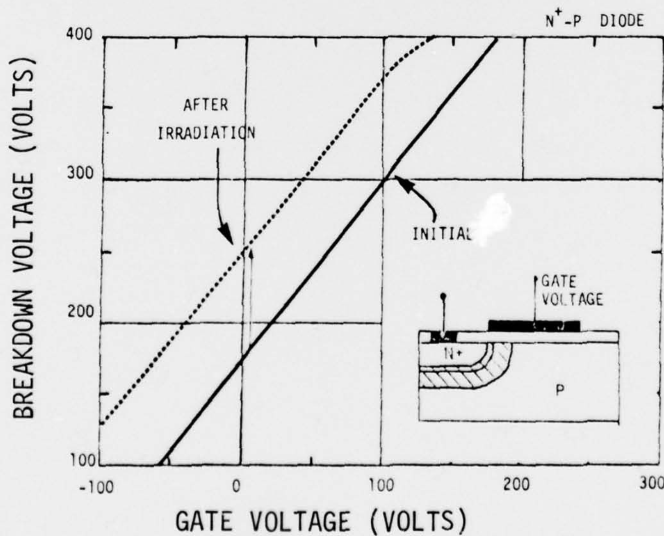

Figure 2.38. Breakdown voltage vs. gate voltage characteristics of an n^+-p gate-controlled diode before and after X-irradiation.[49] The radiation dose was $1.5x10^5$ Rads. The device was irradiated with +10 volts applied to the gate and V_J=0. The doping concentration of the p-substrate was $5x10^{14}$ cm^{-3}; the oxide thickness was 1.2 μ.

2.3.4 Integrated Circuits

One assumption used in the analysis of n-p-n and p-n-p transistors was that they represented the basic bipolar mechanisms found in all bipolar devices. The only difference would be in the physical parameters. At present, we see no reason to change this assumption. In fact, the data used to verify the analysis for emitter crowding appears to verify the above generalization (i.e., elements (transistors) of an I^2L integrated circuit showed the same radiation effects at high currents as did discrete transistors).

For integrated circuits (ICs), we can expect to make the same application of the models discussed in Section 2.2. We would expect even more dependence on geometry due to the complexity and size requirements and especially due to the low current levels usually desired for low power consumption. This low current requirement increases the importance of the surface effects.

SECTION 3

3.0 CONCLUSIONS

This investigation assessed the theoretical understanding of surface effects in bipolar structures. Estimations were made on key physical parameters such as the electric field in the oxide, distribution of oxide charges and traps and their production rate. The formulation of the means to use these relationships in hardness assurance applications leads to a comparison between the theoretical calculations and experimental data.

The theoretical model predictions made for the un-irradiated case compared favorably with the experimental data. Minor discrepancies between the higher V_{BE} predicted and measured values for gate voltage necessary to maximize the surface velocity term, I_{SO}, appeared to be the result of assuming that the minority carrier concentration was constant across the base surface region. This assumption was used to simplify the evaluation of the model. A more rigorous approach would most likely correct this difference.

The radiation inclusive model compared favorably with the low V_{BE} data and higher V_{BE} (at low dose) data. Critical parameters determined under these conditions:

a) surface potential, ϕ_s,

b) surface state density, N_{SS},

c) acceptor dopant concentration,

d) emitter periphery,

e) emitter periphery - emitter area ratio, and

f) base surface area (between the E-B junction and base contact) for n-p-n transistors and the emitter and collector surfaces for p-n-p's.

The distributions of the surface potential and surface states over the base and E-B metallurgical junction regions (for n-p-n transistors) and over the E-B metallurgical junction and emitter regions (for p-n-p transistors) are extremely critical. Estimates of these critical parameters must be generated for accurate predictions, especially at low and moderate dose levels. This is because the build-up of trapped oxide charge was found to be an important parameter for low to moderate dose levels. The surface state density becomes dominant at moderate to high dose levels. To match experimental data the surface state density distribution had to assume a significant uniform,field invariant build-up in addition to the field dependent mechanisms. Thus even for low field regions in the oxide, large changes in base current can occur.

The dopant of the p-type material is also an important factor in determining the gain degradation effects. For n-p-n transistors, the greater the base doping, the more surface potential required to induce increases in surface base currents. For p-n-p transistors, the emitter doping concentration plays an important role in determining the increase in base current expected per dose.

These statements are based on the assumption that positive charge is induced in the oxide and, that a positive surface potential increases with dose. At low currents this assumption appears to be valid. At high currents, the "effective" surface potential decreases with higher dose in the gated transistor

data indicating an unknown dependency near the surface, possibly injection related. This fact had not previously been noted and is important in applying the models correctly to these structures. For the normal transistor, this new effect does not appear to be as dominant and the model may be useful as defined.

The other critical parameters identified for use in hardness assurance controls were geometry related. They determine the magnitude (and thus the importance) of each surface base current term under various conditions of application and dose.

For other types of bipolar structures, the same basic mechanisms can be assumed. The effects on each type of structure will depend on the dominance of a particular mechanism for that structure and its application. The comparisons will rely heavily on assumptions of some of the critical parameters (e.g., the lateral surface emitter doping profile for p-n-p transistors).

Estimates which are required for direct application of existing models to predict the long-term ionization response of bipolar transistors are:

1) the interplay of the oxide charge with the interface density to produce the surface potential,

2) the rate of buildup of the uniform field-independent and field-dependent oxide charge and interface density in bipolar devices,

3) the minority carrier concentration at the surface of the base and/or emitter, and

4) the effect of the gate, if any, on the surface potential, interface state build-up, oxide charge or minority carrier concentration.

These estimates have not previously been addressed by other investigators.

Future experiments need to provide information on a number of the assumed parameters. We need to know the energy distribution of N_{ss} in the band gap. More MOS studies may aid in determining the true mechanism(s) of N_{ss} generation. Needed yet are estimates of cross-sections and their dependencies (if any) on V_{BE} and radiation. The surface potential as a function of radiation is, of course, essential. The problem is compounded by needing the minority carrier concentration as a function of position to calculate the recombination rate, but the carrier concentration is dependent on the recombination rate. This is needed for both the base and the emitter regions so that both n-p-n and p-n-p device types may be explored.

For the application of this model in hardness assurance techniques, the restrictions are not as great. This is because a hardness assurance calculation usually only requires some upperbound which a designer can use to estimate the need for shielding or other design "tricks" to qualify the design for the system. In this report we have shown that (for n-p-n transistors) by identifying the surface geometry of the transistor elements in bipolar devices, measuring the base doping through the emitter-base breakdown voltage, and using the worst case values for the build-up of Q_{ox} and N_{ss}, an upperbound calculation is possible. It remains to form this into a more useful method and to determine in more detail by experimentation some of the assumptions that had to be made before the method could be generalized to p-n-p transistors and other bipolar devices. This program has therefore taken a major step toward developing a hardness assurance technique that is based on the basic physics of the device and its interaction with ionizing radiation.

REFERENCES

1. Phillips, A. B., Transistor Engineering, Mc-Graw-Hill, New York (1962).

2. Larin, Frank, Radiation Effects in Semiconductors, John Wiley & Sons, New York (1968).

3. Hart, A. R., J. B. Smyth Jr., and V. A. J. van Lint, Parameter Sensitivities for Hardness Assurance: Displacement Effects in Bipolar Transistors, MRC/SD-R-20, Mission Research Corporation/San Diego, December 1977.

4. Blice, R. D. and J. A. Manarin, Neutron Hardness Assurance for Bipolar Transistors through Determination of Physical Parameters, AFWL-TR-74-327, Air Force Weapons Laboratory, July 1976.

5. Shockley, W., and W. T. Read, "Statistics of the Recombination of Holes and Electrons," Physics Review, Vol. 87, p. 835 (1952).

6. Hall, R. N., "Electron-Hole Recombination in Germanium," Physics Review, Vol. 87, p. 387 (1952).

7. Sivo, L. L., Transistor Nonlinear Damage, Document No. D180-14225-1 (under Contract No. ONR-N00014-72-C-0026), Boeing, p. 27, May 1972.

8. Grove, A. S., and D. J. Fitzgerald, "Surface Effects on p-n Junctions: Characteristics of Surface Space-Charge Regions under Non-Equilibrium Conditions," Solid State Electronics, Vol. 9, p. 783 (1966).

9. Mitchell, J. P., IEEE Trans. on Electronic Devices, ED-14, p. 764 (1967), and Grove, A. S., and E. H. Snow, Proceedings IEEE, Vol. 54, p. 894 (1966).

10. Sze, S. M., Physics of Semiconductors, John Wiley & sons, Inc., New York (1969) p. 27.

11. Ibid., p.432.

12. Grove, A. S., Physics and Technology of Semiconductor Devices, John Wiley & Sons, (1967) p. 268.

13. Sze, S. M., op. cit., p. 436.

14. Grove, A. S., op. cit., p. 302.

15. Reddi, V. G. K., "Influence of Surface Conditions on Silicon Planar Transistor Current Gain," Solid State Electronics, Vol. 10, p. 305 (1967).

16. Many, A., Y. Goldstein, and N. B. Grover, Semiconductor Surfaces, John Wiley & Sons, Inc., New York (1965) p. 200.

17. Smyth, J. B., Jr., V. A. J. van Lint, "Parameter Sensitivities for Hardness Assurance: Displacement Effects in Bipolar Transistors," IEEE Trans. on Nucl. Science, Vol. NS-24, No. 6, p. 2093, December 1977.

18. Sivo, L. L., IEEE Trans. on Nucl. Sci., NS-19, No. 6, p. 313-319 (December 1972).

19. Bruncke, W. C., et. al., Report No. 03-74-33, Final Contract Report N00164-73-C-0420, Texas Instruments (November 1974).

20. Fitzgerald, D. G., and A. S. Grove, Proceedings IEEE, Vol. 54, p. 1601-1602 (November 1966).

21. Brown, G. A., Report No. 03-77-10, Contract Final Report, N00164-75-C-0280, Texas Instruments (March 1977).

22. Snow, E. H., A. S. Grove, and D. J. Fitzgerald, "Effects of Ionizing Radiation on Oxidized Silicon Surfaces and Planar Devices," Proceedings IEEE, Vol. 55, No. 7, p. 1174 (July 1967).

23. Nelson, D. L., and R. J. Sweet, "Mechanisms of Ionizing Radiation Surface Effects on Transistors," IEEE Trans. on Nucl. Sci., Vol. NS-13, No. 6, p. 197 (December 1966).

24. Winokur, P. S., et. al., "Dependence of Interface State Buildup on Hole Generation and Transport in Irradiated MOS Capacitors," IEEE Trans. on Nucl. Sci., Vol. NS-23, No. 6, p. 1580 (December 1976).

25. Goben, C. A., and C. H. Irani, "Electric Field Strength Dependence of Surface Damage in Oxide Passivated Silicon Planar Transistors," IEEE Trans. on Nucl. Sci., NS-17, No. 6, p. 18 (December 1970).

26. Sah, C. T., and L. C. Sah, Origins of Interface States and Oxide Charges Generated by Ionizing Radiation in Metal-Oxide Structures, HDL-CR-76-164-1, Harry Diamond Laboratories, p. 54 (January 1976).

27. Sze, S. M., op. cit., p. 454.

28. Sivo, L. L., op. cit., p. 40.

29. Ibid., p. 113.

30. Bauerlein, R., "Investigation of the Surface Ionization Effect on Planar Silicon Bipolar Transistors and the Improvement of the Resistance to Radiation by an Irradiation-Annealing Treatment," IEEE Trans. on Nucl. Sci., NS-17, No. 6, p. 52 (December 1970).

31. Srour, J. R., et. al., Radiation Effects on Semiconductor Materials and Devices, Harry Diamond Laboratories Tech. Report,171-4, p. 97, December 1973.

32. Measel, P. R., and R. R. Brown, "Low Dose Ionization-Induced Failures in Active Bipolar Transistors," IEEE Trans. on Nucl. Sci., NS-15, No. 6, p. 228 (December 1968).

33. Raymond, J. P., and R. L. Pease, "A Comparative Evaluation of Integrated Injection Logic," IEEE Trans. on Nucl. Sci., NS-24, No. 6, p. 2331 (December 1977).

34. Sivo, L. L., op. cit. p. 53.

35. Ibid., p. 42.

36. Greegor, R. B., and L. L. Sivo, Effects of Process Variations on Total-Dose Sensitivities of Bipolar Oxides, Document No. D180-20519-1 (under Contract ONR-N00014-76-C-0678 available from Director, NRL, Washington, D.C.) Boeing, p. 20 (April 15, 1977).

37. Sivo, L. L., op. cit., p. 55 - 58.

38. Greegor, R. B., op. cit., p. 1174.

39. Stanley, A. G., Correlation of Surface Structure and Ionizing Radiation Effects on Bipolar Transistors, JPL Letter Report 900-778 (Contract NAS7-100 for DNA), Jet Propulsion Laboratories, p.4 (February 1, 1977).

40. Stanley, A. G., and K. E. Martin, Statistical Analysis of Long-Term Ionization Effects on Bipolar Transistors, JPL Report 365-J-46-76, (Preliminary); Jet Propulsion Laboratories (November 23, 1976).

41. Snow, et. al., op. cit., p. 1174.

42. Radiation Effects on Semiconductor Devices, HDL-DS-77-1, Harry Diamond Laboratories, p. 74 (May 1977).

43. Sivo, L. L., op. cit., p. 67.

44. Ibid., p. 63.

45. Prince, J. L., and R. A. Stehlin, "Efforts of Co^{60} Gamma Radiation on Noise Parameters of Bipolar Transistors," IEEE Trans. on Nucl. Sci., Vol. NS-18, No. 6, p. 404 (December 1971).

46. Sivo, L. L., op. cit., p. 72.

47. Stanley, Alan, G., and William E. Price, "Irradiate-Anneal Screening of Total Dose Effects in Semiconductor Devices," IEEE Trans., on Nucl. Sci., Vol. NS-23, No. 6, p. 2038 (December 1976).

48. Neamen, D., et. al., "Permanent Ionizing Radiation Effects in Dielectrically Bounded Field Effect Transistors," IEEE Trans. on Nucl. Sci., Vol. NS-20, p. 160 (December 1973).

APPENDIX A
FIELD-INDUCED DEPLETION LAYER

The properties exhibited by depletion layers at and near the $Si\text{-}SiO_2$ interface have been studied extensively.[A1-A6] Surface effects on p-n junctions are primarily due to the fact that ionic charges above the interface will induce an image charge in the semiconductor and thereby lead to the formation of surface space-charge regions or depletion layers. This is illustrated schematically in Figure A-1 where we show an idealized plane p-n junction structure. When a surface space-charge region is formed, it also modifies the metallurgical junction space-charge region near the surface and leads to changes in device characteristics.

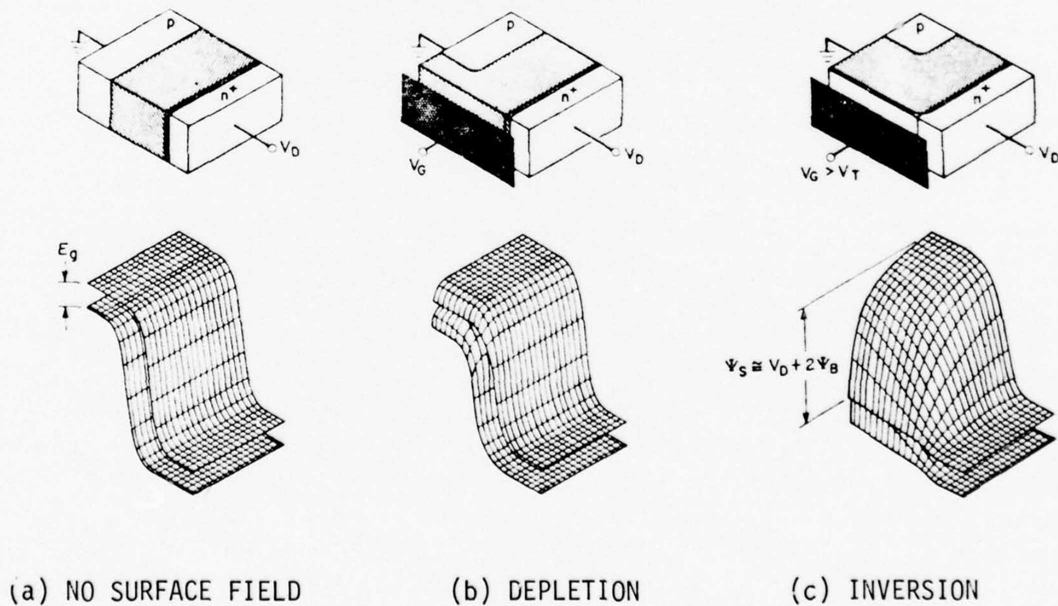

(a) NO SURFACE FIELD (b) DEPLETION (c) INVERSION

Figure A-1. The idealized junction and energy band diagrams under non-equilibrium conditions.

For a small positive voltage (V_G) applied to a gate over the oxide, a negative charge will be induced in the semiconductor near the surface due to holes being pushed away from the vicinity of the interface, leaving behind a depletion region consisting of uncompensated acceptor ions as illustrated in Figure A-2. The charge per unit area induced in the semiconductor (Q_s) will then be given by the charge contained within this depletion region,

$$Q_s = - qN_A X_d \ , \tag{A1}$$

where X_d is the width of the surface depletion region and N_A is the original acceptor concentration. The semiconductor is originally assumed neutral in charge.

(a) Depletion of majority carriers from surface.

(b) Inversion: accumulation of minority carriers near surface.

Figure A-2. Energy bands and charge distribution under various bias conditions, in the absence of surface states and work function differences.

If we increase V_G, the width of the surface depletion region will increase. Correspondingly, the total electrostatic potential variation in the silicon, as represented by the bending of the energy bands will increase.

For high positive gate voltages, an inversion layer is formed. The width of the surface depletion region reaches a maximum at this point.

When the surface region of the semiconductor is depleted and the charge within the semiconductor is given by Equation (A1), integration of Poisson's equation yields the distribution of the electrostatic potential in the surface depletion region as

$$\phi = \phi_s \left(1 - \frac{x}{X_d}\right)^2 \qquad \text{(A2)}$$

where x = distance from the surface into the semiconductor and the surface potential, ϕ_s, designates the total bending of the semiconductor energy bands given by

$$\phi_s = \frac{qN_A X_d^2}{2K_s \varepsilon_0} \quad . \qquad \text{(A3)}$$

The theory of surface space-charge regions for the depletion and inversion cases is analogous to the theory of one-sided step junctions in almost every detail.

The surface potential ϕ_s at strong inversion is given by $\phi_s(\text{inv}) = V_J + 2\phi_F$ where V_J = applied junction potential and ϕ_F = Fermi potential. The surface potential ϕ_s at strong inversion will be larger in the presence of a reverse bias V_R and smaller in the presence of a forward applied junction bias V_F.

The maximum width of the depletion region is given by

$$X_{d(max)} = \sqrt{\frac{2K_s \varepsilon_0 (V_J + 2\phi_F)}{qN_A}} \qquad \text{(A4)}$$

The result of a surface potential applied such that $\phi_s = V_J + 2\phi_F$ is that a "symmetrical" depletion layer is formed. In the case of a p-type

the bands are bent such that the donor concentration induced at the surface has the same value of that of the acceptor concentration within the crystal and thus yields the appearance of a symmetric junction.

In general, the surface recombination-generation (R-G) current due to recombination of carriers in a normal depletion region is very difficult to define exactly because neither the carrier concentration nor the recombination rate per carrier is constant across the depletion layer. The carrier concentration for a symmetrical junction at equilibrium (solid lines) and with a forward bias (dashed lines) is shown in Figure A-3. While the increase in the minority carrier concentration at the edge of the depletion layer follows the Boltzmann dependence of exp (βV), the carrier concentration at the center of the depletion layer is increased by only exp ($\beta V/2$) ($\beta V \equiv q/kT$).

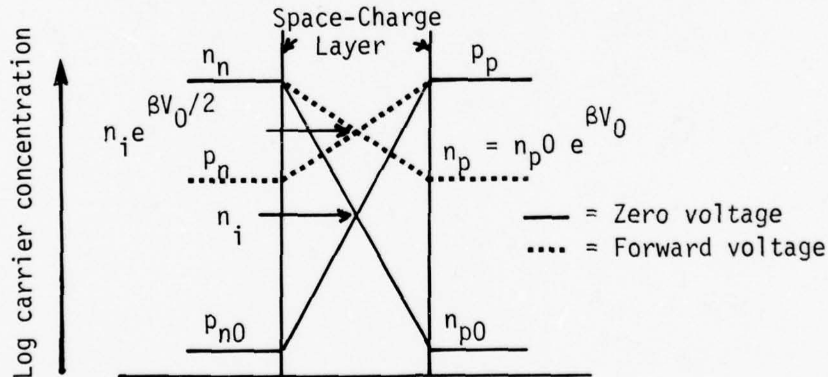

Figure A-3. The carrier concentration in the depletion layer with a forward junction voltage.

In practice, a good approximation fo (R-G currents can be obtained from a relation in the form;†

† This has the same form as the E-B depletion layer recombination-generation term described by Larin.

$$I_{DL} = q(\text{effective volume})\ (\text{recombination rate/carrier})\ (\text{effective carrier concentration}) \qquad (A5)$$

For the surface depletion layer (field-induced from charges in oxide) the effective volume for recombinations is the fraction $\pi kT/q2\phi_F$ of the total volume of the depletion layer where ϕ_F is the Fermi potential.

The total effective field-induced depletion layer (FIDL) volume is

$$\text{vol} = \frac{\pi\ kT}{2q\phi_F} AX \qquad (A6)$$

The recombination rate is the intrinsic recombination rate per carrier or R_i. The effective carrier concentration is not the concentration at the center of the gap but it is experimentally determined to be about halfway between the center and the edge of thejunction. The voltage dependence of the carrier concentrations is approximately exp $(qV_0/1.5kT)$ over the regions of interest.

Thus the maximum recombination generation current in the inverted field-induced depletion layer is

$$I_{FIDL_{max}} = .5q \frac{\pi\ kT}{2\phi_F q}\ \chi_{d_{max}}\ A_1\ n_i\ R_i\ e^{\beta V/1.5}\ \text{Amps.} \qquad (A7)$$

where A_1 is the surface area that is inverted (i.e., $\phi_s \geq 2\phi_F$).

REFERENCES

A-1 Grove, A. S., and D. J. Fitzgerald, "Surface Effects on p-n Junctions: Characteristics of Surface Space-Charge Regions under Non-Equilibrium Conditions", Solid-State Electronics, Vol. 9, 1966; p. 783.

A-2 Reddi, V. G. K., "Influence of Surface Conditions on Silicon Planar Transistor Current Gain", Solid-State Electronics, Vol. 10, 1967; p. 305.

A-3 Sah, Chih-Tang, Robert N. Noyce, and William Shockley, "Carrier Generation and Recombination in p-n Junctions and p-n Junction Characteristics", Proceedings of the IEEE, Vol. 45, No. 9, September 1957; p. 1228.

A-4 Larin, Frank, Radiation Effects in Semiconductor Devices, John Wiley & Sons, New York (1968) p. 56.

A-5 Sze, S. M., Physics of Semiconductor Devices, John Wiley & Sons, New York (1969) p. 428, 506.

A-6 Grove, A. S., Physics and Technology of Semiconductor Devices, John Wiley & Sons, New York (1967) p. 263.

APPENDIX B
SURFACE RECOMBINATION

This appendix is designed only as a mathematical tool and is intended as an aide to the reader in developing the surface recombination term used in Section 2 from the well known Shockley-Read-Hall relationship. Further information on the recombination-generation process is found in the references at the end of this Appendix.

$$\beta = q/kT \ ,$$

$$C_n = V_{th}\, \sigma_{(n)},$$

$$C_p = V_{th}\, \sigma_{(n)},$$

$$n_s = n\, e^{\beta(\phi_s - \phi_i)} \ ,$$

where

$$n = n_o\, e^{\beta V_{BE}} = n_i\, e^{\beta(\phi_i - \phi_F + V_{BE})}$$

$$p_s = n_i\, e^{\beta(\phi_F - \phi_i)}\, e^{\beta(\phi_s + \phi_i)} \ ,$$

$$n_1 = n_i\, e^{\beta(\phi_s - \phi_t)} \ ,$$

and

$$p_1 = n_i\, e^{\beta(\phi_t - \phi_s)} \ .$$

V_{th} = thermal velocity

σ_n = electron cross-section

σ_p = hole cross-section

N_{ss} = surface state density

V_{BE} = applied emitter-base voltage

ϕ_F = Fermi potential

ϕ_i = intrinsic potential

ϕ_s = surface potential

ϕ_t = trap potential

n_i = intrinsic carrier concentration

n_s, p_s = electron and hole surface densities; respectively.

The net surface recombination rate, U_s, per unit area may be expressed as

$$U_s = \frac{-N_{ss}\, C_n\, C_p(p_s\, n_s - n_i^2)}{C_n(n_1 + n_s) + C_p(p_1 + p_s)}$$

$$= \frac{-N_{ss}\, C_p C_n \left[n_i\, e^{\beta(\phi_F - \phi_i)}\; e^{-\beta(\phi_s - \phi_i)}\, n_i\, e^{\beta(\phi_i - \phi_F + V_{BE} + \phi_s - \phi_i)} - n_i^2\right]}{C_n\left[n_i\, e^{\beta(\phi_s - \phi_t)} + n_i\, e^{\beta(\phi_i - \phi_F + V_{BE} + \phi_s - \phi_i)}\right] + C_p\left[n_i\, e^{\beta(\phi_t - \phi_s)} + n_i\, e^{\beta(\phi_F - \phi_i - \phi_s + \phi_i)}\right]}$$

$$= \frac{-N_{ss}\, C_p\, C_n \frac{n_i^2}{n_i}\left[e^{\beta V_{BE}} - 1\right]}{(C_p C_n)^{\frac{1}{2}}\left[\left(\frac{C_n}{C_p}\right)^{\frac{1}{2}}\left(e^{\beta(\phi_s - \phi_t)} + e^{\beta(\phi_s - \phi_F + V_{BE})}\right) + \left(\frac{C_p}{C_n}\right)^{\frac{1}{2}}\left(e^{\beta(\phi_t - \phi_s)} + e^{\beta(\phi_F - \phi_s)}\right)\right]}$$

Let $\left(\frac{C_p}{C_n}\right)^{\frac{1}{2}} = e^{\beta\phi_o}$; then $\frac{C_p}{C_n} = e^{\beta 2\phi_o}$ and $\phi_o = \frac{\ln(C_p/C_n)}{2\beta}$

thus
$$U_s = \frac{-N_{ss}(C_p\, C_n)^{\frac{1}{2}}\, n_i\left[e^{\beta V_{BE}} - 1\right]}{e^{\beta(-\phi_o)}\left[e^{\beta(\phi_s - \phi_t)} + e^{\beta(\phi_s - \phi_F + V_{BE})}\right] + e^{\beta\phi_o}\left[e^{\beta(\phi_t - \phi_s)} + e^{\beta(\phi_F - \phi_s)}\right]}$$

By rearranging the denominator we obtain

$$U_s = \frac{-N_{ss}(C_p C_n)^{\frac{1}{2}} n_i \left[e^{\beta V_{BE}} - 1\right]}{2\left[\cosh\beta(\phi_s-\phi_t-\phi_o) + e^{\beta V_{BE}/2} \cosh\beta(\phi_s-\phi_F-\phi_o+V_{BE}/2)\right]} \; .$$

The surface current is $I_S = -q\, U_s\, A_s$. Thus

$$I_S = \frac{\frac{1}{2}\, q\, N_{ss}\, A_s\, (C_n C_p)^{\frac{1}{2}}\, n_i \left[e^{\beta V_{BE}} - 1\right]}{\cosh\beta(\phi_s-\phi_t-\phi_o) + e^{\beta V_{BE}/2} \cosh\, \beta(\phi_s-\phi_F-\phi_o+V_{BE}/2)} \quad \text{Amps.}$$

This is the form of the surface recombination-generation introduced in Section 2.

REFERENCES

B-1 Sze, S. M., Physics of Semiconductor Devices, John Wiley & Sons, New York (1969), pps. 96-104.

B-2 Grove, A. S., Physics and Technology of Semiconductor Devices, John Wiley & Sons, New York (1967), pps. 117-148.

B-3 Wang, Shyh, Solid State Electronics, McGraw-Hill, New York (1966), pps. 275-282.

B-4 Shockley, W., and W. T. Read Jr., "Statistics of the Recombinations of Electrons and Holes", Physical Review, Vol. 87, No. 5, September 1952, p. 835.

B-5 Sah, Chih-Tang, R. N. Noyce, and W. Shockley, "Carrier Generation and Recombination in P-N Junctions a[illegible] P-N Junction Characteristics", Proceedings of the IRE, Vol. 45, No. [illegible], September 1957, p. 1228.

APPENDIX C

DESCRIPTION OF "BULK" BASE CURRENT TERMS IN DC GAIN COMPONENTS

We propose a physical parameter model for gain of an n-p-n bipolar transistor which segregates the transistor into five basic current components. The ideal current-voltage characteristics are derived on the basis of the following four assumptions: (1) the abrupt depletion-layer approximation, i.e., the built-in potential and applied voltages are supported by a dipole layer with abrupt boundaries, and outside the boundaries the semiconductor is assumed to be neutral; (2) the Boltzmann approximation, i.e., throughout the depletion layer, the Boltzmann relations are valid; (3) the low injection assumption, i.e., the injected minority carrier densities are small compared with the majority-carrier densities; and (4) the facts that no generation current exists in the depletion layer, and the electron and hole currents are constant through the depletion layer. The term, gain (h_{FE}) refers to the forward common-emitter transistor gain with a reverse-bias and collector-base junction.

The five major contributions to the gain which can also represent the dominant elements in bipolar microcircuits, are:

a) recombination in base region, $\frac{I_{RB}}{I_C}$

b) an emitter efficiency related term; $\frac{I'_D}{I_C}$

c) recombination-generation in emitter-base depletion layer, $\frac{I_{RG}}{I_C}$

d) collector-base junction leakage, $\frac{I_{CBO}}{I_C}$, and

e) surface recombination, $\frac{I_S}{I_C}$.

Contributions, c through e, are similar mechanisms but occur in different regions of the transistor structure.

These components form an expression for gain defined as:

$$\frac{1}{h_{FE}} = \frac{I_B}{I_C} = \frac{I_{RB}}{I_C} + \frac{I'_D}{I_C} + \frac{I_{RG}}{I_C} - \frac{I_{CBO}}{I_C} + \frac{I_S}{I_C} \qquad \text{(C-1)}$$

Figure C-1 describes the location of each contribution. The form of each contribution in physical parameter terms was obtained mainly from understanding provided by Phillips[C-1] and Larin.[C-2] Comparison of our model with data provided by Blice[C-3] and Larin[C-4] for the pre-irradiation condition was used to confirm the accuracy of each term.

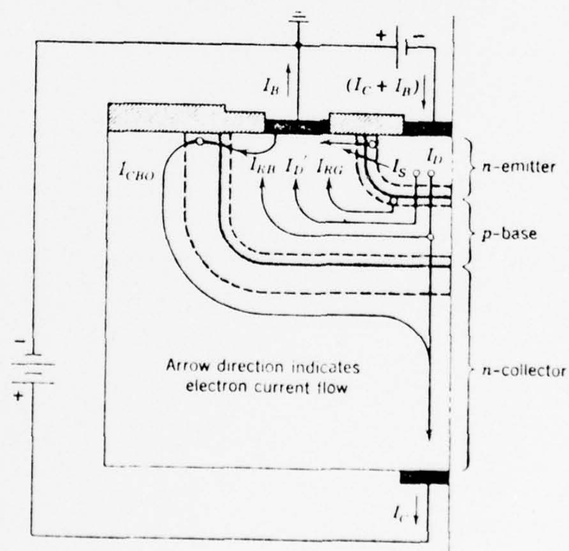

Figure C-1. A schematic representation of the five base current components.

Our model for gain of a bipolar NPN planar transistor at moderate collector currents[†] is given by the following expressions for each contribution in equation (C-1).

$$\frac{I_{RB}}{I_C} = \frac{W_b^2}{2\,D_{nb}\,\tau_{nb}} \left(\frac{1}{1+Z}\right) \left(\frac{1}{1+\left(\frac{\tau_\infty}{\tau_{nb}}-1\right)(Z)}\right) \qquad \text{(C-2a)}$$

$$\frac{I'_D}{I_C} = \frac{D_{pe}\left(N_B\,W_b\right)}{D_{nb}\,N_E\,L_{pe}} \left(\frac{1}{1-Z^2}\right) \qquad \text{(C-2b)}$$

$$\frac{I_{RG}}{I_C} = \frac{\pi\,\chi_e\,R_i\,n_i\,W_b \quad I_D^{2/3}}{D_{nb}\,N_B\,\ln\left(\frac{N_E N_B}{n_i^2}\right)\left(\frac{q\,A_e\,D_{nb}\,n_i^2}{W_b\,N_B}\right)^{2/3}} \left(\frac{1-Z}{Z\,(1+Z)}\right) \qquad \text{(C-2c)}$$

$$\frac{I_{CBO}}{I_C} = \frac{A_c\,\chi_c\,n_i\,R_i\,W_b}{A_e\,D_{nb}\,N_B} \left(\frac{1-Z}{Z\,(1+Z)}\right) \qquad \text{(C-2d)}$$

$$\frac{I_S}{I_C} = \frac{I_{SO}\,e^{qV_{BE}/2kT}}{I_C} \qquad \text{(C-2e)}$$

where

$$I_{RB} = \frac{qA_e W_b n_{po}}{2\tau_n}\, e^{qV_{BE}/kT}$$

$$I'_D = \frac{qA_e D_p p_{no}}{(D_p \tau_p)^{1/2}}\, e^{qV_{BE}/kT}$$

$$I_{RG} = \frac{q\pi A_e \chi_e R_i n_i}{\ell n\left(\frac{n_n}{n_{po}}\right)}\, e^{qV_{BE}/1.5\,kT}$$

[†]For low collector currents where I_{CBO} may affect the measured value of I_C, the following expressions using V_{BE} must be used.

$$I_s = I_{so}\, e^{qV_{BE}/2\,kT}$$

and

$$I_{CBO} = qA_c X_c n_i R_i$$

$$\nu = \frac{y - 1 + \sqrt{1 + 6y + y^2}}{4}$$

$$\nu_e = \frac{\nu N_B \left(\nu N_B + N_B\right)}{N_E^{\,2}}$$

$$y = \frac{q\, R_{BB}\, W_b^{\,2}\, I_D}{kT\, A_e\, b} \quad \text{for an NPN transistor}^{C-5} = \frac{n_i^{\,2}}{N_B^{\,2}} \; \frac{I_C}{I_{DC}}$$

$$Z = \frac{\nu}{1 + \nu} = \text{injection ratio in base region}$$

$$Z_e = \frac{\nu_e}{1 + \nu_e} = \text{injection ratio in emitter region}$$

$$b = \frac{\mu_{nb}}{\mu_{pb}} \quad \text{for p-type base}^{C-6}$$

R_{BB} = base sheet resistivity (Ω/square) =

$$\frac{1}{q\, \mu_{pb\,(eff)} \left(N_B\, W_b\right)_{(eff)}} \approx \frac{b}{q\, \mu_{nb}\, N_B\, W_b} \quad \left(\begin{array}{l}\text{uniform}\\ \text{base -}\\ \text{no}\\ \text{grading}\end{array}\right)$$

W_b = width of base (including base pushout)[C-7] = $W_{bo} + \Delta W_b$

$$\Delta W_b = \frac{N_C}{a_2} \ln\left(\frac{q\, A_e\, v_{s1}\, N_C}{q\, A_e\, v_{s1}\, N_C - I_C}\right)$$

for $\quad I_C < q\, A_e\, v_{s1}\, N_C \left[1 - \exp\left(-a_2\, W_C / N_C\right)\right]$

a_2 = linear grade constant[C-8]

$$\frac{1}{a_2} \approx \left(\frac{2 + W_{bo}/W_e}{1 + W_{bo}/W_e}\right)\left(\frac{W_{bo}}{2\ N_C}\right) \frac{1}{\ln\left[\frac{N_B}{N_C} + 1\right]}$$

v_{sl} = scattering-limited velocity = 10^7 cm/sec.

W_{bo} = base width (vertical in Figure C-1) without base pushout (cm)

W_e = emitter depth to base region (cm)

k = Boltzmann's constant = 8.63×10^{-5} ev/°K

T = Absolute temperature (°k)

A_e = Area of emitter-base junction (cm^2)

A_c = Area of collector-base junction (cm^2)

I_D = Emitter diffusion current into base region (Amps) $\approx I_C$ for moderate currents

D_{nb} = Electron diffusion constant in base = $\frac{kT\ \mu_{nb}}{q}$ (cm^2/sec)

D_{pe} = Hole diffusion constant in emitter = $\frac{kT\ \mu_{pe}}{q}$ (cm^2/sec)

τ_{nb} = Electron minority carrier lifetime in base (sec^{-1})

τ_{∞} = High level minority carrier lifetime in base (sec^{-1})

L_{nb} = Electron diffusion length in base region = $\left(D_{nb}\ \tau_{nb}\right)^{\frac{1}{2}}$ (cm)

L_{pe} = Hole diffusion length in emitter = $\left(D_{pe}\ \tau_{pe}\right)^{\frac{1}{2}}$ (cm)

μ_{pe} = Hole mobility in emitter region (cm^2/v-sec)

μ_{nb} = Electron mobility in base region (cm^2/v-sec)

N_B = Impurity concentration in uniform base (cm^{-3})

N_E = Impurity concentration in uniform emitter (cm^{-3})

N_C = Collector donor impurity concentration (assumed uniform) (cm^{-3})

n_i = Intrinsic carrier concentration = 1.5×10^{10} cm^{-3}

n_n = Majority electron concentration in the n region (cm^{-3})

n_{po} = Minority electron concentration in base region at equilibrium (cm^{-3}) = n_i^2 / N_B

I_{DO} = Extrapolated normal diffusion current (Amps)

I_D = Forward biased diffusion current (Amps) $I_D \approx I_C$

X_e = Width of the emitter-base depletion layer (cm)

$$= 3.73 \times 10^3 \left(\frac{\psi_o - V_{BE}}{N_B} \right)^{1/2} \quad \text{for uniform base}$$

$$V_{BE} = \frac{kT}{q} \ln \left(\frac{I_C}{I_{DO}} \right) \quad \text{where} \quad I_{DO} = \frac{q\, A_e\, D_{nb}\, n_{po}}{W_b} = \frac{q\, A_e\, D_{nb}\, n_i^2}{W_b\, N_B}$$

X_c = Width of the base-collector depletion layer (cm)

R_i = Intrinsic carrier recombination rate (sec^{-1})

$$\psi_o = \frac{kT}{q} \ln \left(\frac{n_n}{n_{po}} \right) \text{(volts)} = \frac{kT}{q} \ln \left(\frac{N_E\ N_B}{n_i^2} \right) \text{(volts)}$$

The Z terms in each part of equation (C-2) represent the injection level dependencies. Even though a term may not show I_C directly, the Z terms include the I_C dependence. The expression for Z could be substituted into each part of equation (C-2) but it was felt that it would be more instructive to keep the injection ratio dependencies separated so that their origins could remain identifiable. Base pushout (ΔW_b) technique has a limiting condition on its validity vs. I_C to take into account the different collector thicknesses when epitaxial processing techniques are used.

The factor in equation (C-2a),

$$\frac{1}{\left(1 + \left(\frac{\tau_\infty}{\tau_{\mu b}} - 1\right) Z\right)}$$

is used to correct the minority carrier lifetime, τ_{nb}, for its injection dependence. It is determined from point defect statistical capture considerations.

The model includes high injection effects and base pushout (Kirk Effect) but does not include other effects directly in the model such as:

- emitter crowding
- graded base
- contribution due to surface effects (I_{CBO_S} and I_S)

Saturation and inverse gain have not been addressed here.

The two sets of data used for verifying our model were obtained from Larin and Blice (See Table C-1).[C-2,C-3]

Table C-1: Data used for comparison with Larin and Blice.

Parameter	Larin's 2N1613 Value (NPN)	Blice's 2N2222 Value (NPN)
W_e	4×10^{-4} cm	2×10^{-4} cm
W_{bo}	2×10^{-4} cm	2.7×10^{-5} cm
W_c	7.5×10^{-3} cm	4×10^{-4} cm
N_E	3×10^{18} atoms/cm^3	2×10^{18} atoms/cm^3
N_B	5×10^{16} atoms/cm^3	9.5×10^{16} atoms/cm^3
N_C	1.5×10^{15} atoms/cm^3	7×10^{15} atoms/cm^3
τ_{pe}	1×10^{-8} sec	1.35×10^{-8} sec
τ_{nb}	1×10^{-7} sec	6.65×10^{-7} sec
A_e	1×10^{-3} cm^2	2.9×10^{-4} cm^2
A_c	4×10^{-3} cm^2	1.13×10^{-3} cm^2
R_i	1.5×10^5/sec	3.7×10^5/sec
n_i	1.5×10^{10} carriers/cm	1.5×10^{10} carriers/cm
n_{po}	4.5×10^3 carriers/cm	2.3×10^3 carriers/cm
n_n	3×10^{18} carriers/cm	2×10^{18} carriers/cm
τ_i	6.7×10^{-6} sec	6.7×10^{-6} sec

Table C-1: Data used for comparison with Larin and Blice. (Cont'd)

Parameter	Larin's 2N1613 Value (NPN)	Blice's 2N2222 Value (NPN)
D_{nb}	1.66×10^{1} cm^2/sec	1.4×10^{1} (Note 1)
D_{pe}	1.95 cm^2/sec	2.34 (Note 1)
L_{nb}	1.28×10^{-3} cm	3.1×10^{-3}
L_{pe}	1.4×10^{-4} cm	1.8×10^{-4}
X_{eo}	1.6×10^{-5} cm	1.1×10^{-5}
R_{BB}	2.2×10^{3} $\Omega/\square$	7.4×10^{4}
μ_{nb}	6.4×10^{2} cm^2/volt-sec	5.4×10^{2}
μ_{pe}	7.5×10^{1} cm^2/volt-sec	9.0×10^{1}
X_c	3.2×10^{-4} cm	3.9×10^{-5}
I_{SO}	1×10^{-10}	3.1×10^{-15}
$\frac{\tau_{\infty}}{\tau_{nb}}$	0.5	0.5 - (estimate)
ψ_{oe}	0.886	0.894

Note 1. Ref. C-14 and C-15 refer to a modification in the diffusion constants due to electric fields for high field intensities. We assume in this model that the fields required for this effect to be significant are not present and therefore Phillips[1] can be used to determine diffusion constants from mobility and impurity concentrations.

Larin supplied in detail the physical parameter values used in his discussions which corresponded to a reference transistor with size intermediate between small switching transistors and large power transistors corresponding to device types such as 2N1613, 2N1893, 2N697, 2N1711, 2N3439 and 2N1290. Most experimental data used by Larin was for the 2N1613. For Blice, a different set of data was used and applied to a different form of a transistor model. Some of the values used by Blice were estimated from the referenced report. Both comparisons should agree in terms of the slope for each contribution versus collector current and the relative contribution from each term.

The comparison of the model presented in this report in equation (C-2) with Larin's data is shown in Figure C-2. Each contribution has a similar slope and relative placement in magnitude. The only variation of our model from Larin's data is the high injection effects for $\frac{I_D'}{I_C}$. This increase in $\frac{I_D'}{I_C}$ for high injection in Larin's data is due to emitter crowding. Emitter crowding has not previously been explicitly defined in terms of physical parameters, so this additional complexity will be discussed qualitatively in a separate section.

For Blice's transistor, the relative importance of the $\frac{I_{RB}}{I_C}$ contribution compared to the $\frac{I_D'}{I_C}$ contribution is reversed from Larin's. This reversal, shown in Figure C-3, is also predicted by our model since different physical parameter values were used by Blice than by Larin. Our model appears to be in good agreement with the most recent comparisons and models of Blice except for a constant factor on I_D'/I_C. Since some of the values that Blice used are not given, the source of this constant

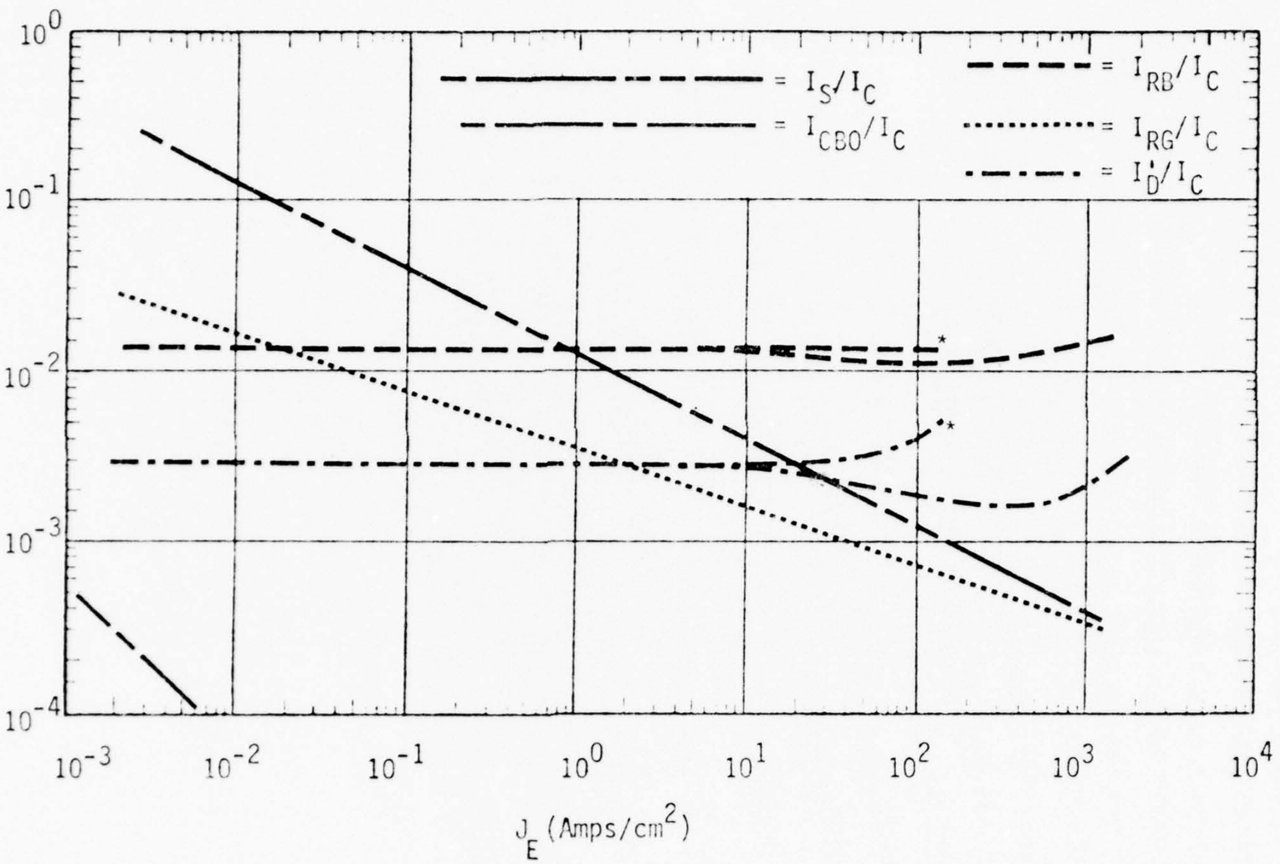

Figure C-2. Component comparison of I_B/I_C vs. I_C between Larin's model and ours presented here. * indicates Larin's curve when different. Larin's upturn of I'_D/I_C is due to measured crowding.

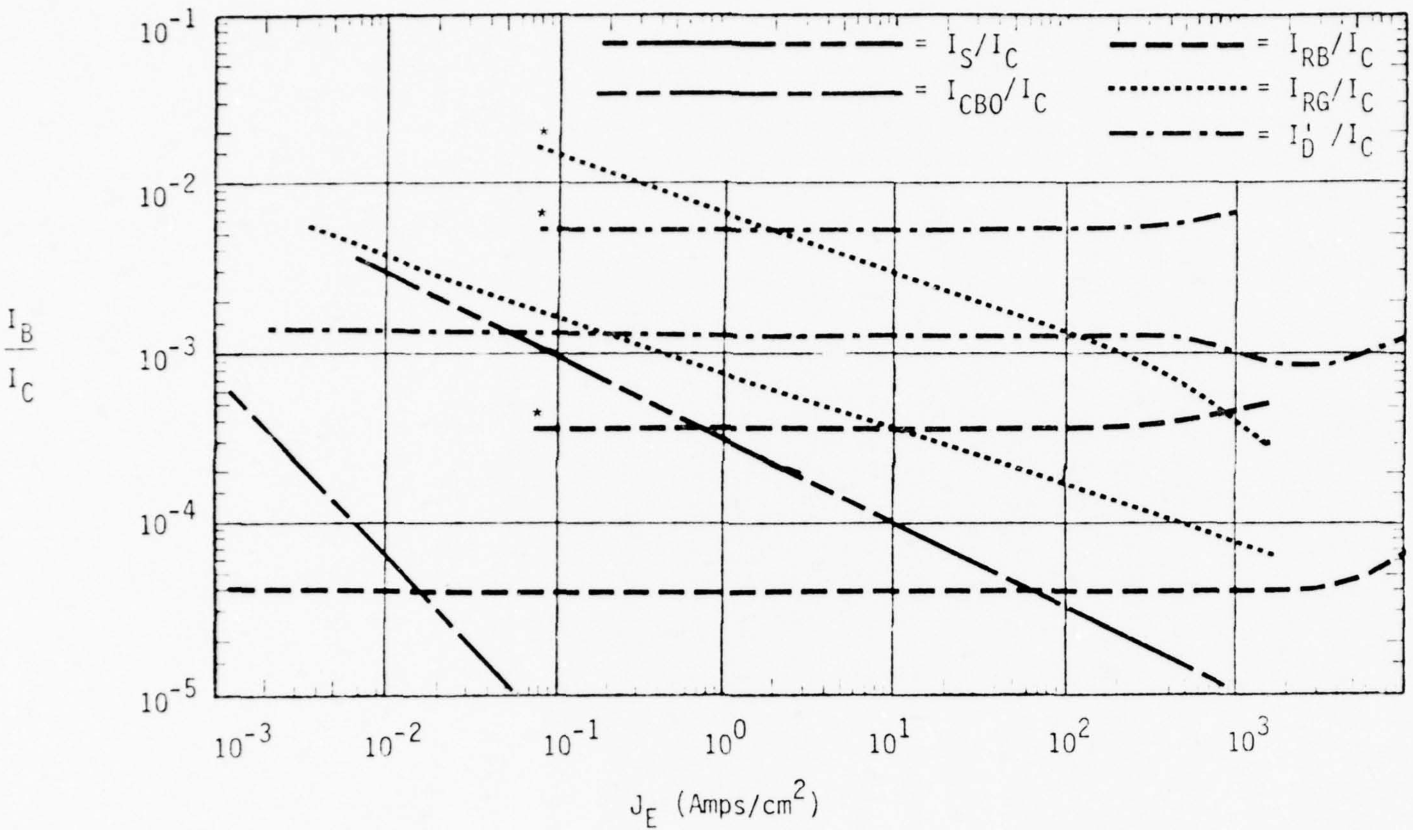

Figure C-3. Component comparison of I_B/I_C vs. I_C between Blice's model and ours presented here when applied to Blice's 2N2222. *Indicates Blice's curve.

could not be identified. The $\frac{I'_D}{I_C}$ and $\frac{I_{RG}}{I_C}$ terms also compare in slope except at very high injection level. The $\frac{I'_D}{I_C}$ term for Blice turns up sooner than our model. Also the $\frac{I_{RG}}{I_C}$ term in Blice's model decreases sublinearly at high injection while our model decreases superlinearly. Both of these discrepancies occur near the point when the models begin to break down and could be the result of the assumptions used in this unknown area. This is influenced by emitter crowding.

Emitter Crowding

The construction of an epitaxial bipolar transistor usually requires that the base contact be positioned at the surface of the base region. As a result there is a finite resistance difference from the base contact to various points under the emitter diffusion (in the thin base region under the emitter well). The base current that flows from the base contact to the base region under the emitter produces a voltage gradient over this base region. The maximum potential occurs furthest from the base contact. If the external emitter bias voltage is assumed to be applied uniformly over the entire base-emitter junction, then the effect of the internal base voltage is to produce a net junction potential that decreases from the periphery edge to the center of the emitter. The higher edge forward potential causes a crowding of the injected emitter current into the peripheral areas of the emitter well, thus an effective reduction in the active cross-sectional area. The internal base bias may be such that the injected carrier density in the center of the emitter junction may be practically zero.[C-10] Since the injection ratio, Z, for a given current is dependent on the active cross-sectional area, A_e, a reduction in A_e increases Z and thus for the same J_e on Figures C-2 and C-3, the Z dependence would be stronger (at high injection). The only term in $\frac{I_B}{I_C}$ that depends strongly on Z for turn-up at high Z is $\frac{I'_D}{I_C}$. The other terms are only weakly

dependent on a decrease in A_e . Therefore emitter crowding will make the $\frac{I'_D}{I_C}$ term increase at a lower J_e . Larin's data for $\frac{I'_D}{I_C}$ includes emitter crowding which used measured $V_{BE} - I_C$ characteristic for a typical transistor.[C-11]

Graded Base

In a graded base structure an electric field is established in the base by the majority carriers to maintain space charge neutrality. The effect of a graded base is to effectively increase the diffusion constant, D_{nb}. In the $\frac{I'_D}{I_C}$ term there is also another factor which is dependent on the grading of the base. This term is $(N_B W_b)$.[C-12] Actually this term was obtained for a uniform base from the general expression

$$\int_0^{W_b} N(x)\, dx \; .$$

For a linear grading profile, this term $\approx 1/2\; N_B W_b$. The approximation that can be made for graded base is therefore to divide each contribution in the gain equation by some factor > 1.

The results of the pre-irradiation comparisons of our model with Larin and Blice were very good in that each model indicated the same relative contribution to the gain and the same dependency on I_C . Larin's absolute values compared more favorably than Blice's. This was due to a higher confidence in establishing the actual values used by Larin.

Also, many of the terms that contributed to the gain equation had the same form as Larin. The model therefore represents an adequate definition of existing understanding of the relationship between the gain of a bipolar transistor and the physical parameters for both low and high injection.

REFERENCES

C-1. Phillips, A. B., Transistor Engineering and Introduction to Integrated Semiconductor Circuits, McGraw-Hill Book Co., New York (1962).

C-2. Larin, Frank, Radiation Effects in Semiconductor Devices, John Wiley & Sons, Inc., New York (1968).

C-3. Blice, R. D., and J. A. Munarin, Neutron Hardness Assurance for Bipolar Transistors through Determination of Physical Parameters, AFWL-TR-74-327, Air Force Weapons Laboratory, July 1976, p. 101.

C-4. Larin, op. cit., p. 70.

C-5. Phillips, op. cit., p. 229.

C-6. Ibid., p. 69.

C-7. Blice, op. cit., p. 133.

C-8. Ibid, p. 57.

C-9 Larin, op. cit., p. 51.

C-10. Phillips, op. cit., p. 241.

C-11. Larin, op. cit., p. 98.

C-12. Phillips, op. cit., p. 192.

APPENDIX D

LONG TERM IONIZATION

A major factor in the degradation of gain of bipolar transistors due to effects of long term ionizing radiation is the creation of electron-hole pairs in the passivating oxide layer over the pn junctions and subsequent trapping of a fraction of the holes at the oxide-silicon interface. In an npn transistor, holes are trapped at the interface in the base region. In addition the surface state trap density is increased in this region. The resultant change in surface potential increases the surface recombination velocity thereby providing a sink for base current.

In the present program, IRT has calculated the oxide field due to fringing of the junction field, the effective generation rate of holes in the oxide under irradiation, the trapping of holes at the interface and the creation of interface states, and the resultant change in surface potential of the silicon as a function of distance from the geometrical junction. Calculations have been made for representative device dimensions, junction biases, and hole and interface state generation rates.

The nature of these calculations and the results are described in a form suitable for inclusion as an appendix to the MRC report on this program.

APPENDIX D

ELECTRIC FIELDS AND SURFACE POTENTIALS AT OXIDE-SILICON INTERFACE

D-1 INTRODUCTION

The surface recombination rate depends on the surface potential (relative to the bulk) which, in turn, depends on the electrical field normal to the interface. In this Appendix, estimates are made for these surface electric fields and potentials in the transistor base region (1) due to fringing of the emitter-base junction fields near where this junction intersects the silicon surface and (2) due to the oxide charge and interface states that result from radiation. The methods of calculating the fields and surface potentials before irradiation are discussed in Paragraph D.2 and the effect of radiation is considered in Paragraph D.3.

D.2 ELECTRIC FIELDS AND SURFACE POTENTIALS BEFORE IRRADIATION

The following is the method used to obtain the normal electric fields and surface potentials at the interface before irradiation.

The configuration for which the electric fields were determined is shown in Figure D-1 in which a semi-infinite slab of silicon with dielectric constant K_2 is in contact along the X-axis with a semi-infinite slab of SiO_2 with dielectric constant K_1. A step pn junction is taken along the y-axis in the silicon with the positively charged depletion region with uniform charge density ρ extending from $0<x<a$ and the negatively charged region extending from $-b<x<0$.

The electric field at any point is initially calculated by neglecting the presence of the two media with different dielectric constants and by integrating the field equation over the entire charge distribution. The presence of the interface between two regions with different dielectric constants is then accounted for by use of the method of images.

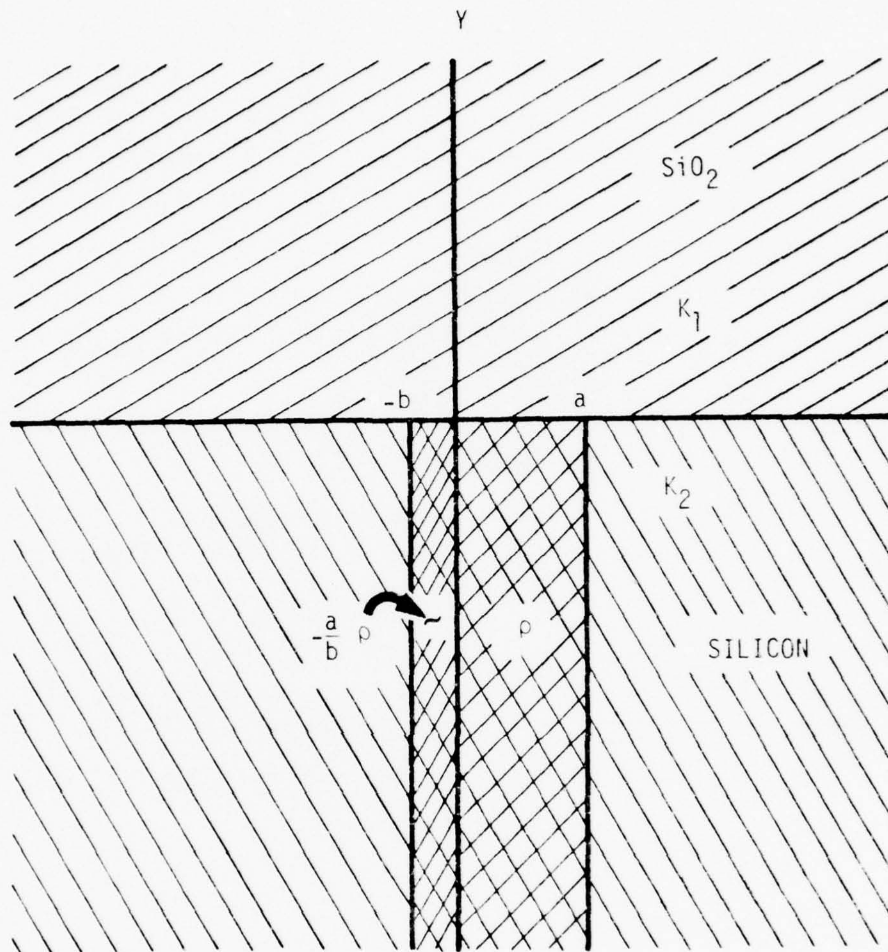

RT-16130

Figure D-1. Charge distribution and configuration for initial calculation of electric fields given in equations D1 and D2.

From Reference D-1, the electrostatic potential inside and outside a solid dielectric cylinder of infinite length due to a line charge of strength q per unit length located outside the dielectric cylinder and parallel to its axis is given by the following set of image charges. The potential inside the dielectric cylinder is just the potential due to a line charge of strength 2q/(1+K) located at the position of the real charge. Here K is the ratio of the dielectric constant of the cylinder to that of the surrounding medium. That is,

$$\phi_{inside} = \frac{2q \ln R}{(1+K)\, 2\pi K_2 \varepsilon_o}$$

where ε_o is the permittivity of free space and R is the radial distance from the real charge.

On the other hand, the potential outside the cylinder is the sum of the potentials from three line charges, (1) the real charge at its normal position, (2) an effective charge [q(1-K)/(1+K)] located at the inversion point of the real charge (i.e., at a^2/r_o from the center of the dielectric cylinder of radius "a" with the real charge at r_o), and (3) an effective charge [-q(1-K)/(1+K)] located at the centerline of the cylinder. For all of these potentials, the dielectric constant to use is the dielectric constant (K_2) of the surrounding medium (Si), not the dielectric cylinder (SiO_2). The effect of the cylinder's dielectric constant enters in through the parameter K.

For semi-infinite planes, the same image procedure can be used except that the effective charge at the origin [-q(1-K)/(1+K)] can be ignored because it recedes to infinity when the cylinder is transformed into a plane. This charge at infinity will be canceled by an equal and opposite charge at at infinity because we will always be dealing with equal and opposite real charges in the Si. Another difference for a planar geometry is that the image point is the same distance from the plane as the real charge.

Equations D-1 and D-2 give the components of the electric field in the silicon and in the oxide both parallel (x) and perpendicular (y) to the interface for the assumed charge distributions and configuration shown in Figure D-1.

$$E_x = \frac{2A\rho}{4\pi(1+K)K_2\varepsilon_o}\left\{\frac{\pi}{A}\left[|x|\left(1+\frac{a}{b}\right) - |a-x| - \frac{a}{b}|x+b|\right]\right. \tag{D1}$$

$$-2x\left(1+\frac{a}{b}\right)\tan^{-1}\frac{y}{x} + 2\left[(a-x)\tan^{-1}\frac{y}{a-x} + \frac{a}{b}(x-b)\tan^{-1}\frac{y}{x+b}\right]$$

$$\left. + y\left[\log\frac{(a-x)^2+y^2}{x^2+y^2} + \frac{a}{b}\log\frac{(x-b)^2+y^2}{x^2+y^2}\right]\right\}$$

$$E_y = \frac{-2A\rho}{4\pi(1+K)K_2\varepsilon_o}\left\{2y\left[\tan^{-1}\frac{a-x}{y} + \tan^{-1}\frac{x}{y} - \frac{a}{b}\left(\tan^{-1}\frac{x+b}{y} - \tan^{-1}\frac{x}{y}\right)\right]\right. \tag{D2}$$

$$+ x\left[\log\frac{x^2+y^2}{(a-x)^2+y^2} + \frac{a}{b}\log\frac{x^2+y^2}{(x+b)^2+y^2}\right]$$

$$\left. - a\log\frac{(x+b)^2+y^2}{(x-a)^2+y^2}\right\} \quad .$$

In the oxide $(y > 0)$ $A = 1$ and in the silicon $(y < 0)$ $A = K$.

The above fields are however not correct for the physical problem because the fields in the bulk of the Si are not zero, as they should be. In a real device, the electric fields that cross the interface from the oxide to the silicon cause depletion or accumulation regions in the silicon near the interface, which produces just enough net charge in the silicon at the interface to terminate the electric field lines and shield the bulk silicon. As a first order attempt to take this into account, surface charge was added along the interface to try to cancel the normal component of the electric field. The local surface charge density was taken as

$$\sigma = 2K_2\varepsilon_o E_y/[2/(1+K)]$$

where E_y is the local normal electric field in the silicon at the interface,

the factor in the denominator is due to images, and the initial factor of 2 is because, for an isolated sheet of charge, half of the field lines extend out from each side of the sheet. If E_y were uniform to infinity, this correction term would be exact. However, because E_y is not uniform, it is only approximately correct. No surface charge is added in the depletion region of the junction because that area is already fully depleted and no additional space charge can be developed.

The total electric fields are now due to the original depletion region (Eq. D1 and D2) and a spatially varying negative surface charge density on the p side of the junction and a positive surface charge density on the n side. A simple computer program was written to evaluate Eq. D1 and D2, to determine the required surface charge density σ, and then to calculate the effect of σ on the electric fields. Care was taken to make the total positive and negative charge on either side of the junction due to σ exactly equal to each other and to use a sufficiently large lateral distribution of σ so that the fields in the region of interest were hardly affected by terminating the integration at a finite distance.

The results of this calculation indicate that this first-order correction did a good job of reducing the y components of the electric fields in the bulk silicon essentially to zero, but it produced a relatively small x component of the field in the silicon. In principle, one could try some additional correction to try to further reduce the fields in the bulk of the silicon to zero. However, since the normal electric fields near the interface are the main fields of interest for this analysis and since this first-order correction seems to be adequate for these fields, no additional iterations were attempted.

The surface potentials as a function of the normal electric field at the surface are shown in Figure D-2.

The surface potential ϕ_s of the silicon as a function of the normal electric field, E_s, in the silicon at the interface is determined by integration of the appropriate one-dimensional Poisson equation from the bulk of the silicon out to the surface and is given by the following relation (Ref. D-2).

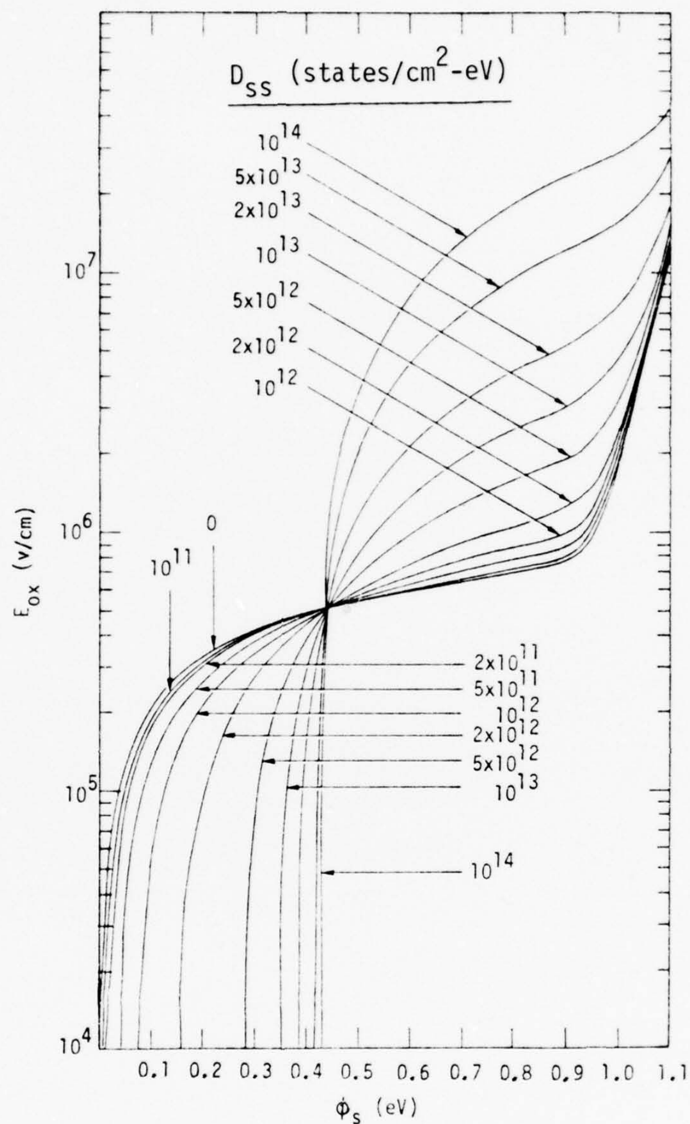

Figure D-2. Dependence of surface potential ϕ_s on interface electric field in silicon dioxide, for various values of surface state density D_{SS} (in units of $(cm^2\ eV)^{-1}$). The zero of surface potential is taken at flat band condition. Acceptor concentration in the silicon is $2 \times 10^{17}\ cm^{-3}$.

$$E_s = \frac{2}{\beta L_D}\left[\left(e^{-\beta\phi_s} + \beta\phi_s - 1\right) + \frac{n_{po}}{p_{po}}\left(e^{\beta\phi_s} - \beta\phi_s - 1\right)\right]^{1/2}$$

where $\beta = \frac{q}{kT}$, L_D is the intrinsic Debye length for holes = $\left[2K_2\varepsilon_o/qp_{po}\beta\right]^{1/2}$, and n_{po} and p_{po} are the equilibrium bulk concentration of holes and electrons. Figure D-2 shows this relationship for $p_{po} = 2 \times 10^{17} cm^{-3}$ and for a surface field in the direction which will take the surface to depletion and subsequently inversion.

Also shown in Figure D-2 is the effect of inclusion of surface states which serve to terminate a fraction of an externally applied electric field. These surface states are taken to be acceptors (neutral above the Fermi level and negative below) in the upper half of the band gap, and donors (positive above the Fermi level and neutral below) in the lower half of the band gap. The surface state density is assumed to be independent of position in the band gap.

From this figure one may determine the silicon surface potential for any given oxide surface field $E_{ox} = E_{Si}/K$ and surface state density D_{ss}.

D.3. CHANGE IN ELECTRIC FIELDS AND SURFACE POTENTIALS DUE TO RADIATION

The holes that are generated in the SiO_2 by the ionizing radiation will be swept toward the interface between the SiO_2 and the p silicon (base region for the present NPN devices) by the electric fields described in Section D-2, and some of the holes will be trapped at the interface. The electrons from the SiO_2 are driven by the electric fields toward the n emitter, which they enter. They then proceed to the p base where they annihilate the holes that escaped from the SiO_2 or terminate the electric flux lines from the trapped holes in the oxide. Thus, to first order, the effect of the radiation-induced charge is just a local increase in the electric field across the interface (equal to $\Delta E_y = \sigma_h/K_2\varepsilon_o$ in the silicon, where σ_h is the surface density of trapped holes), and the fields in the bulk of the oxide are unchanged. Of course, there are second order effects that have not been considered here because they are believed to be unimportant for this study.

The surface density of trapped holes per unit dose is a function of the effective generation rate of holes in the oxide, the distance from which holes can be pulled to the interface, and the probability of capture of the holes at the interface. The effective generation rate is assumed to be limited by geminate recombination, which is a function of the electric field in the oxide.

Estimates of the effect of geminate recombination on the survival rate of holes can be made from measurements on charge carrier transport in the oxide of MOS capacitors (Refs. D-3, D-4), Below electric fields of about 10^6 V/cm the survival rate varies between 3.5 and 7.5×10^{-7} $(V/cm)^{-1}$. From the work of McLean, Boesch, and McGarrity (Ref. D-5), (also on MOS capacitors with clean oxides) we estimate that at room temperature 9% of the holes reaching the interface are trapped there. Consequently we take for the fraction of initially generated holes which are trapped in the oxide at the interface the value 6×10^{-8} $(V/cm)^{-1}$. Using this value and the generally accepted value of 18 eV needed to initially create an electron-hole pair with radiation (Ref. D-6), we can determine that the oxide interface charge generation rate is 7.77×10^{-18} coul/cm^2-rad-(V/cm) in 1 μm thick oxide.

We also assume that interface states are produced by hole motion to the interface, rather than by direct interaction by the irradiation (Ref. D-7), We have assumed, somewhat arbitrarily, that interface states are generated at five times the rate of generation of oxide charge.

Use of these generation rates for oxide charge and interface state density allow calculation of both the total interface electric field and the resulting surface potential, from graphs similar to Figure D-2, as a function of total dose at any position along the interface. Note that, again the first order, the oxide field is not altered by the presence of oxide charge, which is assumed to be at the interface; consequently the oxide field does not vary with dose. The thickness over which holes are collected is taken as the oxide thickness times the secant of the average angle which the electric field makes to the normal to the interface. The electric field, which determines the fraction of holes escaping geminant recombination, is taken as the average of the field at the interface and

at the point at which the average field direction intersects the outer surface of the oxide.

The variation of surface potential as a function of distance from the junction, at various values of total dose, is shown in Figure D-3, for zero bias across the base emitter junction, and in Figure D-4 for $V_{BE} = +0.5V$.

A calculation was also made of the magnitude of the fringing field from the collector-base junction in the vicinity of the emitter-base junction for $V_{CB} = -10V$ and an emitter-collector separation of 115μm. This field was found to be negligible ($\lesssim 2\%$) compared to the field from the emitter-base junction.

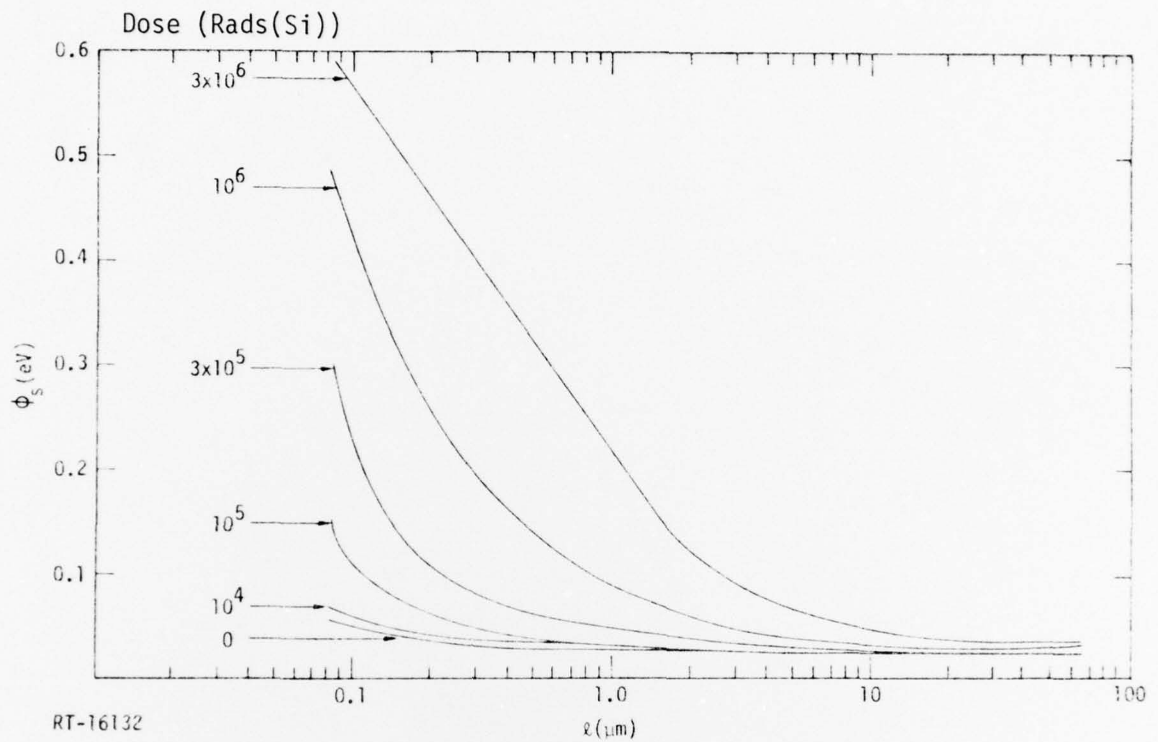

Figure D-3, Variation of surface potential ϕ_s as a function of distance into the base region from the emitter-base junction for various values of total dose. Base doping: $N_A = 2 \times 10^{17}$ cm^{-3}; emitter doping $N_D = 3 \times 10^{20}$ cm^{-3}. Oxide thickness: 0.6 μm. The emitter-base bias is 0. initial values of oxide charge, Q_{ss}, and surface state density, D_{ss} are 10^{11} cm^{-2} and 10^{11} cm^{-2} eV^{-1} respectively.

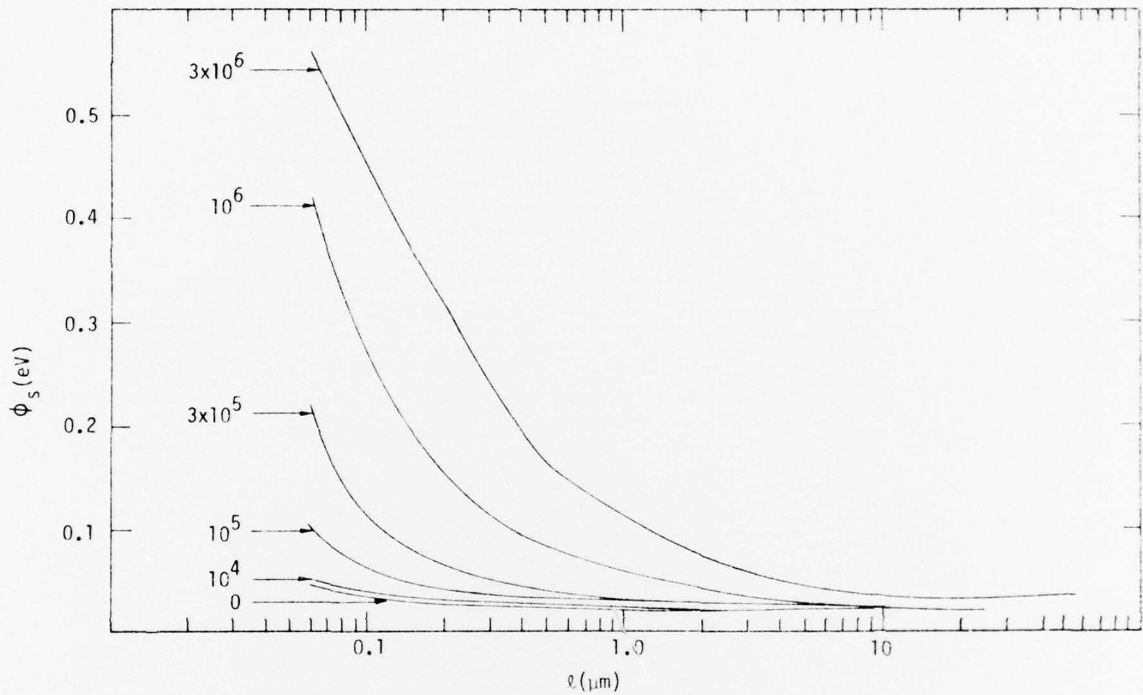

RT-16133

Figure D-4, Variation of surface potential ϕ, as a function of distance into the base region from the emitter-base junction for various values of total dose. Base doping: $N_A = 2 \times 10^{17}$ cm^{-3}; emitter doping: $N_D = 3 \times 10^{20}$ cm^{-3}. Oxide thickness: 0.6 μm. $V_{BE} = +0.5$ volts. Initial values of oxide charge, Q_{ss} and surface state density D_{ss} are $Q_{ss} = 10^{11}$ cm^{-2} and $D_{ss} = 10^{11}$ cm^{-2} eV^{-1}.

REFERENCES

D-1. W. R. Smythe, Static and Dynamic Electricity, McGraw-Hill, New York, 1950, p 68.

D-2. S. M. Sze, Physics of Semiconductor Devices, Wiley and Sons, 1969, p 431.

D-3. J. R. Srour, O. L. Curtis, Jr., and K. Y. Chu, "Charge Transport Studies in SiO_2: Processing Effects and Implications for Radiation Hardening," IEEE Trans. Nucl. Sci., NS-21, 73 (1974).

D-4. D. P. Snowden and T. M. Flanagan, "Transient Response to High-Energy Electron Irradiation," IEEE Trans. Nucl. Sci. NS-22, 2516 (1975).

D-5. F. B. McLean, H. E. Boesch, and J. M. McGarrity, "Hole Transport and Recovery Characteristic of SiO_2 Gate Insulators," IEEE Trans. Nucl. Sci. NS-23, 1506 (1977).

D-6. J. R. Srour, S. Othmer, O. L. Curtis, Jr., and K. Y. Chu, "Radiation Indirect Charge Transport and Charge Build-Up in SiO_2 Films at Low Temperatures," IEEE Trans. Nucl. Sci. NS-23, 1513 (1976).

D-7. C. T. Sah, "Origin of Interface States and Oxide Charges Generated by Ionizing Radiation," IEEE Trans. Nucl. Sci. NS-23, 1563 (1976).

APPENDIX E

RECOMBINATION CENTER EFFECTIVE CONCENTRATION

For a reverse-biased depletion surface area with single-level centers, the generation rate per unit area, U_s, may be expressed in terms of the Shockley-Read-Hall recombination-generation theory and given by:[E-1]

$$U_s = \frac{\sigma_{sn}\ \sigma_{sp}\ V_{th}\ N_{ss}\ n_i}{\sigma_{sn}\ \exp\left[\beta(E_{st} - E_i)\right] + \sigma_{sp}\ \exp\left[\beta(E_i - E_{st})\right]}$$

where N_{ss} is the number of single-level surface recombination-generation centers per unit area, σ_{sn} and σ_{sp} are the centers capture cross-sections for electrons and holes respectively, V_{th} is the thermal velocity, $\beta = q/kT$, E_i is the intrinsic energy level, and E_{st} is the center's energy level. If we assume that the center energy $E_{st} = E_i$ and that $\sigma_{sn} = \sigma_{sp} = \sigma_s$ then:[E-2]

$$U_s = \sigma_s\ V_{th}\ n_i\ N_{ss}$$

For a uniform energy distribution of the center, D_{ss}, within the forbidden band gap, the generation rate becomes:

$$U_s = \sigma_{sn}\ \sigma_{sp}\ V_{th}\ D_{ss}\ n_i \int_{E_c}^{E_v} \frac{d\ E_{st}}{\sigma_{sn}\ \exp\left[\beta(E_{st} - E_i)\right] + \sigma_{sp}\ \exp\left[\beta(E_i - E_{st})\right]}$$

where D_{ss} (centers/cm^2- eV) designates the density of surface centers uniformly spaced in the energy gap between E_V and E_c (the valence and conduction bands) respectively.

If we let $x = E_{st} - E_i$, then $dx = d\,E_{st}$ and we have

$$U_s = \sigma_{sn}\,\sigma_{sp}\,V_{th}\,D_{ss}\,n_i \int_{E_c - E_i}^{E_v - E_i} \frac{dx}{\sigma_{sn}\,e^{\beta x} + \sigma_{sp}\,e^{-\beta x}}$$

$$= \sigma_{sn}\,\sigma_{sp}\,V_{th}\,D_{ss}\,n_i\,\frac{1}{\beta}\,\frac{1}{(\sigma_{sn}\,\sigma_{sp})^{\frac{1}{2}}}\,\tan^{-1}\left(e^{\beta x}\left(\frac{\sigma_{sn}}{\sigma_{sp}}\right)^{\frac{1}{2}}\right)\Bigg|_{\text{limits}}$$

but $\tan^{-1}\left(e^{\beta x}\left(\frac{\sigma_{sn}}{\sigma_{sp}}\right)^{\frac{1}{2}}\right)\Bigg|_{\text{limits}} \Longrightarrow \frac{\pi}{2}$

$$U_s = \sigma_{sn}\,\sigma_{sp}\,V_{th}\,D_{ss}\,n_i\,\frac{\pi\,kT}{2q}\,\frac{1}{(\sigma_{sn}\sigma_{sp})^{\frac{1}{2}}}$$

$$U_s = (\sigma_{sn}\sigma_{sp})^{\frac{1}{2}}\,V_{th}\,n_i\,\frac{\pi\,kT}{2q}\,D_{ss}\,.$$

Under the assumption that $\sigma_{sn} = \sigma_{sp} = \sigma_s$, this expression becomes:

$$U_s = \sigma_s\,V_{th}\,n_i\,\frac{\pi\,kT}{2q}\,D_{ss}$$

thus $\frac{\pi\,kT}{2q}\,D_{ss} = N_{ss}\,.$

This indicates that the principal contribution to recombination-generation process is due to the surface states centered around the intrinsic energy of the gap.

REFERENCES

E-1 Sze, S.M., Physics of Semiconductor Devices, John Wiley & Sons, New York (1969), p. 103.

E-2 Grove, A. S., and D. J. Fitzgerald, "Surface Effects on p-n Junctions: Characteristics of Surface Space-Charge Regions under Non-Equilibrium Conditions", Solid State Electronics, Vol. 9 (1966), pps. 783-806.

DISTRIBUTION LIST

DEPARTMENT OF DEFENSE

Assistant to the Secretary of Defense
Atomic Energy
ATTN: Executive Assistant

Defense Communication Engineer Center
ATTN: Code R720, C. Stansberry
ATTN: Code R410

Defense Documentation Center
Cameron Station
12 cy ATTN: DD

Commander
Defense Electronic Supply Center
ATTN: DESC-ECS

Director
Defense Intelligence Agency
ATTN: DB-4C
ATTN: DT-1B

Director Defense Nuclear Agency
ATTN: DDST
ATTN: RAEV
4 cy ATTN: TITL

Commander
Field Command, Defense Nuclear Agency
ATTN: FCPR

Joint Chiefs of Staff
ATTN: J-3, WWMCCS, Evaluation Office

Chief
Livermore Division, Fld. Command, DNA
Lawrence Livermore Laboratory
ATTN: FCPRL

National Communications System
ATTN: NCS-TS, C. Bodson

Director
National Security Agency
ATTN: R-52, O. Van Gunten

Under Secy. of Def. for Rsch. & Engrg.
ATTN: Strategic & Space Systems (OS)

DEPARTMENT OF THE ARMY

Commander
Aberdeen Proving Ground
ATTN: STEAP, R. Harrison

Director
BMD Advanced Technology Center
Huntsville Office
ATTN: F. Hoke

Commander
BMD Systems Command
ATTN: BMDSC-HEN

DEPARTMENT OF THE ARMY (Continued)

Commander Fort Huachuca
ATTN: Tech. Ref. Div.

Commander
Harry Diamond Laboratories
ATTN: DELHD-N-NP
ATTN: DELHD-N-RBG
ATTN: DELHD-N-EM, Chief, Lab. 1000
ATTN: DELHD-N-EMA, J. Miletta
ATTN: J. Thompkins
ATTN: DELHD-N-RBA, J. Rosado

Commander
Redstone Scientific Information Ctr.
U.S. Army R&D Command
ATTN: DRDMI-TBD

Commander
U.S. Army Armament Research & Development Command
ATTN: DRDAR-TSI-E, A. Grinoch
ATTN: DRDAR-TSS, No. 59
ATTN: DRDAR-LCN-F
ATTN: DRDAR-LCN-DP, H. Posternak

Director
U.S. Army Ballistic Research Labs.
ATTN: DRDAR-BLT

U.S. ARMY Communications R&D Command
ATTN: DRSEL-TL-MD, Mr. Gaule
ATTN: DRSEL-TL-IR, E. Hunter
ATTN: DRSEL-NL-RO, R. Brown
ATTN: DRSEL-CT-HDK, A. Cohen

Chief
U.S. Army Communications Sys. Agency
ATTN: CCM-RD-T

Commandant
U.S. Army Engineer School
ATTN: ATSE-CDC

Commander
U.S. Army Material & Mechanics Rsch. Ctr.
ATTN: DRXMR-HH, J. Dignam

Commander
U.S. Army Missile Material Readiness Command
ATTN: Hawk Project Officer, DRCPM-HAER

Commander
U.S. Army Missile R&D Command
ATTN: DRCPM-PE-EA, W. Wagner

Commander U.S. Army Mobility Equip., R&D CMD.
ATTN: DRDME-E, J. Bond, JR.

Commander
U.S. Army Night Vision Laboratory
ATTN: DRSEL-NV-SD, A. Parker
ATTN: DRSEL-NV-SD, J. Carter

DEPARTMENT OF THE ARMY (Continued)

Commander
U.S. Army Nuclear & Chemical Agency
ATTN: Library

Commander U.S. Army Test and Evaluation Comd.
ATTN: DRSTE-EL
ATTN: DRSTE-FA

Director
U.S. Army Tradoc Systems Analysis Activity
ATTN: ATAA-TEC, O. Miller

Commander
U.S. Army Training and Doctrine Comd.
ATTN: ATORI-OP-SW

Project Manager
XM-1, Tank System
ATTN: DRCPM-GCM-SW

DEPARTMENT OF THE NAVY

Commander
Naval Air Systems Command
ATTN: AIR 310
ATTN: AIR 5324K
ATTN: AIR 350F

Commanding Officer
Naval Avionics Facility
ATTN: Branch 942, D. Repass

Commander
Naval Electronic Systems Command
ATTN: Code 504510
ATTN: NAVELEX 51024, C. Watkins
ATTN: PME 117-21

Commanding Officer
Naval Intelligence Support Ctr.
ATTN: NISC, Library

Commander
Naval Ocean Systems Center
ATTN: Code 4471

Superintendent (Code 1424)
Naval Postgraduate School
ATTN: Code 0142

Director Naval Research Laboratory
ATTN: Code 6601, E. Wolicki
ATTN: Code 2627
ATTN: Code 5216
ATTN: Code 6624, J. Ritter
ATTN: Code 4104

Commander
Naval Sea Systems Command
ATTN: SEA-04531

Commander
Naval Ship Engineering Center
ATTN: Code 6174D2

Officer-in-Charge
Naval Surface Weapons Center
ATTN: Code F31
ATTN: Code F30. 130-108

DEPARTMENT OF THE NAVY (Continued)

Commanding Officer
Naval Weapons Evaluation Facility
ATTN: Code AT-6

Commanding Officer
Nuclear Weapons Tng. Center, Pacific
ATTN: Code 32

Director
Strategic Systems Project Office
ATTN: NSP-27334, B. Hahn
ATTN: NSP-2701, J. Pitsenberger

DEPARTMENT OF THE AIR FORCE

Commander
Aeronautical Systems Division, AFSC
ATTN: ASD/ENESS, P. Marth
ATTN: ENACC, R. Fish
ATTN: ASD-YH-EX, Mr. Sunkes

Air Force Aero-Propulsion Laboratory
ATTN: POE-2, J. Wise

Air Force Avionics Laboratory
ATTN: DH, Lt Col McKenzie
ATTN: DHE-2

Air Force Materials Laboratory
ATTN: LTE

Headquarters
Air Force Systems Command
ATTN: DLCA

Air Force Technical Applications Center
ATTN: TFS, M. Schneider

Air Force Weapons Laboratory
ATTN: J. Mullis
ATTN: ELP, TREE Section
ATTN: EL, C. Baum
ATTN: SUL

Headquarters
Electronic Systems Division/IN
ATTN: INDC/21

Headquarters
Electronic Systems Division, AFSC
ATTN: DRI, E. Doherty

Commander
Foreign Technology Division, AFSC
ATTN: ETDP, B. Ballard

Commander
Rome Air Development Center, AFSC
ATTN: RADC/RBRP, C. Lane
ATTN: RBRAC, I. Krulac

Commander
Rome Air Development Center, AFSC
ATTN: ESE, A. Kahan

Space & Missile Systems Organization/MN
Air Force Systems Command
ATTN: MNNG
ATTN: MNNH

DEPARTMENT OF THE AIR FORCE (Continued)

Space & Missile Systems Organization/RS
Air Force Systems Command
ATTN: RSMA, Lt D. Higgins
ATTN: RSMG, Capt Collier

Space & Missile Systems Organization/SK
Air Force Systems Command
ATTN: SKF, P. Stadler

Space & Missile Systems Organization/YA
Air Force Systems Command
ATTN: YAS

Strategic Air Command/XPFS
ATTN: NRI-STINFO, Library
ATTN: XPFS, M. Carra

Director (INWS)
3416th Technical Training Squadron (ATC)
ATTN: TTV

DEPARTMENT OF ENERGY

Albuquerque Operations Office
ATTN: Doc. Con. for WSSB/OSD, R. Shay

University of California
Lawrence Livermore Laboratory
ATTN: Doc. Con. for Technical Information Dept.
ATTN: Doc. Con. for L-389, R. Ott
ATTN: Doc. Con. for L-545, D. Meeker

Los Alamos Scientific Laboratory
ATTN: Doc. Con. for B. Noel

Office of Military Application
ATTN: Doc. Con. for Classified Library

Sandia Laboratories
ATTN: Doc. Con. for F. Coppage
ATTN: Doc. Con. for J. Hood

OTHER GOVERNMENT AGENCIES

Central Intelligence Agency
ATTN: RD/SI, Rm. 5G48, Hq. Bldg.

Department of Transportation
Federal Aviation Administration
Headquarters, SEC. Div., ASE-300
ATTN: ARD-350

DEPARTMENT OF DEFENSE CONTRACTORS

Aerojet Electro-Systems Co.
Div. of Aerojet-General Corp.
ATTN: SV/8711/70

Aerospace Corp.
ATTN: J. Reinheimer
ATTN: S. Bower
ATTN: V. Josephson
ATTN: W. Willis
ATTN: I. Garfunkel
ATTN: R. Crolius

Avco Research & Systems Group
ATTN: W. Broding

DEPARTMENT OF DEFENSE CONTRACTORS (Continued)

Battelle Memorial Institute
ATTN: D. Hamman
ATTN: R. Blazek

BDM Corp.
ATTN: Marketing
ATTN: D. Alexander

Bendix Corp.
Communication Division
ATTN: Document Control

Bendix Corp.
Research Laboratories Division
ATTN: M. Frank

Boeing Co.
ATTN: 8K-38
ATTN: H. Wicklein
ATTN: R. Caldwell

Booz-Allen and Hamilton, Inc.
ATTN: R. Chrisner

Brown Engineering Company, Inc.
Cummings Research Park
ATTN: J. McSwain

Burroughs Corp.
Federal and Special Systems Group
ATTN: Product Eval. Lab.

California Institute of Technology
Jet Propulsion Lab.
ATTN: A. Stanley
ATTN: J. Bryden

Charles Stark Draper Lab, Inc.
ATTN: P. Kelly
ATTN: R. Haltmaier

Computer Sciences Corp.
ATTN: A. Schiff

Cutler-Hammer, Inc.
AIL Division
ATTN: Central Tech. Files, A. Anthony

University of Denver
Colorado Seminary
Denver Research Institute
ATTN: Sec. Officer for F. Venditti

E-Systems, Inc.
ECI Division
ATTN: R. French

E-Systems, Inc.
Greenville Division
ATTN: Division Library
ATTN: Library 8-50100

Effects Technology, Inc.
ATTN: E. Steele

Ex-Cal, Inc,
ATTN: R. Dickhaut

DEPARTMENT OF DEFENSE CONTRACTORS (Continued)

Fairchild Camera and Instrument Corp.
ATTN: Sec. Con. for D. Myers

Fairchild Industries, Inc.
Sherman Fairchild Technology Center
ATTN: B. Patton

University of Florida
ATTN: Security Officer for H. Sisler

Ford Aerospace & Communications Corp.
ATTN: E. Poncelet, Jr.
ATTN: K. Attinger
ATTN: Tech. Info. Services

Ford Aerospace & Communications, Corp.
ATTN: D. McMorrow
ATTN: E. Hahn
ATTN: Technical Library
ATTN: S. Crawford

Franklin Institute
ATTN: R. Thompson

Garrett Corp.
ATTN: Dept. 93-9, Weir

General Electric Co., Space Division
ATTN: D. Tasca
ATTN: VFSC, 4230M, J. Peden
ATTN: L. Chasen
ATTN: L. Sivo
ATTN: J. Andrews
ATTN: D. Long
ATTN: L. Jeffers

General Electric Co.
Re-Entry & Environmental Systems Div.
ATTN: W. Patterson
ATTN: J. Palchefsky, Jr.
ATTN: Tech. Lib.

General Electric Co.
Ordnance Systems
ATTN: J. Reidl

General Electric Co.
Aircraft Engine Business Group
ATTN: R. Hellen

General Electric Co.-TEMPO
Center for Advanced Studies
ATTN: DASIAC
ATTN: R. Rutherford
ATTN: W. McNamara
ATTN: M. Espig

General Electric Co.-TEMPO
Alexandria Office
ATTN: DASIAC

General Research Corp.
Santa Barbara Division
ATTN: Technical Information Office

Georgia Institute of Technology
Office of Contract Administration
ATTN: Rsch. Security Coordinator for H. Denny

DEPARTMENT OF DEFENSE CONTRACTORS (Continued)

Goodyear Aerospace Corp.
Arizona Division
ATTN: Security Control Station

GTE Sylvania, Inc.
Electronics Systems Grp-Eastern Div.
ATTN: L. Blaisdell
ATTN: C. Thornhill

GTE Sylvania, Inc.
ATTN: J. Waldron

Harris Corp.
Electronics Systems Division
ATTN: C. Davis
ATTN: W. Abare

Harris Corp.
Harris Semiconductor Division
ATTN: Mngr., Linear Eng.
ATTN: Mngr., Bipolar Digital Eng.

Hazeltine Corp.
ATTN: Tech. Info. Ctr., M. Waite

Honeywell, Inc.
Avionics Division
ATTN: MS 725-5

Hughes Aircraft Co.
ATTN: K. Walker
ATTN: J. Singletary
ATTN: D. Binder
ATTN: CTDC 6/E110

Hughes Aircraft Co.
ATTN: M S A620, E. Smith

IBM Corp.
ATTN: Mono Memory Systems
ATTN: Electromagnetic Compatability

Institute for Defense Analyses
ATTN: Tech. Info. Services

International Tel. & Telegraph Corp.
ATTN: Dept. 608

IRT Corp.
ATTN: Systems Effects Division
ATTN: Physics Division
ATTN: R. Mertz
ATTN: MDC

JAYCOR
ATTN: R. Sullivan

Johns Hopkins University
Applied Physics Lab.
ATTN: P. Partridge

Kaman Sciences Corp.
ATTN: President
ATTN: Dir., Science & Technology Div.
ATTN: W. Ware
ATTN: W. Rich
ATTN: J. Lubell

DEPARTMENT OF DEFENSE CONTRACTORS (Continued)

Litton Systems, Inc.
Guidance & Control Systems Division
ATTN: J. Retzler
ATTN: V. Ashby

Lockheed Missiles & Space Co., Inc.
ATTN: L. Rossi
ATTN: E. Smith
ATTN: B. Kimura
ATTN: D. Wolfhard

Lockheed Missiles & Space Co., Inc.
ATTN: Reports Library

M.I.T. Lincoln Lab.
ATTN: Library, A-082

Martin Marietta Corp.
Orlando Division
ATTN: TIC/MP-30

Martin Marietta Corp.
Denver Division
ATTN: Research Library
ATTN: P. Kase

McDonnell Douglas Corp.
ATTN: T. Ender
ATTN: Library

McDonnell Douglas Corp.
ATTN: P. Albrecht

Mission Research Corp.
ATTN: M. Van. Blaricum
5 cy ATTN: Technical Library

Mission Research Corp.
EM System Applications Division
ATTN: D. Merewether

Mission Research Corp.-San Diego
ATTN: V. Van Lint
ATTN: J. Raymond
ATTN: A. Hart
ATTN: J. Smyth, Jr.

National Academy of Sciences
ATTN: Committee on Atmospheric Sciences for R. Shane

Northrop Corp.
Northrop Research and Technology Ctr.
ATTN: J. Srour
ATTN: O. Curtis, Jr.

Northrop Corp.
Electronic Division
ATTN: D. Strobel

University of Oklahoma
Research Institute
ATTN: R. Wood

Physics International Co.
ATTN: Division 6000
ATTN: J. Shea

DEPARTMENT OF DEFENSE CONTRACTORS (Continued)

Power Conversion Technology, Inc.
ATTN: V. Fargo

R & D Associates
ATTN: C. MacDonald
ATTN: W. Karzas
ATTN: S. Rogers

Rand Corp.
ATTN: C. Crain

Raytheon Co.
ATTN: G. Joshi

Raytheon Co.
ATTN: H. Flescher

RCA Corp.
Government Systems Division
Astro Electronics
ATTN: G. Brucker

RCA Corp.
David Sarnoff Research Center
ATTN: Office N103
ATTN: Security Dept., L. Minich

Research Triangle Institute
ATTN: Sec. Officer for Eng. Div., M. Simons, Jr.

Rockwell International Corp.
ATTN: K. Hull
ATTN: HA10, J. Bell
ATTN: N. Rudie

Rockwell International Corp.
Space Division
ATTN: D. Stevens
ATTN: TIC D/41-092 AJ01

Rockwell International Corp.
ATTN: TIC BA08

Rockwell International Corp.
Collins Divisions
ATTN: A. Langenfeld
ATTN: TIC 106-216

Sanders Associates, Inc.
ATTN: M. Aitel
ATTN: L. Brodeur

Science Applications, Inc.
ATTN: L. Scott
ATTN: J. Beyster

Science Applications, Inc.
Huntsville Division
ATTN: N. Byrn

Science Applications, Inc.
ATTN: W. Chadsey

Singer Co.
Data Systems
ATTN: Tech. Info. Center

DEPARTMENT OF DEFENSE CONTRACTORS (Continued)

Sperry Rand Corp.
Sperry Microwave Electronics
ATTN: Engineering Laboratory

Sperry Rand Corp.
Sperry Division
ATTN: P. Maraffino
ATTN: C. Craig
ATTN: R. Viola

Sperry Rand Corp.
Sperry Flight Systems
ATTN: D. Schow

Spire Corp.
ATTN: R. Little

SRI International
ATTN: P. Dolan

Sundstrand Corp.
ATTN: Research Department

Tetra Tech, Inc.
ATTN: T. Simpson

Texas Instruments, Inc.
ATTN: D. Manus

DEPARTMENT OF DEFENSE CONTRACTORS (Continued)

TRW Defense & Space Sys. Group
ATTN: R. Webb
ATTN: H. Holloway
ATTN: Technical Information Center
ATTN: Vulnerability & Hardness Laboratory
ATTN: A. Narevsky
2 cy ATTN: O. Adams
2 cy ATTN: R. Plebuch

TRW Defense & Space Sys. Group
San Bernardino Operations
ATTN: F. Fay
ATTN: R. Kitter

TRW Systems and Energy
ATTN: G. Spehar
ATTN: R. Mathews
ATTN: D. Millward

Vought Corp.
ATTN: Library
ATTN: R. Tomme

Westinghouse Electric Corp.
Defense and Electronic Systems Ctr.
ATTN: H. Kalapaca
ATTN: MS 3330